The Investigation of a Multi-turn Time-of-Flight Mass Spectrometer

Michisato Toyoda

Department of Physics, Graduate School of Science,

Osaka University

Contents

I. Introduction

In space science, mass spectrometry (MS) plays a key role in the analysis of material from planetary and cometary surfaces. Mass spectrometry is able to provide information on (1) the isotope ratios of the elements and (2) the possibility of the existence of organic compounds. On recent space missions mass analyzers have often been employed for this purpose. In the Viking mission, a miniature Nier-Johnson type double focusing sector instrument was used [1-1]. And in the Cassini mission, launched in October 1997, a quadrupole mass analyzer is carried on the Huygens-Probe [1-2]. Major past missions employed mass spectrometers are listed in Table 1-1 [1-3]. It is necessary that an instrument is small and light to carry on a spacecraft. In the case of the COSAC project of ROSETTA mission, the allowed weight, size and electric power is 1100 g, 300 × 350 × 80 mm and 5 W, respectively. Moreover the required mass resolution is 3000. The investigation and development of a mass spectrometer having high performance in spite of its small size and lightweight are very important.

Magnetic sector instruments are commonly used for the measurement of isotope ratios, elemental composition, etc. in geochemistry and space science. The mass spectrometers of this type were adopted in various planetary and cometary investigation. They have advantages (1) high resolution, (2) high accuracy for quantitative analysis and (3) wide dynamic rage. However, there is a demerit that the instrument becomes heavy because magnets are used.

Quadrupole mass filters (QMS) are recently getting popular in space investigation because this type of mass spectrometers are light. However, the QMS usually suffers from (1) low resolution, (2) low sensitivity and (3) a limitation in the mass range.

With the development of high-speed data acquisition and data analysis methods, it is now possible to use a time-of-flight (TOF) instrument as a light but powerful mass spectrometer for space research. Here, the time-of-flight mass spectrometry

Year (launch)	Target	Mission		Mass spectrometer	Object for measurement	Resource	Remark
1972	**Moon**	**Apollo**		**Single focusing type**	Ar, Ne, H	**9.1kg (inc. electric circuit)**	atmosphere
1975	**Mars**	**Viking**	Atmosphere	**Mattauch-Herzog type**	CO_2, N_2, Ar	**20 kg (inc. electric circuit)**	
			GC/MS	**Nier-Johnson type**	organic matters		
1978	**Venus**	**Pioneer - Venus**	Large probe	**Single focusing type**	CO_2, N_2, Ar		
			Bus	**Mattauch-Herzog type**			
1985	**Halley Comet**	**Giotto**		**non-standard type double focusing energy analyzer**	H_2O,CO, CO_2,NH_3, CH_4		
1988	**Phobos**	**Phobos**	LIMA-D	**TOF mass spectrometer**		**81.5 kg**	laser heating
			DION	**Quadrupole mass spectrometer**		**23.9 kg**	secondary ion bombardment
1989	**Jupiter**	**Galileo**		**Quadrupole mass spectrometer**	chemical composition of atmosphere	**13kg, 13W**	atmosphere
1997	Saturn	Cassini	Huygens probe	Quadrupole mass spectrometer	GC/MS atomospher	17.3 kg, 41W (ave.)	
			Cassini orbiter	Quadrupole mass spectrometer	atmosphere of Titan	**10.3 kg**	

Table 1-1 Major past missions employed mass spectrometers.

(TOF/MS) is discussed in detail.

TOF/MS was first postulated in 1946 [1-4]. Stephens suggested that ions having different m/z values (m [u] is the mass of the ion and z [e] is the charge) would possess different velocities after acceleration from an ion source, and consequently would separate into groups spreading out in space. If the acceleration voltage is known the mass to charge ratio of the ions can be calculated from the time taken to travel a known distance as :

$$\frac{m}{z} = 1.929 \times 10^{8} \frac{V T^2}{L^2} \tag{1-1}$$

where V [V] is the acceleration voltage, T [s] is the flight time and L [m] is the flight path length.

The merits of the TOF mass spectrometer are :

(1) The mass range is ultimate.

(2) TOF mass spectrometers can detect all ions from low to high mass successively, and no ions are lost by the scanning process which is often used in other type of mass spectrometers.

A major limitation of TOF mass spectrometer, however, was its relatively poor mass resolution and poor ion transmission. In order to improve the mass resolution and the ion transmission, the following methods were successfully introduced.

(1) In order to minimize the effects of spatial and velocity dispersions on time resolution, two-stage acceleration, time-lag focusing [1-5] and orthogonal acceleration ion sources [1-6] were developed.

(2) In order to compensate for energy distribution among ions generated in the ion source, electric mirrors were proposed and constructed by Mamyrin et al. in 1973 [1-7].

(3) In order to accomplish high resolution and high transmission, Poschenrieder proposed the mass spectrometers consisting of electric sectors in 1971 [1-8]. They satisfied angular and energy time focusing conditions. Spatial focusing can also be achieved to increase ion transmission efficiency. As an example of this method, a

TOF mass spectrometer consisting of four toroidal electric sectors was constructed and examined by Sakurai et al. in 1985 [1-9]. It realizes triple time focusing and triple space focusing.

(4) In order to obtain a long flight path, multi-turn geometries using electric sectors were proposed by Poschenrieder [1-8], Matsuo et al. [1-10] and Sakurai [1-11]. For the same purpose, electrostatic multi-pass mirror systems were proposed by Wollnik [1-12].

Since the mass resolution of a TOF mass spectrometer is proportional to the path length under the condition of constant ion-packet-width during the flight, it will be necessary to use a multi-turn optical system in order to achieve the desired resolution within the physical limitations imposed by the spacecraft. However, if a multi-turn optical system does not satisfy the 'perfect focusing condition', ion beam diverges. Therefore, the mass resolution and the ion transmission decrease with an increasing number of turns around the system. To avoid this problem, the ion optical system should satisfy the 'perfect focusing condition.'

The purpose of this thesis is to investigate and to develop a small and light multi-turn TOF mass spectrometer suitable for a planetary and cometary research mission. A multi-turn TOF mass spectrometer was newly designed and constructed as a laboratory model of COSAC project of ROSETTA mission. The performance of this mass spectrometer was examined.

The outline of this thesis is as follows :

Chapter II :

The computer program 'TRIO-DRAW' was developed to calculate and display ion trajectories. It was also developed to simulate overall ion optical characteristics such as image shape and mass resolution and flight time information [1-13]. This program was used to design a multi-turn TOF mass spectrometer. The features of this program are described.

Chapter III :

The ion optics of a multi-turn TOF mass spectrometer which satisfies the 'perfect space and time focusing' was investigated [1-14]. By introducing symmetry in the arrangement of sectors, multiple time and space focusing can be easily satisfied [1-14, 1-15]. Using this principle, the ion optical systems for a multi-turn TOF mass spectrometer are proposed.

Chapter IV :

One of these proposed TOF mass spectrometer systems has been constructed as a laboratory model of COSAC project of ROSETTA mission [1-16, 1-17]. It consists of four cylindrical electrostatic sectors and eight electric quadrupole lenses. In order to inject and eject ions, a linear type TOF mass spectrometer was combined. Four electric quadrupole triplets were used to achieve perfect space focusing of the linear type TOF mass spectrometer. The instrument was named 'MULTUM Linear plus.' The technical data for the construction are reported.

Chapter V :

The results of the examination of the performance of 'MULTUM Linear plus' are described. The relationship between the mass resolution or ion transmission and the number of cycles of the ions through the ion optical system is presented.

References

[1-1] Biemann, K., *Origin of Life,* **5** (1974), 417.

[1-2] Niemann, H., S. Atreya, S. J. Bauer, K. Biemann, B. Block et al., *ESA report,* **85** (1997).

[1-3] http://www.nasa.gov, http://nssdc.gsfc.nasa.gov/planetary/

[1-4] W.E. Stephens, *Phys. Rev.*, **69** (1946), 691.

[1-5] W. C. Wiley and I. H. McLaren, *Rev. Sci. Instrum.*, **26** (1955), 1150 - 1157.

[1-6] J.H.J. Dawson and M. Guilhaus, *Rapid. Commun. Mass Spectrom.*, **3** (1989), 155-159.

[1-7] B. A. Mamyrin, V. I. Karataev, D. V. Shmikk and V. A. Zagulin, *Sov. Phys. JETP*, **37** (1973), 45.

[1-8] W. P. Poschenrieder, *Int. J. Mass Spectrom. and Ion Phys.*, **9** (1972), 357-373.

[1-9] T. Sakurai, Y. Fujita, T. Matsuo, H. Matsuda, I. Katakuse and K. Miseki, *Int. J. Mass Spectrom. and Ion Proc.*, **66** (1985), 283-290.

[1-10] T. Matsuo, M. Toyoda, T. Sakurai and M. Ishihara, *J. Mass Spectrom.*, **32** (1997), 1179-1185.

[1-11] T. Sakurai, H. Nakabishi, T. Hiasa and K. Okanishi, *Nucl. Instrum. Methods A*, **427** (1999), 182-186.

[1-12] H. Wollnik and M. Przewloka, *Int. J. Mass Spectrom. and Ion Proc.*, **96** (1990), 267-274.

[1-13] M. Toyoda and T. Matsuo, *Nucl. Instrum. Methods A*, **427** (1999), 375-381.

[1-14] M. Ishihara, M. Toyoda and T. Matsuo, *Int. J. Mass Spectrom. and Ion Proc.*, **197** (2000), 179-189.

[1-15] T. Sakurai, T. Matsuo and H. Matsuda, *Int. J. Mass Spectrom. and Ion Proc.*, **63** (1985), 273-287.

[1-16] T. Matsuo, M. Ishihara, M. Toyoda, H. Ito, S. Yamaguchi, R. Roll and H. Rosenbauer, *Advances in Space Research*, **23** (1999), 341-348.

[1-17] M. Toyoda, M. Ishihara, S. Yamaguchi, H. Ito, T. Matsuo, R. Roll and H. Rosenbauer, *J. Mass Spectrom.*, **35** (2000), 163-167.

II. Computer Program 'TRIO-DRAW' for Displaying Ion Trajectory and Flight Time

2.1 Introduction

When we design a high-performance mass spectrometer, we take the following two processes. First, we must determine the physical parameters of the mass spectrometer, e.g. the radius and the aperture angle of the electric or magnetic sector, the length of the quadrupole lens or that of the drift space. Several computer codes, e.g. TRANSPORT [2-1], TRIO [2-2], GIOS [2-3], etc. were already developed for this purpose. Secondly, we should simulate the ion optical overall characteristics of a proposed system before determining the final dimensions. It is important to calculate the beam envelope of a system under a certain initial conditions of ions in this process. The image shape at a detector plane can be simulated by taking all aberrations into account. From the image shape, the theoretical mass resolution can be obtained. Computer program BEIS was developed for such purpose [2-4]. However, BEIS does not include TOF calculation capability and only run on a personal computer (FACOM FM8 or NEC PC9801). Therefore, the computer program 'TRIO-DRAW' has been newly developed by adding the following new functions.

(1) The functions of TRIO and BEIS are combined in a single program.

(2) Flight time can be calculated in the form of "path length deviation" up to the second order approximation using the transfer matrix method.

(3) Trajectory display

(3a) Three different types of trajectory expression (top view, x-direction, y-direction) are supported.

(3b) Trajectories having different initial conditions (position, angle, energy, mass) are expressed by different colors.

(3c) Path length deviation at certain profile plane is expressed by different color.

(4) Image shape display

(4a) Spatial image shapes at a detector plane are displayed for various initial

conditions.

(4b) Isochronous image shapes at a detector plane are displayed for from various initial conditions.

(5) Estimation of mass resolution

(5a) Theoretical mass resolution under a given initial condition is estimated.

(5b) Theoretical mass resolution in TOF mode is estimated under a given initial condition.

(6) The program is written using FORTRAN and C languages. Outputs of the images are given by a Postscript file.

2.2 The transfer matrix method

2.2.1 The transfer matrix method for the geometrical trajectory

Generally, there are two methods to calculate the ion trajectories in electromagnetic fields :

(1) The transfer matrix method

An arbitrary ion trajectory is defined by its ion optical position vector $\mathbf{P}(x, \alpha, y, \beta, \gamma, \delta)$. The field elements (electric and magnetic sectors, electric and magnetic quadrupole lenses, etc.) are expressed by transfer matrices. This method is only applicable for a narrow beam originating near the optic axis. The transfer matrix is calculated by using a computer code TRIO [2-2].

(2) The ray tracing method

Numerical expressions in the field elements of electromagnetic fields are derived from solutions to Maxwell's equations. Then the ion trajectory can be determined by finding the solution to the path equation. In this method, there are no restrictions to the beam characteristics such as parallaxial approximations. Computer program ELECTRA has been developed using this method [2-5].

Relating to the field calculation accuracies and computing time, the first method is preferred to the second. In this thesis, the transfer matrix method is used.

The coordinate system (x, y, z) is defined with its origin on the optical axis, with the z direction along the optical axis as shown in Fig. 2-1. In principle, ion trajectories in electric or magnetic fields can be calculated by solving the equations of motion. The geometrical trajectory of an arbitrary particle can be expressed by an ion optical position vector $\mathbf{P}(x, \alpha, y, \beta, \gamma, \delta)$. Here, x, y and α, β denote the lateral and angular deviations of the ion from the optical axis. The mass and energy deviations, γ and δ, are defined as:

$$m / e = \left(m_0 / e_0\right)\left(1+\gamma\right), \quad U / e = \left(U_0 / e_0\right)\left(1+\delta\right) \tag{2-1}$$

where m, U and e are respectively the mass, energy and charge of an arbitrary ion and m_0, U_0, e_0 are those of a reference ion. The ion optical position vector $\mathbf{P}$ for any arbitrary position is a function of the initial vector $\mathbf{P_0}(x_0, \alpha_0, y_0, \beta_0, \gamma, \delta)$. Since exact analytical solutions can not be obtained generally, power series expansions are the normal way to express results :

$$\begin{aligned} x = {} & A(x \mid x)\, x_0 + A(x \mid \alpha)\, \alpha_0 + A(x \mid \gamma)\, \gamma + A(x \mid \delta)\, \delta \\ & \text{(1st order terms)} \\ & + A(x \mid x\, x)\, x_0^2 + A(x \mid x\, \alpha)\, x_0\, \alpha_0 + A(x \mid x\, \gamma)\, x_0\, \gamma + A(x \mid x\, \delta)\, x_0\, \delta + \cdots \\ & \text{(2nd order terms)} \\ & + A(x \mid x\, x\, x)\, x_0^3 + A(x \mid x\, x\, \alpha)\, x_0^2\, \alpha_0 + A(x \mid x\, x\, \gamma)\, x_0^2\, \gamma + A(x \mid x\, x\, \delta)\, x_0^2\, \delta + \cdots \\ & \text{(3rd order terms)} \end{aligned} \tag{2-2.a}$$

$$\begin{aligned} \alpha = {} & A(\alpha \mid x)\, x_0 + A(\alpha \mid \alpha)\, \alpha_0 + A(\alpha \mid \gamma)\, \gamma + A(\alpha \mid \delta)\, \delta \\ & + A(\alpha \mid x\, x)\, x_0^2 + A(\alpha \mid x\, \alpha)\, x_0\, \alpha_0 + A(\alpha \mid x\, \gamma)\, x_0\, \gamma + A(\alpha \mid x\, \delta)\, x_0\, \delta + \cdots \\ & + A(\alpha \mid x\, x\, x)\, x_0^3 + A(\alpha \mid x\, x\, \alpha)\, x_0^2\, \alpha_0 + A(\alpha \mid x\, x\, \gamma)\, x_0^2\, \gamma + A(\alpha \mid x\, x\, \delta)\, x_0^2\, \delta + \cdots \end{aligned} \tag{2-2.b}$$

$$\begin{aligned} y = {} & A(y \mid y)\, y_0 + A(y \mid \beta)\, \beta_0 \\ & + A(y \mid x\, y)\, x_0\, y_0 + A(y \mid x\, \beta)\, x_0\, \beta_0 + A(y \mid \alpha\, y)\, \alpha_0\, y_0 + A(y \mid \alpha\, \beta)\, \alpha_0\, \beta_0 + \cdots \\ & + A(y \mid x\, x\, y)\, x_0^2\, y_0 + A(x \mid x\, x\, \beta)\, x_0^2\, \beta_0 + A(x \mid x\, \alpha\, y)\, x_0\, \alpha_0\, y_0 + \cdots \end{aligned} \tag{2-2.c}$$

$$\begin{aligned} \beta = {} & A(\beta \mid y)\, y_0 + A(\beta \mid \beta)\, \beta_0 \\ & + A(\beta \mid x\, y)\, x_0\, y_0 + A(\beta \mid x\, \beta)\, x_0\, \beta_0 + A(\beta \mid \alpha\, y)\, \alpha_0\, y_0 + A(\beta \mid \alpha\, \beta)\, \alpha_0\, \beta_0 + \cdots \\ & + A(\beta \mid x\, x\, y)\, x_0^2\, y_0 + A(\beta \mid x\, x\, \beta)\, x_0^2\, \beta_0 + A(\beta \mid x\, \alpha\, y)\, x_0\, \alpha_0\, y_0 + \cdots \end{aligned} \tag{2-2.d}$$

$$\gamma = \gamma_0 \tag{2-2.e}$$

$$\delta = \delta_0 \tag{2-2.f}$$

The "transfer coefficients" $A(x \mid x)$, $A(x \mid \alpha)$, ... can be calculated numerically, for example, by the computer program TRIO when the physical parameters, e.g. the

Definition of the coordinate system

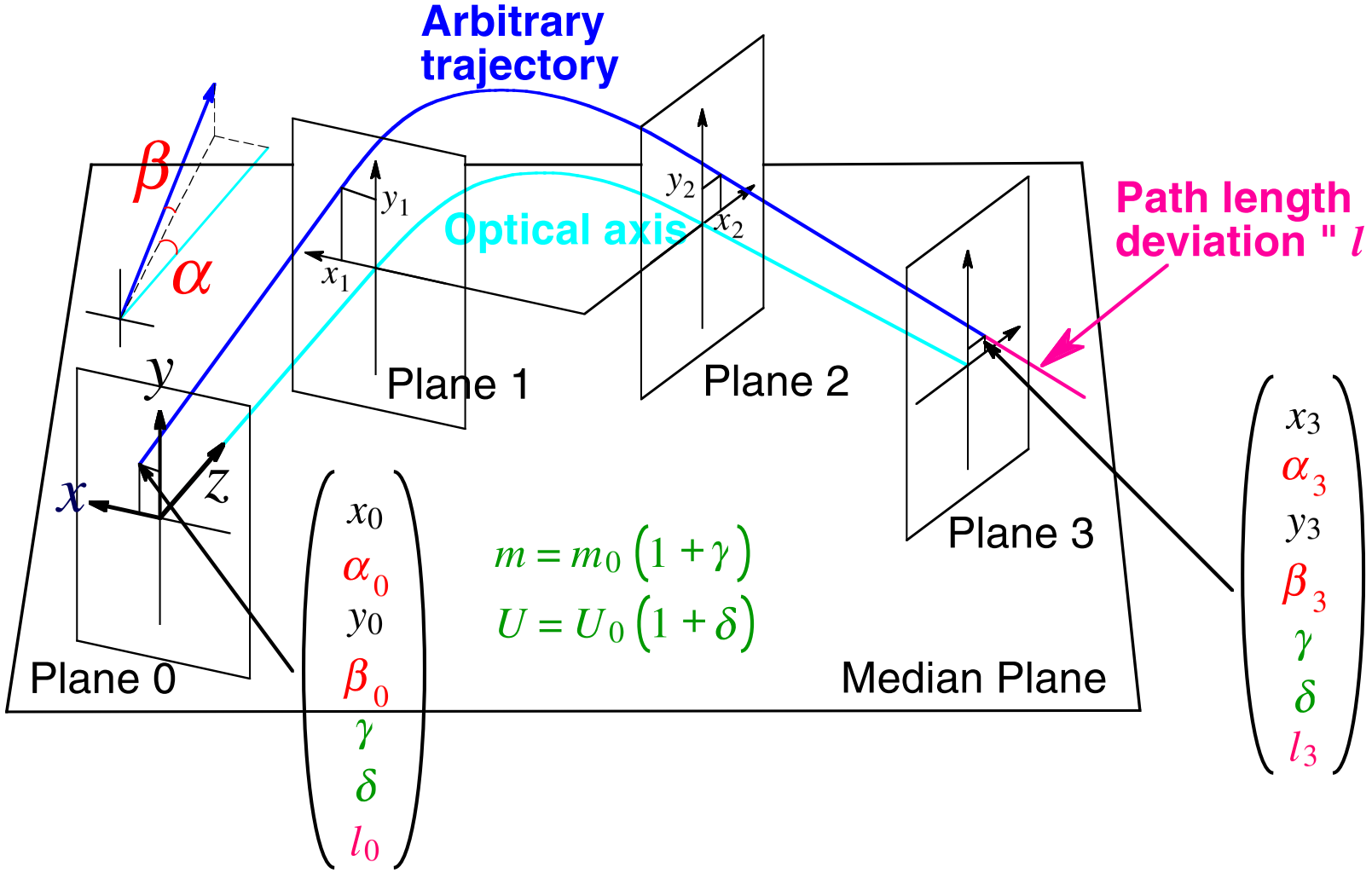

Fig. 2-1 Definition of the coordinate system and of the elements of ion optical position vectors.

radius and the aperture angle of the electric or magnetic sector are given. Eqns. (2-2.a-f) can be expressed as a 6 × 6 matrix A for the first order approximation as ;

$$\begin{pmatrix} x \\ \alpha \\ y \\ \beta \\ \gamma \\ \delta \end{pmatrix} = \begin{pmatrix} A(x\,|\,x) & A(x\,|\,\alpha) & 0 & 0 & A(x\,|\,\gamma) & A(x\,|\,\delta) \\ A(\alpha\,|\,x) & A(\alpha\,|\,\alpha) & 0 & 0 & A(\alpha\,|\,\gamma) & A(\alpha\,|\,\delta) \\ 0 & 0 & A(y\,|\,y) & A(y\,|\,\beta) & 0 & 0 \\ 0 & 0 & A(\beta\,|\,y) & A(\beta\,|\,\beta) & 0 & 0 \\ 0 & 0 & 0 & 0 & 1 & 0 \\ 0 & 0 & 0 & 0 & 0 & 1 \end{pmatrix} \begin{pmatrix} x_0 \\ \alpha_0 \\ y_0 \\ \beta_0 \\ \gamma \\ \delta \end{pmatrix} \tag{2-3}$$

This is the “transfer matrix” which expresses the characteristics of a field. This transfer matrix is very useful when several fields such as electric sectors, quadrupole lenses, drift spaces are combined. The ion optical character of a mass spectrometer, for example, can be condensed into a total transfer matrix R, which is simply obtained by only multiplying the transfer matrices of the individual elements as:

$$R = A_n \times A_{n-1} \times \cdots\cdots \times A_2 \times A_1 \tag{2-4}$$

Focusing conditions of a whole system will be discussed using above the total transfer matrix elements $R(i\,|\,j)$.

2.2.2 The transfer matrix method for the flight time calculation

In order to describe the flight time, the concept of the path length deviation is introduced. The flight time of an arbitrary particle of mass m, energy U and velocity $v = v_0 \sqrt{(1+\delta)/(1+\gamma)}$ (v_0 is the velocity of reference particle. $v_0 = \sqrt{2\,U_0 / m_0}$) is given by

$$T = \int_{s_0}^{s} \frac{ds}{v} = \int_{z_0}^{z} \frac{1}{v} \frac{ds}{dz}\, dz \tag{2-5}$$

Where s and z is the flight path length of an arbitrary particle and a reference particle, respectively, Since $ds\,/\,dz$ is unity on the optical axis, the flight time of the reference particle is given by

$$T_0 = \int_{z_0}^{z} \frac{1}{v_0}\, dz \tag{2-6}$$

From now on, the flight time of an arbitrary particle is described by the time deviation t defined as

$$t = T - T_0 = \int_{z_0}^{z} \left(\frac{1}{v} \frac{ds}{dz} - \frac{1}{v_0} \right) dz \tag{2-7}$$

It is usually difficult to obtain an analytical form of t, therefore t is given by a power series expansion of small quantities, x_0, α_0, y_0, β_0, γ and δ, as

$$t = t_0 + A\,(t \mid x)\, x_0 + A\,(t \mid \alpha)\, \alpha_0 + A\,(t \mid \gamma)\, \gamma + A\,(t \mid \delta)\, \delta + \cdots \tag{2-8}$$

Since t and the coefficients $A(t \mid x)$, $A(t \mid \alpha)$, ... depend on not only physical parameters of ion optical system but also the physical parameters v_0, m_0 and U_0 of the reference particle. However, it is convenient to express the matrix independently of the parameters v_0, m_0 and U_0 of the reference particle. Therefore a new quantity "path length deviation, l" defined by $l = v_0\, t$ is introduced to eliminate v_0. The pass length deviation l can also be expressed by the power series expansion

$$l = l_0 + A\,(l \mid x)\, x_0 + A\,(l \mid \alpha)\, \alpha_0 + A\,(l \mid \gamma)\, \gamma + A\,(l \mid \delta)\, \delta + \cdots \tag{2-9}$$

The coefficients A($l \mid x$), A($l \mid \alpha$), ... depend only on the physical parameters of ion optical systems, and are independent of U_0, v_0 or m_0. They can be calculated by the computer program TRIO-TOF [2-6] or 'unify' [2-7].

In order to express the general trajectory including the path length deviation, the new element of l is added to the original ion optical position vector. The new position vector (x, α, y, β, γ, δ, l) at an arbitrary profile plane is related to the initial position vector (x_0, α_0, y_0, β_0, γ, δ, l_0). In the first order approximation, this relation is expressed by a transfer matrix A in the following way.

$$\begin{pmatrix} x \\ \alpha \\ y \\ \beta \\ \gamma \\ \delta \\ l \end{pmatrix} = \begin{pmatrix} A(x \mid x) & A(x \mid \alpha) & 0 & 0 & A(x \mid \gamma) & A(x \mid \delta) & 0 \\ A(\alpha \mid x) & A(\alpha \mid \alpha) & 0 & 0 & A(\alpha \mid \gamma) & A(\alpha \mid \delta) & 0 \\ 0 & 0 & A(y \mid y) & A(y \mid \beta) & 0 & 0 & 0 \\ 0 & 0 & A(\beta \mid y) & A(\beta \mid \beta) & 0 & 0 & 0 \\ 0 & 0 & 0 & 0 & 1 & 0 & 0 \\ 0 & 0 & 0 & 0 & 0 & 1 & 0 \\ A(l \mid x) & A(l \mid \alpha) & 0 & 0 & A(l \mid \gamma) & A(l \mid \delta) & 1 \end{pmatrix} \begin{pmatrix} x_0 \\ \alpha_0 \\ y_0 \\ \beta_0 \\ \gamma \\ \delta \\ l_0 \end{pmatrix} \tag{2-10}$$

2.3 The functions of the 'TRIO-DRAW' program

2.3.1 Ion trajectory calculation and display

'TRIO-DRAW' supports three different modes (individual beam mode, beam envelope mode, flight-time deviation mode) and three different view (top view, x-direction, y-direction) displays. Top view display shows a plane view of the ion trajectories. This display enables us to estimate the focusing properties of the system, including the beam waist and the size of the instrument. Other displays, x-direction (horizontal plane view) and y-direction (vertical plane view) displays, are linear representations of beam trajectories; similar displays were used in BEIS [2-4]. These displays are written in Postscript language in 'TRIO-DRAW.'

2.3.1.1 Individual beam mode

In this mode only individual initial conditions are given and therefore the superimposition of initial conditions are not taken into account. We consider several ions emitted under a variety of ion source conditions and draw the ion paths through the system. In order to express ion trajectories having different initial conditions, they are drawn by individual colors (green for position x_0, y_0, blue for angle α_0, β_0, red for energy δ and purple for mass γ). All positions of ions at arbitrary profile plane of the system are calculated by the transfer matrix method. Examples for the CQH type mass spectrometer [2-8] are shown in Fig. 2-2. From these figures, we can understand the extent of ion trajectories having respective initial conditions.

2.3.1.2 Beam envelope mode

One method of determining the beam envelope is the calculation of the phase ellipse, which was reported in reference [2-1]. Here we estimate the beam envelope in the same manner as estimated in BEIS. The method of calculation and drawing is similar to individual beam mode, but in this mode the superimposition of initial conditions is taken into account. We can estimate the rough beam envelope by

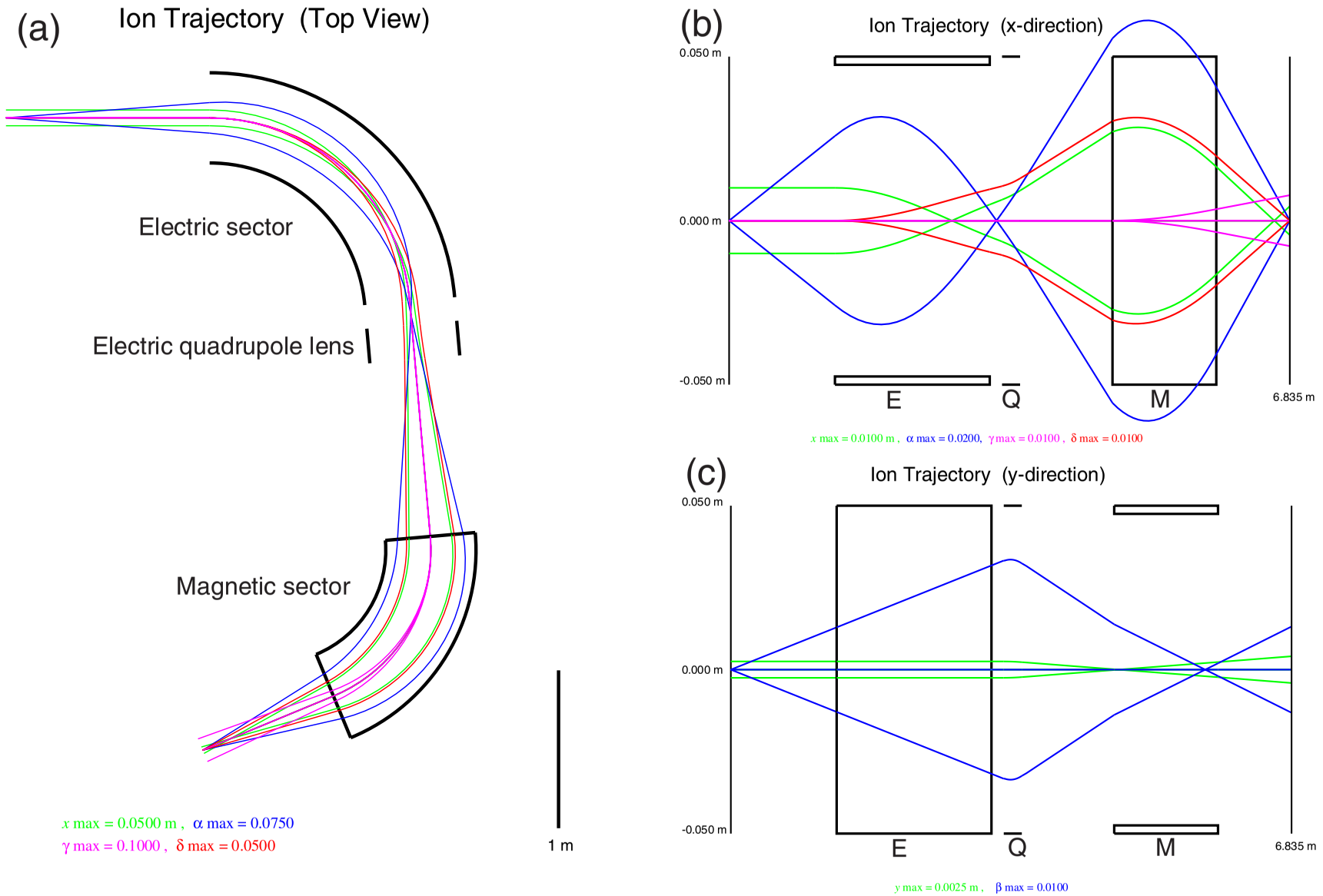

Fig. 2-2 Ion trajectories of the individual beam mode for the CQH-type mass spectrometer. (a)top view, (b) x-direction, (c) y-direction. The flame of electrode, magnet and quadrupole are drawn in arbitrary scale.

connecting the trajectories of the outmost rays. Examples for the CQH-type mass spectrometer are shown in Fig. 2-3. From these figures, the necessary gap width for a magnetic or electric sector can be estimated easily. When the system is already constructed, the necessary conditions for ion source parameters and slit width can be determined.

2.3.1.3 Flight time deviation mode

The degree of path length deviation is dependent on initial conditions and is expressed by color difference accordingly. Examples for the 4-sector TOF mass spectrometer [2-9] are shown in Fig. 2-4. The ion which moved faster and slower than reference particle at the certain profile plane is colored red and blue, respectively. Here, ion trajectories and path length deviations are also calculated by the transfer matrix method. From these figures, we can understand pictorially the isochronous properties of the TOF mass spectrometer.

2.3.2 Image shape calculation and estimation of mass resolution

When the total transfer matrix of the system and the initial conditions are given, the image shape at the detector plane can be calculated. 'TRIO-DRAW' can calculate both the space and flight time image shapes. We choose 10000 ions having random initial conditions for x, y, α, β, δ and calculate the position and the path length deviation at the detector plane for the respective condition. In order to estimate the peak shape as a histogram, the position or the path length deviation is divided into narrow segments; the numbers of ions in each segment is accumulated. The theoretical mass resolution can be estimated from these peak widths. An example of the position image shape of the CQH-type mass spectrometer is shown in Fig. 2-5, and an example of the flight time image shape of the 4-sector TOF mass spectrometer is shown in Fig. 2-6.

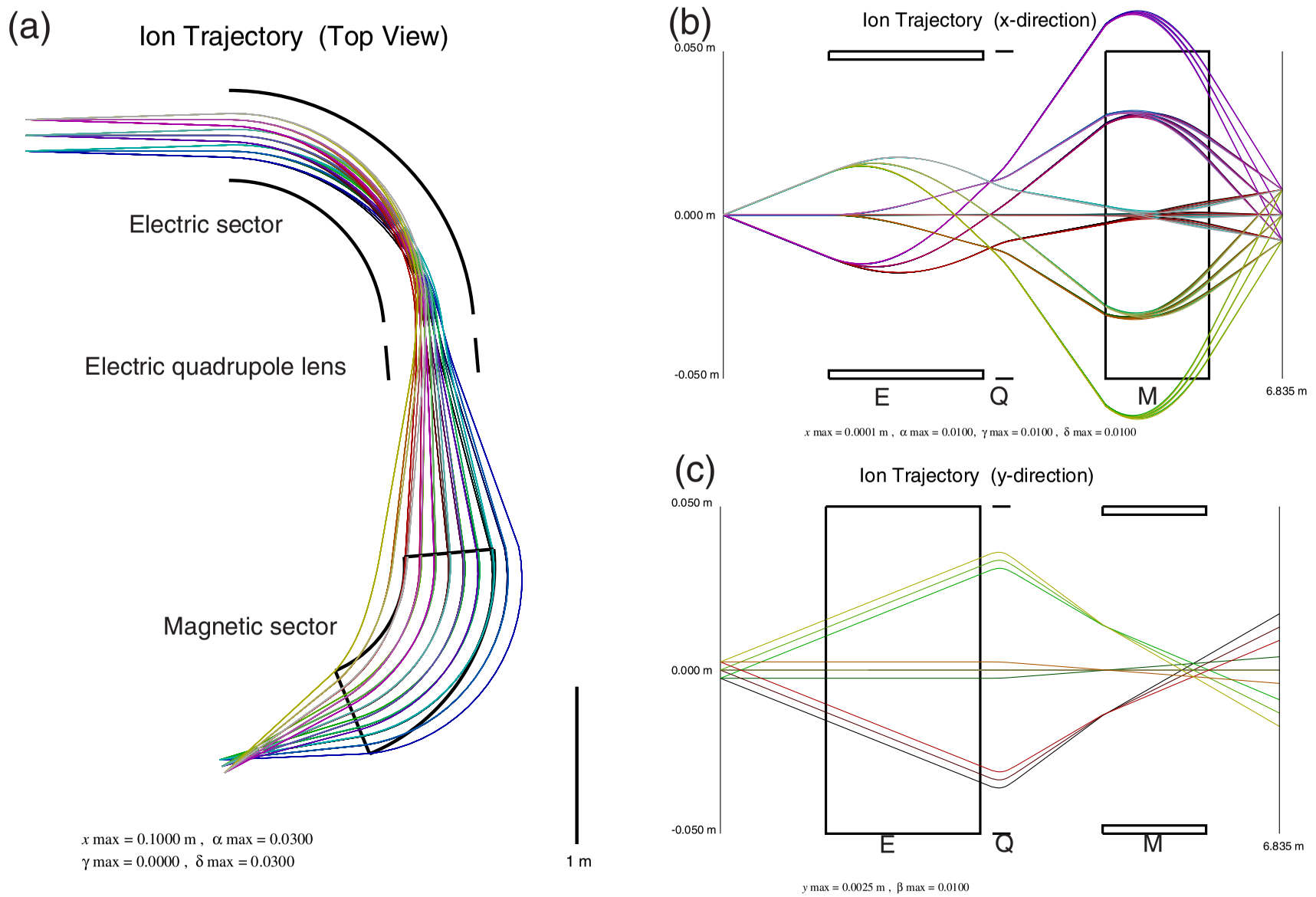

Fig. 2-3 Ion trajectories of the beam envelope mode for the CQH-type mass spectrometer. (a)top view, (b)x-direction, (c)y-direction.

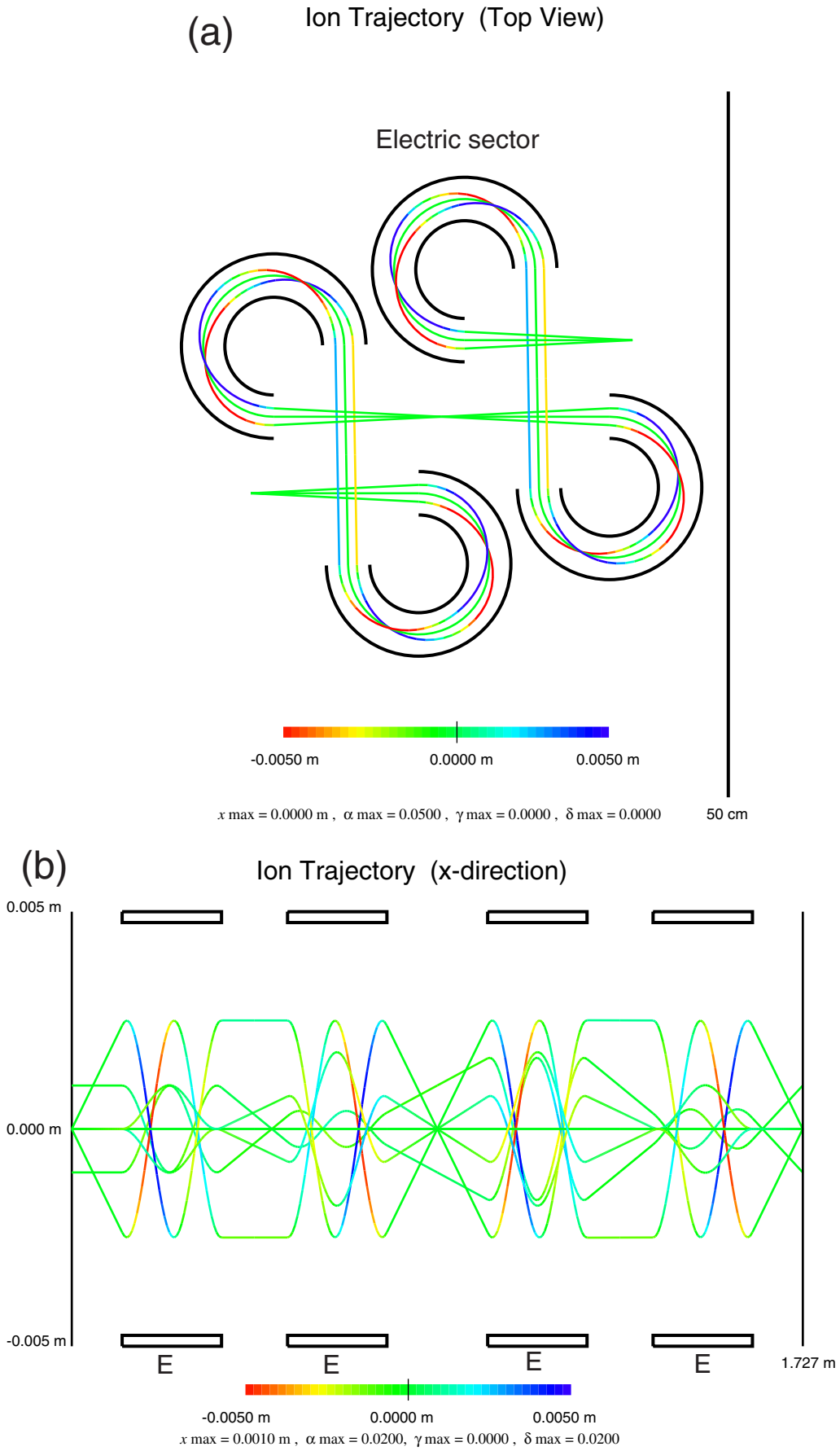

Fig. 2-4 Ion trajectories of the flight time deviation mode for 4 sector TOF mass spectrometer. (a)top view, (b)x-direction.

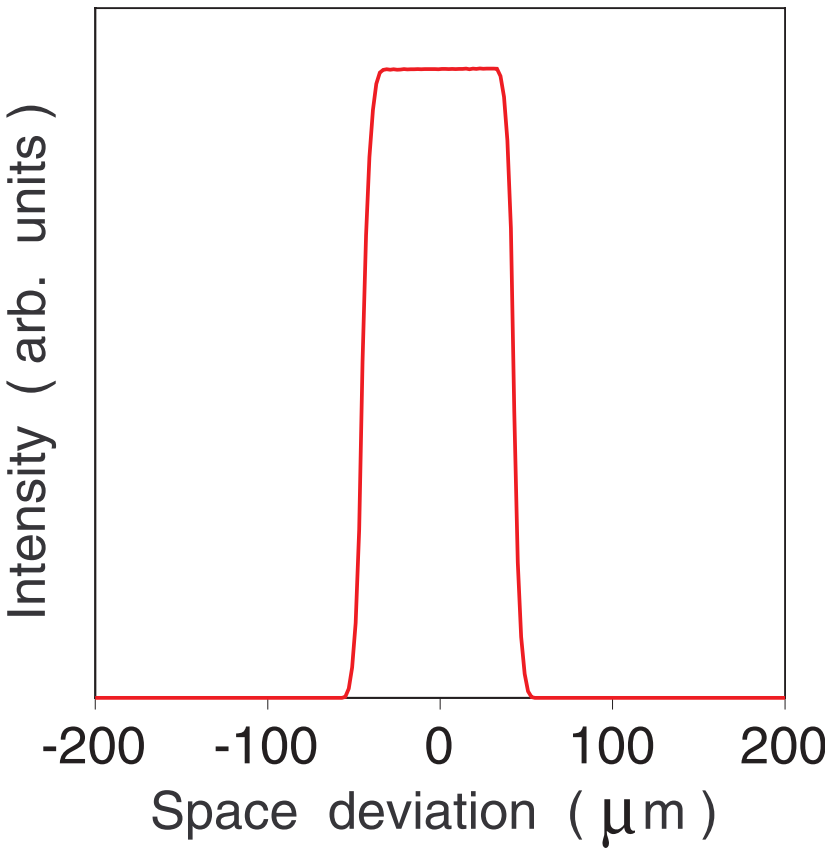

Fig. 2-5 Spatial image shape for the CQH-type mass spectrometer. $x$max = 0.0001 m, αmax = 0.01 rad, δmax = 0.01, $y$max = 0.0025 m, βmax = 0.01 rad. Resolution (10% Valley) = 8244.

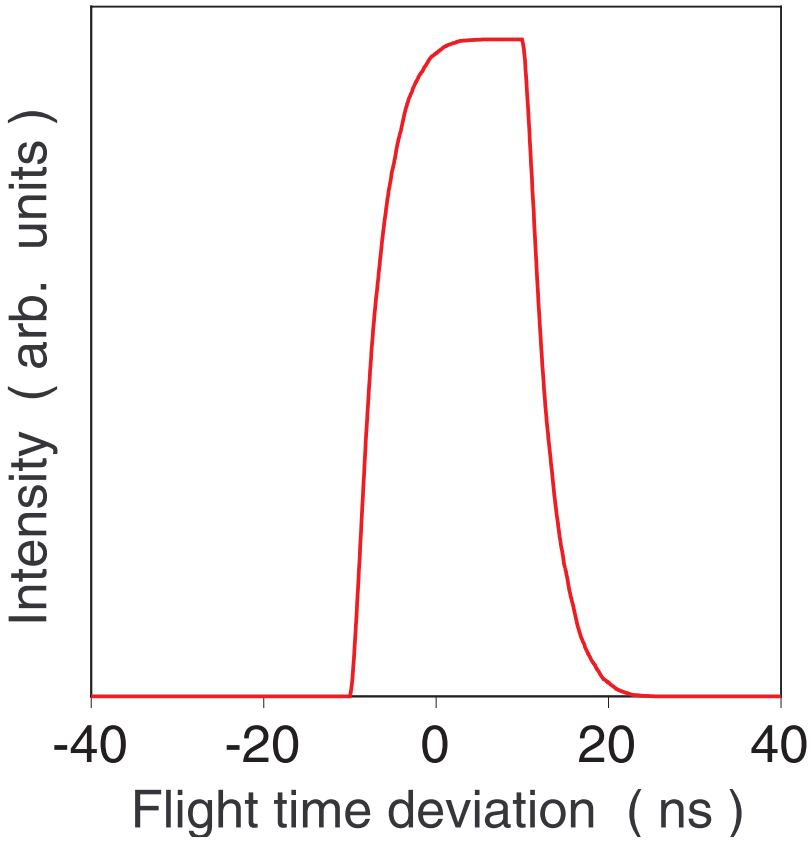

Fig. 2-6 Flight-time image shape for 4-sector TOF mass spectrometer. Pulse width = 20 ns, $x$max = 0.0005 m, αmax = 0.01 rad, δmax = 0.01, $y$max = 0.0025 m, βmax = 0.01 rad, velocity of reference particle = 3.106×10^4 m/s (for example m/z = 100, accelerating voltage = 500 V), Resolution (FWHM) = 1395.

2.3.3 Calculation of 'isochronous plane'

'TRIO-DRAW' can calculate the 'isochronous plane' which shows positions of arbitrary ions having a variety of initial conditions when the reference particle arrives at the detector point. An example of the isochronous plane for the 4-sector TOF mass spectrometer is shown in Fig. 2-7. This figure implies that we can achieve high sensitivity without loosing mass resolution if the detector surface is made to fit this isochronous plane.

2.4 Conclusion

The computer program 'TRIO-DRAW' has been developed, which supports the following features: (i) overall characteristics of an ion optical system can be simulated and displayed, (ii) flight-time information can be obtained in the visual form. This program is very helpful to design a high performance TOF mass spectrometer.

References

[2-1] K. L. Brown et al., *SLAC Report*, **No. 91** (1970).

[2-2] T. Matsuo, H. Matsuda, Y. Fujita and H. Wollnik, *Mass Spectroscopy (Japan)*, **24** (1975), 19.

[2-3] H. Wollnik, J. Brezina, M. Berz and W. Wendel, *GSI-Report THD-26* (1984), 679.

[2-4] T. Matsuo, T. Sakurai, H. Matsuda, H. Nakabushi., *Mass Spectroscopy (Japan)*, **33** (1985), 261.

[2-5] M. Ishihara and T. Matsuo, *Nucl. Instrum. Methods B*, **70** (1992), 445-450.

[2-6] T. Sakurai and T. Matsuo, *J. Mass Spectrom. Sco. Jpn.*, **46** (1998), 437.

[2-7] T. Sakurai, prepareing to the submission.

[2-8] H. Matsuda, *Int. J. Mass Spectrom. Ion Phys.*, **14** (1974), 219.

[2-9] T. Sakurai et. al., *Int. J. Mass Spectrom. Ion Process.*, **66** (1985), 283.

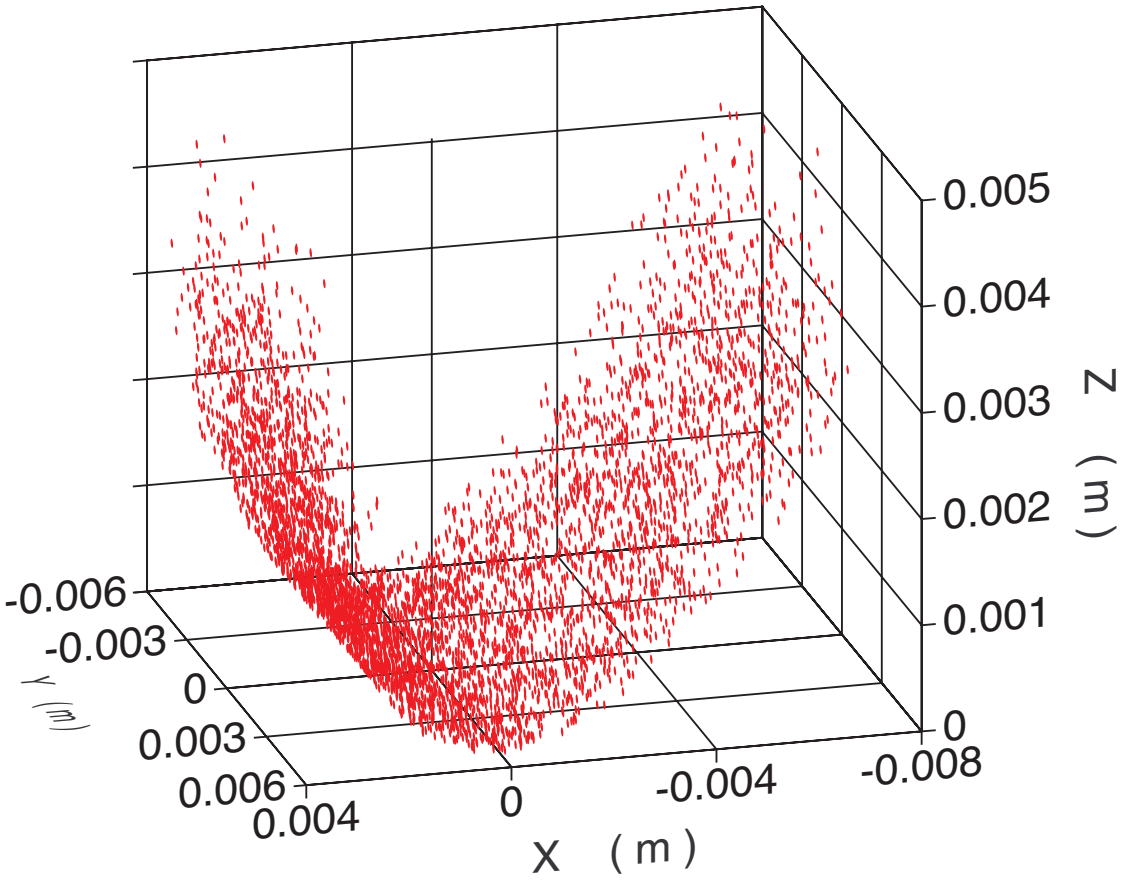

Fig. 2-7 Isochronous plane for 4 sector TOF mass spectrometer. $x$max = 0.005 m, αmax = 0.01 rad, dmax = 0.01, $y$max = 0.005 m, βmax = 0.01 rad.

III. Perfect Space and Time Focusing Ion Optics for Multi-turn Time of Flight Mass Spectrometers

3.1 Introduction

A major limitation of TOF/MS has been its relatively poor mass resolution. Some methods to improve the mass resolution were described in Chapter I in detail. The mass resolution of a TOF mass spectrometer is proportional to the path length. Therefore, it will be necessary to use a multi-turn optical system in order to achieve the desired resolution within the physical limitations imposed by the spacecraft. However, if a multi-turn optical system does not satisfy the 'perfect focusing condition', ion beam diverges. Therefore, the mass resolution and the ion transmission decrease with an increasing number of turns around the system. To avoid this problem, the ion optical systems should satisfy the 'perfect focusing condition.'

The ion optics of a multi-turn TOF mass spectrometer consisting of electric sector fields has been studied [3-1, 3-2]. In this study, it was found that by introducing symmetry in the arrangement of sectors, multiple time and space focusing conditions are easily satisfied [3-2, 3-3]. Using this principle, the ion optical systems for a multi-turn TOF mass spectrometer have been found. In this chapter, the general principle of the perfect space and time focusing conditions for a multi-turn TOF mass spectrometer are discussed. New ion optical systems satisfying the 'perfect focusing' are proposed.

3.2 Ideal perfect space and time focusing condition

In this thesis, the ideal ion optical systems for a multi-turn TOF mass spectrometer are searched, where ions should return to the point of origin in the system; in other words, the absolute values of the position and angle at the detector plane should be the same of those at initial values both in the horizontal and the vertical planes. Such conditions can be expressed using the transfer matrix as

$$R = \begin{pmatrix} \pm 1 & \underline{0} & 0 & 0 & 0 & \underline{0} & 0 \\ \underline{0} & \pm 1 & 0 & 0 & 0 & \underline{0} & 0 \\ 0 & 0 & \pm 1 & \underline{0} & 0 & 0 & 0 \\ 0 & 0 & \underline{0} & \pm 1 & 0 & 0 & 0 \\ 0 & 0 & 0 & 0 & 1 & 0 & 0 \\ 0 & 0 & 0 & 0 & 0 & 1 & 0 \\ \underline{0} & \underline{0} & 0 & 0 & R(l \mid \gamma) & \underline{0} & 1 \end{pmatrix} \qquad (3\text{-}1)$$

It should be noted here that the character $\underline{0}$ (zero with underline) means the matrix element which should be forced to be zero, while 0 (zero without underline) means always zero from the definition. In the present works, since only electric sectors or electric quadrupole lenses are used, the conditions $R(x \mid \gamma) = 0$ and $R(\alpha \mid \gamma) = 0$ are always fulfilled.

Angular focusing ($R(x \mid \alpha) = 0$), energy focusing ($R(x \mid \delta) = 0$) and the condition $R(x \mid x) = \pm 1$ for lateral magnification are required to conserve the absolute value of the lateral deviation ($|x| = |x_0|$) in the horizontal direction. In the same manner, angular focusing ($R(y \mid \beta) = 0$) and the condition $R(y \mid y) = \pm 1$ for lateral magnification are required to conserve the absolute value of the lateral deviation ($|y| = |y_0|$) in the vertical direction. Moreover $R(\alpha \mid x) = R(\alpha \mid \delta) = 0$ and $R(\alpha \mid \alpha) = \pm 1$ are required to conserve the absolute value of the angle ($|\alpha| = |\alpha_0|$) in the horizontal direction and $R(\beta \mid y) = 0$ and $R(\beta \mid \beta) = \pm 1$ are required to conserve the absolute value of the angle ($|\beta| = |\beta_0|$) in the vertical direction. In the case of TOF mass spectrometer, triple time focusing $R(l \mid x) = R(l \mid \alpha) = R(l \mid \delta) = 0$ is also required. Accordingly, we require the "nine-fold focusing", i.e. the nine $\underline{0}$ elements should be zero to satisfy the perfect space and time focusing. The final goal is to find the ion optical systems whose overall transfer matrix becomes as above. Here, we named the system whose magnification is (+1) as normal image type (N-type) and the (-1) system as inverse image type (I-type).

In our experience, it is easy to find the solution of $R(x \mid x) = \pm 1$ and $R(x \mid \alpha) = 0$, but it is very difficult to satisfy these parameters with $R(\alpha \mid x) = 0$ simultaneously. In order to overcome this difficulty, symmetrical geometries were introduced. The detailed process how to find such solutions will be expressed.

3.3 The symmetrical geometry systems consisting of two units

3.3.1 The transfer matrices of symmetrical geometry systems

The symmetrical arrangement is indispensable because the multiple focusing can be easily satisfied in few conditions [3-3]. In this chapter, only symmetrical systems consisting of electric fields will be treated.

Generally, a symmetrical system consists of two basic units. A system consisting of four units, for example, can be understood as a doubly symmetric system of two units. Therefore, it may be worthwhile to explain more details about the characteristics of a symmetrical arrangement consisting of two units.

Here, the matrix A as a basic unit is defined, which is usually obtained by the multiplication of the matrices of drift spaces, electric sectors or electric quadrupole lenses. The point-symmetric matrix A^{*} of A and the plane-symmetric matrix A^{-} from the matrix A can be derived based on the concept of inverse matrix [3-3].

$$A^{*} = \begin{pmatrix} A(\alpha|\alpha) & A(x|\alpha) & 0 & 0 & 0 & -A(x|\alpha)A(\alpha|\delta)+A(x|\delta)A(\alpha|\alpha) & 0 \\ A(\alpha|x) & A(x|x) & 0 & 0 & 0 & -A(x|x)A(\alpha|\delta)+A(x|\delta)A(\alpha|x) & 0 \\ 0 & 0 & A(\beta|\beta) & A(y|\beta) & 0 & 0 & 0 \\ 0 & 0 & A(\beta|y) & A(y|y) & 0 & 0 & 0 \\ 0 & 0 & 0 & 0 & 1 & 0 & 0 \\ 0 & 0 & 0 & 0 & 0 & 1 & 0 \\ -A(\alpha|\alpha)A(l|x)+A(\alpha|x)A(l|\alpha) & -A(x|\alpha)A(l|x)+A(x|x)A(l|\alpha) & 0 & 0 & A(l|\gamma) & \begin{matrix} A(l|\delta)+\left[A(x|\alpha)A(\alpha|\delta)-A(x|\delta)A(\alpha|\alpha)\right]A(l|x) \\ -\left[A(x|x)A(\alpha|\delta)-A(x|\delta)A(\alpha|x)\right]A(l|\alpha) \end{matrix} & 1 \end{pmatrix} \quad (3\text{-}2)$$

$$A^{-} = \begin{pmatrix} A(\alpha|\alpha) & A(x|\alpha) & 0 & 0 & 0 & A(x|\alpha)A(\alpha|\delta)-A(x|\delta)A(\alpha|\alpha) & 0 \\ A(\alpha|x) & A(x|x) & 0 & 0 & 0 & A(x|x)A(\alpha|\delta)-A(x|\delta)A(\alpha|x) & 0 \\ 0 & 0 & A(\beta|\beta) & A(y|\beta) & 0 & 0 & 0 \\ 0 & 0 & A(\beta|y) & A(y|y) & 0 & 0 & 0 \\ 0 & 0 & 0 & 0 & 1 & 0 & 0 \\ 0 & 0 & 0 & 0 & 0 & 1 & 0 \\ A(\alpha|\alpha)A(l|x)-A(\alpha|x)A(l|\alpha) & A(x|\alpha)A(l|x)-A(x|x)A(l|\alpha) & 0 & 0 & A(l|\gamma) & \begin{matrix} A(l|\delta)+\left[A(x|\alpha)A(\alpha|\delta)-A(x|\delta)A(\alpha|\alpha)\right]A(l|x) \\ -\left[A(x|x)A(\alpha|\delta)-A(x|\delta)A(\alpha|x)\right]A(l|\alpha) \end{matrix} & 1 \end{pmatrix} \quad (3\text{-}3)$$

The total transfer matrix of a point symmetric system, $A^{*}A$, can be obtained as

$$A^{*}A$$

$$= \begin{pmatrix} A(x|x)A(\alpha|\alpha)+A(x|\alpha)A(\alpha|x) & 2A(x|\alpha)A(\alpha|\alpha) & 0 & 0 & 0 & 2A(x|\delta)A(\alpha|\alpha) & 0 \\ 2A(x|x)A(\alpha|x) & A(x|x)A(\alpha|\alpha)+A(x|\alpha)A(\alpha|x) & 0 & 0 & 0 & 2A(x|\delta)A(\alpha|x) & 0 \\ 0 & 0 & A(y|y)A(\beta|\beta)+A(y|\beta)A(\beta|y) & 2A(y|\beta)A(\beta|\beta) & 0 & 0 & 0 \\ 0 & 0 & 2A(y|y)A(\beta|y) & A(y|y)A(\beta|\beta)+A(y|\beta)A(\beta|y) & 0 & 0 & 0 \\ 0 & 0 & 0 & 0 & 1 & 0 & 0 \\ 0 & 0 & 0 & 0 & 0 & 1 & 0 \\ -4A(x|\delta)A(\alpha|x) & -4A(x|\delta)A(\alpha|\alpha) & 0 & 0 & 2A(l|\gamma) & 2A(l|\delta)-4A(x|\delta)A(\alpha|\delta) & 1 \end{pmatrix} \quad (3\text{-}4)$$

$$\equiv \begin{pmatrix} [A^{*}A](x|x) & [A^{*}A](x|\alpha) & 0 & 0 & [A^{*}A](x|\gamma) & [A^{*}A](x|\delta) & 0 \\ [A^{*}A](\alpha|x) & [A^{*}A](\alpha|\alpha) & 0 & 0 & [A^{*}A](\alpha|\gamma) & [A^{*}A](\alpha|\delta) & 0 \\ 0 & 0 & [A^{*}A](y|y) & [A^{*}A](y|\beta) & 0 & 0 & 0 \\ 0 & 0 & [A^{*}A](\beta|y) & [A^{*}A](\beta|\beta) & 0 & 0 & 0 \\ 0 & 0 & 0 & 0 & 1 & 0 & 0 \\ 0 & 0 & 0 & 0 & 0 & 1 & 0 \\ [A^{*}A](l|x) & [A^{*}A](l|\alpha) & 0 & 0 & [A^{*}A](l|\gamma) & [A^{*}A](l|\delta) & 1 \end{pmatrix}$$

and in the same manner, that of a plane symmetric system, $A^{-}A$, can be obtained as

$$A^{-}A$$

$$= \begin{pmatrix} A(x|x)A(\alpha|\alpha)+A(x|\alpha)A(\alpha|x) & 2A(x|\alpha)A(\alpha|\alpha) & 0 & 0 & 0 & 2A(x|\alpha)A(\alpha|\delta) & 0 \\ 2A(x|x)A(\alpha|x) & A(x|x)A(\alpha|\alpha)+A(x|\alpha)A(\alpha|x) & 0 & 0 & 0 & 2A(x|x)A(\alpha|\delta) & 0 \\ 0 & 0 & A(y|y)A(\beta|\beta)+A(y|\beta)A(\beta|\beta) & 2A(y|\beta)A(\beta|\beta) & 0 & 0 & 0 \\ 0 & 0 & 2A(y|y)A(\beta|y) & A(y|y)A(\beta|\beta)+A(y|\beta)A(\beta|\beta) & 0 & 0 & 0 \\ 0 & 0 & 0 & 0 & 1 & 0 & 0 \\ 0 & 0 & 0 & 0 & 0 & 1 & 0 \\ 4A(x|x)A(\alpha|\delta) & 4A(x|\alpha)A(\alpha|\delta) & 0 & 0 & 2A(l|\gamma) & 2A(l|\delta)+4A(x|\delta)A(\alpha|\delta) & 1 \end{pmatrix} \quad (3\text{-}5)$$

$$\equiv \begin{pmatrix} [A^{-}A](x|x) & [A^{-}A](x|\alpha) & 0 & 0 & [A^{-}A](x|\gamma) & [A^{-}A](x|\delta) & 0 \\ [A^{-}A](\alpha|x) & [A^{-}A](\alpha|\alpha) & 0 & 0 & [A^{-}A](\alpha|\gamma) & [A^{-}A](\alpha|\delta) & 0 \\ 0 & 0 & [A^{-}A](y|y) & [A^{-}A](y|\beta) & 0 & 0 & 0 \\ 0 & 0 & [A^{-}A](\beta|y) & [A^{-}A](\beta|\beta) & 0 & 0 & 0 \\ 0 & 0 & 0 & 0 & 1 & 0 & 0 \\ 0 & 0 & 0 & 0 & 0 & 1 & 0 \\ [A^{-}A](l|x) & [A^{-}A](l|\alpha) & 0 & 0 & [A^{-}A](l|\gamma) & [A^{-}A](l|\delta) & 1 \end{pmatrix}$$

Where the following relationship [3-4] between the matrix elements of space and time terms are effectively used to simplify the matrix elements.

$$\begin{aligned} A(l \mid x) &= 2\left[A(x \mid x)\, A(\alpha \mid \delta) - A(x \mid \delta)\, A(\alpha \mid x)\right] \\ A(l \mid \alpha) &= 2\left[A(x \mid \alpha)\, A(\alpha \mid \delta) - A(x \mid \delta)\, A(\alpha \mid \alpha)\right] \end{aligned} \tag{3-6}$$

In addition, the conservation of phase-space volume

$$\begin{aligned} A(x \mid x)\, A(\alpha \mid \alpha) - A(x \mid \alpha)\, A(\alpha \mid x) &= 1 \\ A(y \mid y)\, A(\beta \mid \beta) - A(y \mid \beta)\, A(\beta \mid y) &= 1 \end{aligned} \tag{3-7}$$

are also effectively used.

3.3.2 The perfect space focusing condition

One can easily find from Eqns. (3-4), (3-5) that the perfect space focusing conditions in the horizontal plane are expressed as

$$\begin{aligned} &\left[A^{*} A\right](x \mid x) = \left[A^{-} A\right](x \mid x) = A(x \mid x)\, A(\alpha \mid \alpha) + A(x \mid \alpha) A(\alpha \mid x) = \pm 1 \\ &\left[A^{*} A\right](x \mid \alpha) = \left[A^{-} A\right](x \mid \alpha) = 2\, A(x \mid \alpha)\, A(\alpha \mid \alpha) = 0 \\ &\left[A^{*} A\right](\alpha \mid x) = \left[A^{-} A\right](\alpha \mid x) = 2\, A(x \mid x)\, A(\alpha \mid x) = 0 \\ &\left[A^{*} A\right](\alpha \mid \alpha) = \left[A^{-} A\right](\alpha \mid \alpha) = A(x \mid x)\, A(\alpha \mid \alpha) + A(x \mid \alpha) A(\alpha \mid x) = \pm 1 \\ &\left[A^{*} A\right](x \mid \delta) = 2\, A(x \mid \delta)\, A(\alpha \mid \alpha) = 0 \\ &\left[A^{*} A\right](\alpha \mid \delta) = 2\, A(x \mid \delta)\, A(\alpha \mid x) = 0 \\ &\left[A^{-} A\right](x \mid \delta) = 2\, A(x \mid \alpha)\, A(\alpha \mid \delta) = 0 \\ &\left[A^{-} A\right](\alpha \mid \delta) = 2\, A(x \mid x)\, A(\alpha \mid \delta) = 0 \end{aligned} \tag{3-8.a}$$

In the vertical direction, the similar conditions should be satisfied independently.

$$\begin{aligned} &\left[A^{*} A\right](y \mid y) = \left[A^{-} A\right](y \mid y) = A(y \mid y)\, A(\beta \mid \beta) + A(y \mid \beta)\, A(\beta \mid y) = \pm 1 \\ &\left[A^{*} A\right](y \mid \beta) = \left[A^{-} A\right](y \mid \beta) = 2\, A(y \mid \beta)\, A(\beta \mid \beta) = 0 \\ &\left[A^{*} A\right](\beta \mid y) = \left[A^{-} A\right](\beta \mid y) = 2\, A(y \mid y)\, A(\beta \mid y) = 0 \\ &\left[A^{*} A\right](\beta \mid \beta) = \left[A^{-} A\right](\beta \mid \beta) = A(y \mid y)\, A(\beta \mid \beta) + A(y \mid \beta)\, A(\beta \mid y) = \pm 1 \end{aligned} \tag{3-8.b}$$

Accordingly, the four cases in Table 3-1 (a) are the only solutions to fulfill the perfect focusing conditions for the symmetric system. One can understand that there are two cases $A\ (x \mid \alpha) = 0$ or $A\ (\alpha \mid \alpha) = 0$ to satisfy Eqn. (3-8.a-2). In the case $A(x \mid$

$\alpha) = 0$, $A(x \mid x)$ is not zero; otherwise Eqn. (3-7) is not satisfied. As a consequence, $A(\alpha \mid x)$ should be zero to satisfy Eqn. (3-8.a-3). In the same manner, if $A\ (\alpha \mid \alpha) = 0$ in Eqn. (3-8.a-2), $A(x \mid x)$ should be zero.

It can be understood that these types of solutions correspond to the focusing status at the intermediate point, namely, whether ion beams are focussed ($A\ (x \mid \alpha) = 0$) or parallel ($A\ (\alpha \mid \alpha) = 0$). These differences by using the symbol "●" for focusing and "○" for parallel at the intermediate point are expressed. For example, the type of "point symmetric system with intermediate image" can be expressed as "A^{*} ● A" and the type of "plane symmetric system without intermediate image" where the ion beams are parallel at the intermediate point can be expressed as "A^{-} ○ A".

Similar requirements should be satisfied in the vertical direction as shown in Table 3-1 (b). Since there is no energy dispersion in the vertical direction, the required conditions of a point symmetric system are identical to those of a plane symmetric system.

Now, the question becomes how to find the system which satisfies the condition given in Table 3-1. To our knowledge, it is very difficult to find the case of normal image (N-type) : $A(x \mid \alpha) = A(\alpha \mid x) = 0$. On the other hand, the solution of the case of inverse image (I-type) : $A(x \mid x) = A(\alpha \mid \alpha) = 0$ can be easily found by adding to the drift space before and after an arbitrary element and choosing suitable length for each drift space. These processes can be easily understood the following transfer matrix multiplication.

$$
\begin{aligned}
A &= \begin{bmatrix} 1 & L_2 & 0 \\ 0 & 1 & 0 \\ 0 & 0 & 1 \end{bmatrix} \begin{bmatrix} B(x \mid x) & B(x \mid \alpha) & B(x \mid \delta) \\ B(\alpha \mid x) & B(\alpha \mid \alpha) & B(\alpha \mid \delta) \\ 0 & 0 & 1 \end{bmatrix} \begin{bmatrix} 1 & L_1 & 0 \\ 0 & 1 & 0 \\ 0 & 0 & 1 \end{bmatrix} \\
&= \begin{bmatrix} B(x \mid x) + B(\alpha \mid x)\, L_2 & B(x \mid x)\, L_1 + B(x \mid \alpha) + \left[B(\alpha \mid x)\, L_1 + B(\alpha \mid \alpha) \right] L_2 & B(x \mid \delta) + B(\alpha \mid \delta)\, L_2 \\ B(\alpha \mid x) & B(\alpha \mid x)\, L_1 + B(\alpha \mid \alpha) & B(\alpha \mid \delta) \\ 0 & 0 & 1 \end{bmatrix}
\end{aligned}
\tag{3-9}
$$

Here, the matrix B is the transfer matrix of an arbitrary element. Then, by choosing

Type		Required conditions	Characteristics
Point Symmetry	PX1	$A(x \mid x) = 0,\ A(\alpha \mid \alpha) = 0,$ $A(x \mid \delta) = 0$	A^{*} ○ A I - type 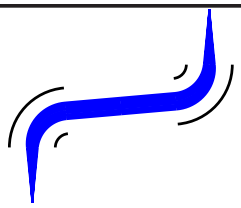
	PX2	$A(x \mid \alpha) = 0,\ A(\alpha \mid x) = 0,$ $A(x \mid \delta) = 0$	A^{*} ● A N - type 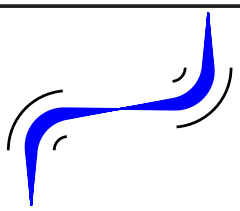
Plane Symmetry	LX1	$A(x \mid x) = 0,\ A(\alpha \mid \alpha) = 0,$ $A(\alpha \mid \delta) = 0$	A^{-} ○ A I - type 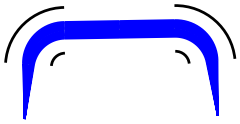
	LX2	$A(x \mid \alpha) = 0,\ A(\alpha \mid x) = 0,$ $A(\alpha \mid \delta) = 0$	A^{-} ● A N - type 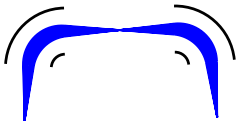

Table 3-1 (a) Four types of solution for the perfect space focusing conditions in the horizontal plane.

Type	Required conditions	Characteristics
Y1	$A(y \mid y) = 0,\ A(\beta \mid \beta) = 0$	A^{s} ○ A I - type
Y2	$A(y \mid \beta) = 0,\ A(\beta \mid y) = 0$	A^{s} ● A N - type

Table 3-1 (b) Two types of solution for the perfect focusing conditions in the vertical plane. The symbol “s” means the symmetries, “ * ” or “ - ”.

the length of drift spaces as $L_1 = -B(\alpha \mid \alpha) / B(\alpha \mid x)$ and $L_2 = -B(x \mid x) / B(\alpha \mid x)$, the condition $A(x \mid x) = A(\alpha \mid \alpha) = 0$ can be satisfied. In contrast, $A(\alpha \mid x) = B(\alpha \mid x)$ is independent of L_1 and L_2. Therefore, it is difficult to satisfy $A(\alpha \mid x) = 0$.

It is not necessary, however, to pursue the solution, $A(x \mid x) = A(\alpha \mid \alpha) = 0$, following the manner described above. It becomes clear that a reasonable solution can be found for even a system of the fixed drift length by choosing a suitable parameters for quadruple lenses or electric sector fields.

3.3.3 The perfect time focusing condition

In an ideal TOF mass spectrometer, all ions of the same mass which leave the ion source slit under the different initial conditions (position, angle and energy) arrive at the detector profile plane simultaneously. Such time focusing condition is expressed from Eqns. (3-4) for a point symmetric system, $A^* A$, as followings.

$$\begin{aligned}
&\left[A^* A\right](l \mid x) = -4\, A(x \mid \delta)\, A(\alpha \mid x) = 0 \\
&\left[A^* A\right](l \mid \alpha) = -4\, A(x \mid \delta)\, A(\alpha \mid \alpha) = 0 \\
&\left[A^* A\right](l \mid \delta) = 2\, A(l \mid \delta) - 4\, A(x \mid \delta)\, A(\alpha \mid \delta) = 0
\end{aligned} \qquad \text{(3-10.a)}$$

Since the condition $A(\alpha \mid x) = A\ (\alpha \mid \alpha) = 0$ is not permitted from Eqn. (3-7), the requirements for the matrix A of the basic units are $A(x \mid \delta) = A(l \mid \delta) = 0$ for a point symmetric system to satisfy the time focusing condition of Eqns. (3-10.a).

For a plane symmetric system, the time focusing condition is expressed as follows from Eqns. (3-5).

$$\begin{aligned}
&\left[A^- A\right](l \mid x) = 4\, A(x \mid x)\, A(\alpha \mid \delta) = 0 \\
&\left[A^- A\right](l \mid \alpha) = 4\, A(x \mid \alpha)\, A(\alpha \mid \delta) = 0 \\
&\left[A^- A\right](l \mid \delta) = 2\, A(l \mid \delta) + 4\, A(x \mid \delta)\, A(\alpha \mid \delta) = 0
\end{aligned} \qquad \text{(3-10.b)}$$

Similarly, since $A(x \mid x) = A\ (x \mid \alpha) = 0$ is not permitted, the requirements for the matrix A of the basic units are $A(\alpha \mid \delta) = A(l \mid \delta) = 0$ for a point symmetric system to satisfy the time focusing condition of Eqns. (3-10.b).

3.3.4 The final form of requirements on the matrix to satisfy the perfect focusing

In the horizontal direction, the final requirements for the matrix A of the basic unit can be summarized in the Table 3-2. In the vertical direction, there is no time term in the first order approximation. Therefore, the final requirements are the same as Table 3-1(b).

3.4 The multi-turn condition

In the previous section, perfect focusing conditions are derived. In addition to these, we have to discuss the geometrical conditions for multi-turn systems, namely the criterion necessary to close the ion optical orbit. These conditions can be expressed in the following way.

3.4.1 Superposition of the entrance position and the exit position

The coordinate of the exit position (x_d, y_d) should coincide with that of the entrance position (x_s, y_s). In principle, the coordinate (x_d, y_d) can be simply calculated after giving the physical parameters of individual optical elements, such as drift length, radius and deflection angle of electrode so on. It may be easier to introduce a simpler constraints depending on the ion optical configuration such as an oval type or a figure-eight type, etc.

3.4.2 Sum of deflection angle rule

In order to connect smoothly to the second turn, the directions of the main optical axis at the entrance and the exit position should coincide with each other. The angle between the direction of the main optical axis at the entrance position and at the exit position can be expressed as a function of only the deflection angles of sectors. Consequently the additional condition to close the orbit can be given explicitly

Type		Required conditions	Characteristics
Point Symmetry	PX1	$A(x \mid x) = 0,\ A(\alpha \mid \alpha) = 0,$ $A(x \mid \delta) = 0,\ A(l \mid \delta) = 0$	A^{*} ○ A I - type
	PX2	$A(x \mid \alpha) = 0,\ A(\alpha \mid x) = 0,$ $A(x \mid \delta) = 0,\ A(l \mid \delta) = 0$	A^{*} ● A N - type
Plane Symmetry	LX1	$A(x \mid x) = 0,\ A(\alpha \mid \alpha) = 0,$ $A(\alpha \mid \delta) = 0,\ A(l \mid \delta) = 0$	A^{-} ○ A I - type
	LX2	$A(x \mid \alpha) = 0,\ A(\alpha \mid x) = 0,$ $A(\alpha \mid \delta) = 0,\ A(l \mid \delta) = 0$	A^{-} ● A N - type

Table 3-2 The perfect focusing conditions of symmetric system consisting of two units in the horizontal direction.

as

$$W_1 + W_2 + ... + W_m = 2\,n\,\pi \quad (n = 0, 1, 2, \cdots) \tag{3-11}$$

where W_i is the deflection angle of the sector and it should be negative value when the deflection of the sector is reversed.

3.5 The double symmetric systems consisting of four units

Any symmetric systems consisting of two basic units which satisfy the perfect focusing has not yet been found up to present. In the next step, the "doubly symmetric geometry" was introduced, namely four units are combined in such way that two units times two units. The purposes are (1) to find a perfect focusing geometry consisting of four units, (2) to find a perfect focusing geometry in the vertical direction as well, and (3) to simplify achievement of a closed trajectory.

Generally, there are four types of combinations as:

(a) Point symmetric system of point symmetric system : $(A^{*}\,A)^{*}\,(A^{*}\,A)$

(b) Plane symmetric system of point symmetric system : $(A^{*}\,A)^{-}\,(A^{*}\,A)$

(c) Point symmetric system of plane symmetric system : $(A^{-}\,A)^{*}\,(A^{-}\,A)$

(d) Plane symmetric system of plane symmetric system : $(A^{-}\,A)^{-}\,(A^{-}\,A)$

The geometries of each of these combinations are showed in Fig. 3-1. In the following sections, the perfect focusing conditions of each system are described.

3.5.1 Point symmetry of point symmetric system : $(A^{*}\,A)^{*}\,(A^{*}\,A)$

The overall transfer matrix can be expressed by the elements of the transfer matrix A (first one fourth) as:

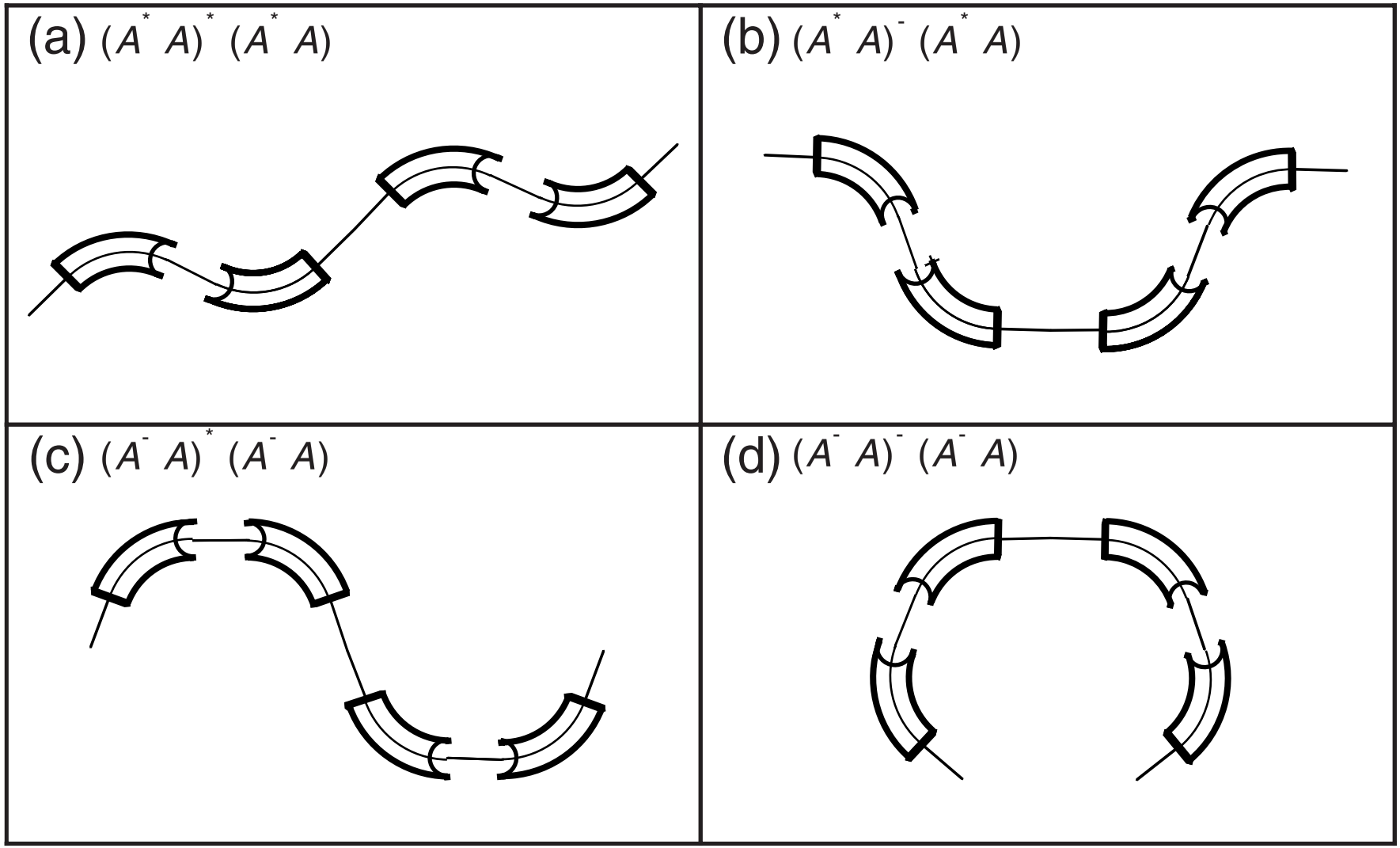

Fig. 3-1 Four geometrical patterns of symmetric systems consisting of four electric sectors.

$$\left(A^{*}A\right)^{*}\left(A^{*}A\right) \tag{3-12}$$

$$= \begin{bmatrix}
8A(x|x)A(x|\alpha)A(\alpha|x)A(\alpha|\alpha)+1 & 4A(x|\alpha)A(\alpha|\alpha)\left(2A(x|x)A(\alpha|\alpha)-1\right) & 0 & 0 & 0 & 4A(x|\delta)A(\alpha|\alpha)\left(2A(x|x)A(\alpha|\alpha)-1\right) & 0 \\
4A(x|x)A(\alpha|x)\left(2A(x|x)A(\alpha|\alpha)-1\right) & 8A(x|x)A(x|\alpha)A(\alpha|x)A(\alpha|\alpha)+1 & 0 & 0 & 0 & 8A(x|x)A(x|\delta)A(\alpha|x)A(\alpha|\alpha) & 0 \\
0 & 0 & 8A(y|y)A(y|\beta)A(\beta|y)A(\beta|\beta)+1 & 4A(y|\beta)A(\beta|\beta)\left(2A(y|y)A(\beta|\beta)-1\right) & 0 & 0 & 0 \\
0 & 0 & 4A(y|y)A(\beta|y)\left(2A(y|y)A(\beta|\beta)-1\right) & 8A(y|y)A(y|\beta)A(\beta|y)A(\beta|\beta)+1 & 0 & 0 & 0 \\
0 & 0 & 0 & 0 & 1 & 0 & 0 \\
0 & 0 & 0 & 0 & 0 & 1 & 0 \\
-16A(x|x)A(x|\delta)A(\alpha|x)A(\alpha|\alpha) & -8A(x|\delta)A(\alpha|\alpha)\left(2A(x|x)A(\alpha|\alpha)-1\right) & 0 & 0 & 4A(l|\gamma) & 4A(l|\delta)-8A(x|\delta)\left(A(\alpha|\delta)+2A(x|\delta)A(\alpha|x)A(\alpha|\alpha)\right) & 1
\end{bmatrix}$$

The perfect focusing conditions are

$$\begin{aligned}
&\left[\left(A^{*}A\right)^{*}\left(A^{*}A\right)\right](x|x) = 8\,A(x|x)\,A(x|\alpha)\,A(\alpha|x)\,A(\alpha|\alpha)+1 = \pm 1 \\
&\left[\left(A^{*}A\right)^{*}\left(A^{*}A\right)\right](x|\alpha) = 4\,A(x|\alpha)\,A(\alpha|\alpha)\left(2\,A(x|x)\,A(\alpha|\alpha)-1\right) = 0 \\
&\left[\left(A^{*}A\right)^{*}\left(A^{*}A\right)\right](x|\delta) = 4\,A(x|\delta)\,A(\alpha|\alpha)\left(2\,A(x|x)\,A(\alpha|\alpha)-1\right) = 0 \\
&\left[\left(A^{*}A\right)^{*}\left(A^{*}A\right)\right](\alpha|x) = 4\,A(x|x)\,A(\alpha|x)\left(2\,A(x|x)\,A(\alpha|\alpha)-1\right) = 0 \\
&\left[\left(A^{*}A\right)^{*}\left(A^{*}A\right)\right](\alpha|\alpha) = 8\,A(x|x)\,A(x|\alpha)\,A(\alpha|x)\,A(\alpha|\alpha)+1 = \pm 1 \\
&\left[\left(A^{*}A\right)^{*}\left(A^{*}A\right)\right](\alpha|\delta) = 8\,A(x|x)\,A(x|\delta)\,A(\alpha|x)\,A(\alpha|\alpha) = 0 \\
&\left[\left(A^{*}A\right)^{*}\left(A^{*}A\right)\right](y|y) = 8\,A(y|y)\,A(y|\beta)\,A(\beta|y)\,A(\beta|\beta)+1 = \pm 1 \\
&\left[\left(A^{*}A\right)^{*}\left(A^{*}A\right)\right](y|\beta) = 4\,A(y|\beta)\,A(\beta|\beta)\left(2\,A(y|y)A(\beta|\beta)-1\right) = 0 \\
&\left[\left(A^{*}A\right)^{*}\left(A^{*}A\right)\right](\beta|y) = 4\,A(y|y)\,A(\beta|y)\ \left(2\,A(y|y)A(\beta|\beta)-1\right) = 0 \\
&\left[\left(A^{*}A\right)^{*}\left(A^{*}A\right)\right](\beta|\beta) = 8\,A(y|y)\,A(y|\beta)\,A(\beta|y)\,A(\beta|\beta)+1 = \pm 1 \\
&\left[\left(A^{*}A\right)^{*}\left(A^{*}A\right)\right](l|x) = -16\,A(x|x)\,A(x|\delta)\,A(\alpha|x)\,A(\alpha|\alpha) = 0 \\
&\left[\left(A^{*}A\right)^{*}\left(A^{*}A\right)\right](l|\alpha) = -8\,A(x|\delta)\,A(\alpha|\alpha)\left(2\,A(x|x)\,A(\alpha|\alpha)-1\right) = 0 \\
&\left[\left(A^{*}A\right)^{*}\left(A^{*}A\right)\right](l|\delta) = 4\,A(l|\delta)-8\,A(x|\delta)\left(A(\alpha|\delta)+2\,A(x|\delta)\,A(\alpha|x)\,A(\alpha|\alpha)\right) = 0
\end{aligned} \tag{3-13}$$

The final required conditions in the horizontal direction are classified in three

cases expressed in Table 3-3. The type of AX1 is similar to the system connecting the type of PX1 in Table 2 with the point symmetric system of PX1. However the number of required conditions to satisfy perfect focusing can be reduced from four to three. The type of AX2 is nothing but the system connecting the type of PX2 with the point symmetric system of PX2. The type of AX3 only appears in the doubly symmetric geometry. Ion beams are parallel at the point after two basic units, while they are not parallel nor focussed after the first units. The number of required conditions can be reduced from four to three.

In the same manner, the final required conditions in the vertical direction are classified in three cases expressed in Table 3-4. In the vertical direction, there is no difference between the point or plane symmetry similar to the symmetric system consisting of two units. Therefore, the same conditions are also required in the following three symmetric systems.

3.5.2 Plane symmetry of point symmetric system : $(A^* A)^- (A^* A)$

The overall transfer matrix of this arrangement is given in the following

$$\left(A^* A\right)^- \left(A^* A\right) \tag{3-14}$$

$$= \begin{bmatrix}
8A(x|x)A(x|\alpha)A(\alpha|x)A(\alpha|\alpha)+1 & 4A(x|\alpha)A(\alpha|\alpha)\left(2A(x|x)A(\alpha|\alpha)-1\right) & 0 & 0 & 0 & 8A(x|\alpha)A(x|\delta)A(\alpha|x)A(\alpha|\alpha) & 0 \\
4A(x|x)A(\alpha|x)\left(2A(x|x)A(\alpha|\alpha)-1\right) & 8A(x|x)A(x|\alpha)A(\alpha|x)A(\alpha|\alpha)+1 & 0 & 0 & 0 & 4A(x|\delta)A(\alpha|x)\left(2A(x|x)A(\alpha|\alpha)-1\right) & 0 \\
0 & 0 & 8A(y|y)A(y|\beta)A(\beta|y)A(\beta|\beta)+1 & 4A(y|\beta)A(\beta|\beta)\left(2A(y|y)A(\beta|\beta)-1\right) & 0 & 0 & 0 \\
0 & 0 & 4A(y|y)A(\beta|y)\left(2A(y|y)A(\beta|\beta)-1\right) & 8A(y|y)A(y|\beta)A(\beta|y)A(\beta|\beta)+1 & 0 & 0 & 0 \\
0 & 0 & 0 & 0 & 1 & 0 & 0 \\
0 & 0 & 0 & 0 & 0 & 1 & 0 \\
8A(x|\delta)A(\alpha|x)\left(2A(x|x)A(\alpha|\alpha)-1\right) & 16A(x|\alpha)A(x|\delta)A(\alpha|x)A(\alpha|\alpha) & 0 & 0 & 4A(l|\gamma)4A(l|\delta)-8A(x|\delta)\left(A(\alpha|\delta)-2A(x|\delta)A(\alpha|x)A(\alpha|\alpha)\right) & 1
\end{bmatrix}$$

The perfect focusing conditions are

Type	Required conditions	Characteristics
AX1	$A(x \mid x) = 0,\ A(\alpha \mid \alpha) = 0,$ $A(l \mid \delta) - 2\,A(x \mid \delta)\,A(\alpha \mid \delta) = 0$	$(A^* \bigcirc A)^* \bullet (A^* \bigcirc A)$ N - type
AX2	$A(x \mid \alpha) = 0,\ A(\alpha \mid x) = 0,$ $A(x \mid \delta) = 0,\ A(l \mid \delta) = 0$	$(A^* \bullet A)^* \bullet (A^* \bullet A)$ N - type
AX3	$2\,A(x \mid x)\,A(\alpha \mid \alpha) - 1 = 0,$ $A(x \mid \delta) = 0,\ A(l \mid \delta) = 0$	$(A^*\,A)^* \bigcirc (A^*\,A)$ I - type

Table 3-3 The perfect focusing conditions of $(A^*\,A)^*\,(A^*\,A)$ geometry in the horizontal direction.

Type	Required conditions	Characteristics
QY1	$A(y \mid y) = 0,\ \ A(\beta \mid \beta) = 0$	$(A^s \bigcirc A)^s \bullet (A^s \bigcirc A)$ N - type
QY2	$A(y \mid \beta) = 0,\ \ A(\beta \mid y) = 0$	$(A^s \bullet A)^s \bullet (A^s \bullet A)$ N - type
QY3	$2\,A(y \mid y)\,A(\beta \mid \beta) - 1 = 0$	$(A^s\,A)^s \bigcirc (A^s\,A)$ I - type

Table 3-4 The perfect focusing conditions of symmetric system consisting of four units in the vertical direction. The symbol “s” means the symmetries, “ * ” or “ - ”.

$$\left[\left(A^{*}A\right)^{-}\left(A^{*}A\right)\right](x\,|\,x) = 8\,A(x\,|\,x)\,A(x\,|\,\alpha)\,A(\alpha\,|\,x)\,A(\alpha\,|\,\alpha) + 1 = \pm 1$$

$$\left[\left(A^{*}A\right)^{-}\left(A^{*}A\right)\right](x\,|\,\alpha) = 4\,A(x\,|\,\alpha)\,A(\alpha\,|\,\alpha)\left(2\,A(x\,|\,x)\,A(\alpha\,|\,\alpha) - 1\right) = 0$$

$$\left[\left(A^{*}A\right)^{-}\left(A^{*}A\right)\right](x\,|\,\delta) = 8\,A(x\,|\,\alpha)\,A(x\,|\,\delta)\,A(\alpha\,|\,x)\,A(\alpha\,|\,\alpha) = 0$$

$$\left[\left(A^{*}A\right)^{-}\left(A^{*}A\right)\right](\alpha\,|\,x) = 4\,A(x\,|\,x)\,A(\alpha\,|\,x)\left(2\,A(x\,|\,x)\,A(\alpha\,|\,\alpha) - 1\right) = 0$$

$$\left[\left(A^{*}A\right)^{-}\left(A^{*}A\right)\right](\alpha\,|\,\alpha) = 8\,A(x\,|\,x)\,A(x\,|\,\alpha)\,A(\alpha\,|\,x)\,A(\alpha\,|\,\alpha) + 1 = \pm 1$$

$$\left[\left(A^{*}A\right)^{-}\left(A^{*}A\right)\right](\alpha\,|\,\delta) = 4\,A(x\,|\,\delta)\,A(\alpha\,|\,x)\left(2\,A(x\,|\,x)\,A(\alpha\,|\,\alpha) - 1\right) = 0$$

$$\left[\left(A^{*}A\right)^{*}\left(A^{*}A\right)\right](y\,|\,y) = 8\,A(y\,|\,y)\,A(y\,|\,\beta)\,A(\beta\,|\,y)\,A(\beta\,|\,\beta) + 1 = \pm 1 \qquad (3\text{-}15)$$

$$\left[\left(A^{*}A\right)^{-}\left(A^{*}A\right)\right](y\,|\,\beta) = 4\,A(y\,|\,\beta)\,A(\beta\,|\,\beta)\left(2\,A(y\,|\,y)\,A(\beta\,|\,\beta) - 1\right) = 0$$

$$\left[\left(A^{*}A\right)^{-}\left(A^{*}A\right)\right](\beta\,|\,y) = 4\,A(y\,|\,y)\,A(\beta\,|\,y)\left(2\,A(y\,|\,y)\,A(\beta\,|\,\beta) - 1\right) = 0$$

$$\left[\left(A^{*}A\right)^{-}\left(A^{*}A\right)\right](\beta\,|\,\beta) = 8\,A(y\,|\,y)\,A(y\,|\,\beta)\,A(\beta\,|\,y)\,A(\beta\,|\,\beta) + 1 = \pm 1$$

$$\left[\left(A^{*}A\right)^{-}\left(A^{*}A\right)\right](l\,|\,x) = 8\,A(x\,|\,\delta)\,A(\alpha\,|\,x)\left(2\,A(x\,|\,x)\,A(\alpha\,|\,\alpha) - 1\right) = 0$$

$$\left[\left(A^{*}A\right)^{-}\left(A^{*}A\right)\right](l\,|\,\alpha) = 16\,A(x\,|\,\alpha)\,A(x\,|\,\delta)\,A(\alpha\,|\,x)\,A(\alpha\,|\,\alpha) = 0$$

$$\left[\left(A^{*}A\right)^{-}\left(A^{*}A\right)\right](l\,|\,\delta) = 4\,A(l\,|\,\delta) - 8\,A(x\,|\,\delta)\left(A(\alpha\,|\,\delta) - 2\,A(x\,|\,\delta)\,A(\alpha\,|\,x)\,A(\alpha\,|\,\alpha)\right) = 0$$

The final required conditions in the horizontal direction are classified in three cases expressed in Table 3-5. The type of BX1 is nothing but the system connecting the type of PX1 in Table 3-2 with the point symmetric system of PX1. The type of BX2 is similar to the system connecting the type of PX2 with the plane symmetric system of PX2. However, the number of required conditions to satisfy perfect focusing can be reduced from four to three. The type of BX3 only appears in the doubly symmetric geometry. Ion beams are parallel at the point after two basic units. The number of required conditions can be reduced from four to three.

The final required conditions in the vertical direction are also classified in three cases expressed in Table 3-4.

Type	Required conditions	Characteristics
BX1	$A(x \mid x) = 0, A(\alpha \mid \alpha) = 0,$ $A(x \mid \delta) = 0, A(l \mid \delta) = 0$	$(A^* \bigcirc A)^- \bullet (A^* \bigcirc A)$ N - type
BX2	$A(x \mid \alpha) = 0, A(\alpha \mid x) = 0,$ $A(l \mid \delta) - 2\,A(x \mid \delta)\,A(\alpha \mid \delta) = 0$	$(A^* \bullet A)^- \bullet (A^* \bullet A)$ N - type
BX3	$2\,A(x \mid x)\,A(\alpha \mid \alpha) - 1 = 0,$ $A(x \mid \delta) = 0, A(l \mid \delta) = 0$	$(A^* A)^- \bigcirc (A^* A)$ I - type

Table 3-5 The perfect focusing conditions of $(A^* A)^- (A^* A)$ geometry in the horizontal direction.

Type	Required conditions	Characteristics
CX1	$A(x \mid x) = 0, A(\alpha \mid \alpha) = 0,$ $A(\alpha \mid \delta) = 0, A(l \mid \delta) = 0$	$(A^- \bigcirc A)^* \bullet (A^- \bigcirc A)$ N - type
CX2	$A(x \mid \alpha) = 0, A(\alpha \mid x) = 0,$ $A(l \mid \delta) + 2\,A(x \mid \delta)\,A(\alpha \mid \delta) = 0$	$(A^- \bullet A)^* \bullet (A^- \bullet A)$ N - type
CX3	$2\,A(x \mid x)\,A(\alpha \mid \alpha) - 1 = 0,$ $A(\alpha \mid \delta) = 0, A(l \mid \delta) = 0$	$(A^- A)^* \bigcirc (A^- A)$ I - type

Table 3-6 The perfect focusing conditions of $(A^- A)^* (A^- A)$ geometry in the horizontal direction.

Type	Required conditions	Characteristics
DX1	$A(x \mid x) = 0, A(\alpha \mid \alpha) = 0,$ $A(l \mid \delta) + 2\,A(x \mid \delta)\,A(\alpha \mid \delta) = 0$	$(A^- \bigcirc A)^- \bullet (A^- \bigcirc A)$ N - type
DX2	$A(x \mid \alpha) = 0, A(\alpha \mid x) = 0,$ $A(\alpha \mid \delta) = 0, A(l \mid \delta) = 0$	$(A^- \bullet A)^- \bullet (A^- \bullet A)$ N - type
DX3	$2\,A(x \mid x)\,A(\alpha \mid \alpha) - 1 = 0,$ $A(\alpha \mid \delta) = 0, A(l \mid \delta) = 0$	$(A^- A)^- \bigcirc (A^- A)$ I - type

Table 3-7 The perfect focusing conditions of $(A^- A)^- (A^- A)$ geometry in the horizontal direction.

3.5.3 Point symmetry of plane symmetric system : $(A^{-}A)^{*}(A^{-}A)$

The overall transfer matrix of this arrangement is given in the following

$$\left(A^{-}A\right)^{*}\left(A^{-}A\right) \tag{3-16}$$

$$= \begin{bmatrix}
8A(x|x)A(x|\alpha)A(\alpha|x)A(\alpha|\alpha)+1 & 4A(x|\alpha)A(\alpha|\alpha)\left(2A(x|x)A(\alpha|\alpha)-1\right) & 0 & 0 & 0 & 4A(x|\alpha)A(\alpha|\delta)\left(2A(x|x)A(\alpha|\alpha)-1\right) & 0 \\
4A(x|x)A(\alpha|x)\left(2A(x|x)A(\alpha|\alpha)-1\right) & 8A(x|x)A(x|\alpha)A(\alpha|x)A(\alpha|\alpha)+1 & 0 & 0 & 0 & 8A(x|x)A(x|\alpha)A(\alpha|x)A(\alpha|\delta) & 0 \\
0 & 0 & 8A(y|y)A(y|\beta)A(\beta|y)A(\beta|\beta)+1 & 4A(y|\beta)A(\beta|\beta)\left(2A(y|y)A(\beta|\beta)-1\right) & 0 & 0 & 0 \\
0 & 0 & 4A(y|y)A(\beta|y)\left(2A(y|y)A(\beta|\beta)-1\right) & 8A(y|y)A(y|\beta)A(\beta|y)A(\beta|\beta)+1 & 0 & 0 & 0 \\
0 & 0 & 0 & 0 & 1 & 0 & 0 \\
0 & 0 & 0 & 0 & 0 & 1 & 0 \\
-16A(x|x)A(x|\alpha)A(\alpha|x)A(\alpha|\delta) & -8A(x|\alpha)A(\alpha|\delta)\left(2A(x|x)A(\alpha|\alpha)-1\right) & 0 & 0 & 4A(l|\gamma)4A(l|\delta)+8A(\alpha|\delta)\left(A(x|\delta)-2A(x|x)A(x|\alpha)A(\alpha|\delta)\right) & 1 &
\end{bmatrix}$$

The perfect focusing conditions are

$$\left[\left(A^{-}A\right)^{*}\left(A^{-}A\right)\right](x\,|\,x) = 8\,A(x\,|\,x)\,A(x\,|\,\alpha)\,A(\alpha\,|\,x)\,A(\alpha\,|\,\alpha) + 1 = \pm 1$$

$$\left[\left(A^{-}A\right)^{*}\left(A^{-}A\right)\right](x\,|\,\alpha) = 4\,A(x\,|\,\alpha)\,A(\alpha\,|\,\alpha)\left(2\,A(x\,|\,x)\,A(\alpha\,|\,\alpha) - 1\right) = 0$$

$$\left[\left(A^{-}A\right)^{*}\left(A^{-}A\right)\right](x\,|\,\delta) = 4\,A(x\,|\,\alpha)\,A(\alpha\,|\,\delta)\left(2\,A(x\,|\,x)\,A(\alpha\,|\,\alpha) - 1\right) = 0$$

$$\left[\left(A^{-}A\right)^{*}\left(A^{-}A\right)\right](\alpha\,|\,x) = 4\,A(x\,|\,x)\,A(\alpha\,|\,x)\left(2\,A(x\,|\,x)\,A(\alpha\,|\,\alpha) - 1\right) = 0$$

$$\left[\left(A^{-}A\right)^{*}\left(A^{-}A\right)\right](\alpha\,|\,\alpha) = 8\,A(x\,|\,x)\,A(x\,|\,\alpha)\,A(\alpha\,|\,x)\,A(\alpha\,|\,\alpha) + 1 = \pm 1$$

$$\left[\left(A^{-}A\right)^{*}\left(A^{-}A\right)\right](\alpha\,|\,\delta) = 8\,A(x\,|\,x)\,A(x\,|\,\alpha)\,A(\alpha\,|\,x)\,A(\alpha\,|\,\delta) = 0$$

$$\left[\left(A^{-}A\right)^{*}\left(A^{-}A\right)\right](y\,|\,y) = 8\,A(y\,|\,y)\,A(y\,|\,\beta)\,A(\beta\,|\,y)\,A(\beta\,|\,\beta) + 1 = \pm 1 \qquad (3\text{-}17)$$

$$\left[\left(A^{-}A\right)^{*}\left(A^{-}A\right)\right](y\,|\,\beta) = 4\,A(y\,|\,\beta)\,A(\beta\,|\,\beta)\left(2\,A(y\,|\,y)A(\beta\,|\,\beta) - 1\right) = 0$$

$$\left[\left(A^{-}A\right)^{*}\left(A^{-}A\right)\right](\beta\,|\,y) = 4\,A(y\,|\,y)\,A(\beta\,|\,y)\,\left(2\,A(y\,|\,y)A(\beta\,|\,\beta) - 1\right) = 0$$

$$\left[\left(A^{-}A\right)^{*}\left(A^{-}A\right)\right](\beta\,|\,\beta) = 8\,A(y\,|\,y)\,A(y\,|\,\beta)\,A(\beta\,|\,y)\,A(\beta\,|\,\beta) + 1 = \pm 1$$

$$\left[\left(A^{-}A\right)^{*}\left(A^{-}A\right)\right](l\,|\,x) = -16\,A(x\,|\,x)\,A(x\,|\,\alpha)\,A(\alpha\,|\,x)\,A(\alpha\,|\,\delta) = 0$$

$$\left[\left(A^{-}A\right)^{*}\left(A^{-}A\right)\right](l\,|\,\alpha) = -8\,A(x\,|\,\alpha)\,A(\alpha\,|\,\delta)\left(2\,A(x\,|\,x)\,A(\alpha\,|\,\alpha) - 1\right) = 0$$

$$\left[\left(A^{-}A\right)^{*}\left(A^{-}A\right)\right](l\,|\,\delta) = 4\,A(l\,|\,\delta) + 8\,A(\alpha\,|\,\delta)\left(A(x\,|\,\delta) - 2\,A(x\,|\,x)\,A(x\,|\,\alpha)\,A(\alpha\,|\,\delta)\right) = 0$$

The final required conditions in the horizontal direction are classified in three cases expressed in Table 3-6. The type of CX1 is nothing but the system connecting the type of LX1 in Table 3-2 with the plane symmetric system of LX1. The type of CX2 is similar to the system connecting the type of LX2 with the plane symmetric system of LX2. However the number of required conditions to satisfy perfect focusing can be reduced from four to three. The type of CX3 only appears in the doubly symmetric geometry. Ion beams are parallel at the point after two basic units. The number of required conditions can be reduced from four to three.

The final required conditions in the vertical direction are also classified in three cases expressed in Table 3-4.

3.5.4 Plane symmetry of plane symmetric system : $(A^{-}A)^{-}(A^{-}A)$

The overall transfer matrix of this arrangement is given in the following

$$\left(A^{-}A\right)^{-}\left(A^{-}A\right) \tag{3-18}$$

$$= \begin{bmatrix}
8A(x|x)A(x|\alpha)A(\alpha|x)A(\alpha|\alpha)+1 & 4A(x|\alpha)A(\alpha|\alpha)\left(2A(x|x)A(\alpha|\alpha)-1\right) & 0 & 0 & 0 & 8A(x|x)A(x|\alpha)A(\alpha|\alpha)A(\alpha|\delta) & 0 \\
4A(x|x)A(\alpha|x)\left(2A(x|x)A(\alpha|\alpha)-1\right) & 8A(x|x)A(x|\alpha)A(\alpha|x)A(\alpha|\alpha)+1 & 0 & 0 & 0 & 4A(x|x)A(\alpha|\delta)\left(2A(x|x)A(\alpha|\alpha)-1\right) & 0 \\
0 & 0 & 8A(y|y)A(y|\beta)A(\beta|y)A(\beta|\beta)+1 & 4A(y|\beta)A(\beta|\beta)\left(2A(y|y)A(\beta|\beta)-1\right) & 0 & 0 & 0 \\
0 & 0 & 4A(y|y)A(\beta|y)\left(2A(y|y)A(\beta|\beta)-1\right) & 8A(y|y)A(y|\beta)A(\beta|y)A(\beta|\beta)+1 & 0 & 0 & 0 \\
0 & 0 & 0 & 0 & 1 & 0 & 0 \\
0 & 0 & 0 & 0 & 0 & 1 & 0 \\
8A(x|x)A(\alpha|\delta)\left(2A(x|x)A(\alpha|\alpha)-1\right) & 16A(x|x)A(x|\alpha)A(\alpha|\alpha)A(\alpha|\delta) & 0 & 0 & 4A(l|\gamma)\,4A(l|\delta)+8A(\alpha|\delta)\left(A(x|\delta)+2A(x|x)A(x|\alpha)A(\alpha|\delta)\right) & 1
\end{bmatrix}$$

The perfect focusing conditions are

$$
\begin{aligned}
&\left[\left(A^{-}A\right)^{-}\left(A^{-}A\right)\right](x\,|\,x) = 8\,A(x\,|\,x)\,A(x\,|\,\alpha)\,A(\alpha\,|\,x)\,A(\alpha\,|\,\alpha) + 1 = \pm 1\\
&\left[\left(A^{-}A\right)^{-}\left(A^{-}A\right)\right](x\,|\,\alpha) = 4\,A(x\,|\,\alpha)\,A(\alpha\,|\,\alpha)\left(2\,A(x\,|\,x)\,A(\alpha\,|\,\alpha) - 1\right) = 0\\
&\left[\left(A^{-}A\right)^{-}\left(A^{-}A\right)\right](x\,|\,\delta) = 8\,A(x\,|\,x)\,A(x\,|\,\alpha)\,A(\alpha\,|\,\alpha)\,A(\alpha\,|\,\delta) = 0\\
&\left[\left(A^{-}A\right)^{-}\left(A^{-}A\right)\right](\alpha\,|\,x) = 4\,A(x\,|\,x)\,A(\alpha\,|\,x)\left(2\,A(x\,|\,x)\,A(\alpha\,|\,\alpha) - 1\right) = 0\\
&\left[\left(A^{-}A\right)^{-}\left(A^{-}A\right)\right](\alpha\,|\,\alpha) = 8\,A(x\,|\,x)\,A(x\,|\,\alpha)\,A(\alpha\,|\,x)\,A(\alpha\,|\,\alpha) + 1 = \pm 1\\
&\left[\left(A^{-}A\right)^{-}\left(A^{-}A\right)\right](\alpha\,|\,\delta) = 4\,A(x\,|\,x)\,A(\alpha\,|\,\delta)\left(2\,A(x\,|\,x)\,A(\alpha\,|\,\alpha) - 1\right) = 0\\
&\left[\left(A^{-}A\right)^{-}\left(A^{-}A\right)\right](y\,|\,y) = 8\,A(y\,|\,y)\,A(y\,|\,\beta)\,A(\beta\,|\,y)\,A(\beta\,|\,\beta) + 1 = \pm 1\\
&\left[\left(A^{-}A\right)^{-}\left(A^{-}A\right)\right](y\,|\,\beta) = 4\,A(y\,|\,\beta)\,A(\beta\,|\,\beta)\left(2\,A(y\,|\,y)\,A(\beta\,|\,\beta) - 1\right) = 0\\
&\left[\left(A^{-}A\right)^{-}\left(A^{-}A\right)\right](\beta\,|\,y) = 4\,A(y\,|\,y)\,A(\beta\,|\,y)\left(2\,A(y\,|\,y)\,A(\beta\,|\,\beta) - 1\right) = 0\\
&\left[\left(A^{-}A\right)^{-}\left(A^{-}A\right)\right](\beta\,|\,\beta) = 8\,A(y\,|\,y)\,A(y\,|\,\beta)\,A(\beta\,|\,y)\,A(\beta\,|\,\beta) + 1 = \pm 1\\
&\left[\left(A^{-}A\right)^{-}\left(A^{-}A\right)\right](l\,|\,x) = 8\,A(x\,|\,x)\,A(\alpha\,|\,\delta)\left(2\,A(x\,|\,x)\,A(\alpha\,|\,\alpha) - 1\right) = 0\\
&\left[\left(A^{-}A\right)^{-}\left(A^{-}A\right)\right](l\,|\,\alpha) = 16\,A(x\,|\,x)\,A(x\,|\,\alpha)\,A(\alpha\,|\,\alpha)\,A(\alpha\,|\,\delta) = 0\\
&\left[\left(A^{-}A\right)^{-}\left(A^{-}A\right)\right](l\,|\,\delta) = 4\,A(l\,|\,\delta) + 8\,A(\alpha\,|\,\delta)\left(A(x\,|\,\delta) + 2\,A(x\,|\,x)\,A(x\,|\,\alpha)\,A(\alpha\,|\,\delta)\right) = 0
\end{aligned}
\qquad (3\text{-}19)
$$

The final required conditions in the horizontal direction are classified in three cases expressed in Table 3-7. The type of DX1 is similar to the system connecting the type of LX1 in Table 3-2 with the plane symmetric system of LX1. However the number of required conditions to satisfy perfect focusing can be reduced from four to three. The type of DX2 is nothing but the system connecting the type of LX2 with the plane symmetric system of LX2. The type of DX3 only appears in the doubly symmetric geometry. Ion beams are parallel at the point after two basic units. The number of required conditions can be reduced from four to three.

The final required conditions in the vertical direction are also classified in three cases expressed in Table 3-4.

3.6 Examples of the system satisfying the perfect focusing condition

Several ion optical systems for a multi-turn TOF mass spectrometer which satisfies the perfect focusing have been found by using the principle described in the section 3.5. In this section, the characteristics of three perfect focusing systems are discussed.

3.6.1 MULTUM geometry

'MULTUM' geometry consists of four cylindrical electrostatic sectors and eight electric quadrupole lenses. The ion optical parameters and the total transfer matrix elements of 'MULTUM' are given in Table 3-8. The ion trajectories simulated by TRIO-DRAW are shown in Fig. 3-2. The basic unit is comprised of four drift spaces, two electric quadrupole lenses and a cylindrical electrostatic sector. This system consists of BX1 type in the horizontal direction and QY3 type in the vertical direction. In the horizontal direction, the perfect focusing is satisfied and the image type is the inverse (I-type) after half cycle (two units). Therefore, the image type at one cycle (four units) is the normal (N-type). In the vertical direction, the perfect focusing is satisfied at only one cycle and the image type is the inverse (I-type).

3.6.2 Figure - eight type geometry

'Figure - eight type' geometry consists of two cylindrical electrostatic sectors and eight electric quadrupole lenses. The ion optical parameters and the total transfer matrix elements of 'Figure - eight type' are given in Table 3-9. The ion trajectories simulated by TRIO-DRAW are shown in Fig. 3-3. The basic unit is comprised of six drift spaces, four electric quadrupole lenses and a cylindrical electrostatic sector. This system consists of AX1 type in the horizontal direction and QY1 type in the vertical direction. The perfect focusing is satisfied after two cycles (four units) and the image type is the N-type in both the horizontal and the vertical direction. This system must be operated 2 cycles as a basis whether only two electric sectors are needed.

```
Drift Space             DL = 0.0461
Electrostatic Q-lens entrance         QR= 0.0050  NQ1= 2
Electrostatic Q-lens                QKE=-36.1600  QLE=  0.0100
Electrostatic Q-lens exit             QR= 0.0050  NQ2= 2
Drift Space             DL = 0.0218
Toroidal ESA entrance   RO1= 0.0000  GAP= 0.0038  NE1= 2
Toroidal ESA            AE = 0.0500  WE = 156.87  C1 = 0.0000  C2 = 0.0000
Toroidal ESA exit       RO2= 0.0000  GAP= 0.0038  NE2= 2
Drift Space             DL = 0.0661
Electrostatic Q-lens entrance         QR= 0.0050  NQ1= 2
Electrostatic Q-lens                QKE=-21.0220  QLE=  0.0100
Electrostatic Q-lens exit             QR= 0.0050  NQ2= 2
Drift Space             DL = 0.0300
```

A-MATRIX

	X	A	C	D	XX	XA	XC	XD	AA	AC
X	-0.00005	-0.08619	0.00000	0.00000	0.10052	5.78695	0.00000	2.98495	0.44564	0.00000
A	11.60185	-0.00010	0.00000	-0.37245	389.78232	120.01601	0.00000	15.51453	7.18874	0.00000
T	0.00006	0.06433	0.16044	0.00000	-29.66154	-7.21246	0.00003	-0.99933	-0.34118	0.03216

	AD	CC	CD	DD	YY	YB	BB
X	0.11518	0.00000	0.00000	-0.02990	0.00017	-0.00001	0.00000
A	0.45282	0.00000	0.00000	-0.21624	60.60295	-3.30910	0.04517
T	0.03937	-0.04011	0.00000	0.10596	7.96619	-0.10649	0.07544

	Y	B
Y	-2.13396	0.12469
B	-4.00992	-0.23431

```
Deflection Is In Reverse Sense
Drift Space             DL = 0.0300
Electrostatic Q-lens entrance         QR= 0.0050  NQ1= 2
Electrostatic Q-lens                QKE=-21.0220  QLE=  0.0100
Electrostatic Q-lens exit             QR= 0.0050  NQ2= 2
Drift Space             DL = 0.0661
Toroidal ESA entrance   RO1= 0.0000  GAP= 0.0038  NE1= 2
Toroidal ESA            AE = 0.0500  WE = 156.87  C1 = 0.0000  C2 = 0.0000
Toroidal ESA exit       RO2= 0.0000  GAP= 0.0038  NE2= 2
Drift Space             DL = 0.0218
Electrostatic Q-lens entrance         QR= 0.0050  NQ1= 2
Electrostatic Q-lens                QKE=-36.1600  QLE=  0.0100
Electrostatic Q-lens exit             QR= 0.0050  NQ2= 2
Drift Space             DL = 0.0461
Deflection Is In Reverse Sense
```

A-MATRIX

	X	A	C	D	XX	XA	XC	XD	AA	AC
X	-0.99998	0.00002	0.00000	-0.00001	-0.18005	-20.66408	0.00000	0.00300	-0.00080	0.00000
A	-0.00115	-0.99998	0.00000	-0.00002	0.07630	0.33638	0.00000	69.33239	10.32843	0.00000
T	0.00005	0.00000	0.32088	0.00000	-59.23941	0.01312	0.00002	2.46016	-0.01772	0.00000

	AD	CC	CD	DD	YY	YB	BB
X	-0.07840	0.00000	0.00000	0.00000	-4.08301	-0.00001	0.01394
A	-0.00701	0.00000	0.00000	-0.69418	0.00011	-0.00022	0.00002
T	-0.00033	-0.08022	0.00000	0.16726	30.06317	-0.21298	0.10264

	Y	B
Y	0.00002	-0.05843
B	17.11404	0.00002

contitue on the next page

```
Deflection Is In Reverse Sense
Drift Space             DL = 0.0461
Electrostatic Q-lens entrance         QR= 0.0050  NQ1= 2
Electrostatic Q-lens                QKE=-36.1600  QLE=  0.0100
Electrostatic Q-lens exit             QR= 0.0050  NQ2= 2
Drift Space             DL = 0.0218
Toroidal ESA entrance   RO1= 0.0000  GAP= 0.0038  NE1= 2
Toroidal ESA            AE = 0.0500  WE = 156.87  C1 = 0.0000  C2 = 0.0000
Toroidal ESA exit       RO2= 0.0000  GAP= 0.0038  NE2= 2
Drift Space             DL = 0.0661
Electrostatic Q-lens entrance         QR= 0.0050  NQ1= 2
Electrostatic Q-lens                QKE=-21.0220  QLE=  0.0100
Electrostatic Q-lens exit             QR= 0.0050  NQ2= 2
Drift Space             DL = 0.0300
Deflection Is In Reverse Sense
  A-MATRIX
        X         A         C         D          XX         XA         XC         XD         AA         AC
X     0.00015   0.08619   0.00000   0.00000   -0.11373   -5.81573   0.00000   -8.96105   -1.33575   0.00000
A   -11.60165   0.00029   0.00000   0.37235 -391.99530 -359.75702   0.00000  -15.49629   -7.19677   0.00000
T     0.00018   0.06433   0.48133   0.00000  -88.91306   -7.21925   0.00009   -2.99970   -1.02316   0.03216
        AD         CC         CD         DD         YY         YB         BB
X    -0.11459   0.00000   0.00000   0.08970    0.00015    0.00001    0.00000
A    -1.36352   0.00000   0.00000   0.21619  -60.60001   -3.30903   -0.04518
T     0.03943  -0.12033   0.00000   0.31787   52.15980   -0.10645    0.12984
        Y         B
Y     2.13387   0.12469
B    -4.00999   0.23430
Drift Space             DL = 0.0300
Electrostatic Q-lens entrance         QR= 0.0050  NQ1= 2
Electrostatic Q-lens                QKE=-21.0220  QLE=  0.0100
Electrostatic Q-lens exit             QR= 0.0050  NQ2= 2
Drift Space             DL = 0.0661
Toroidal ESA entrance   RO1= 0.0000  GAP= 0.0038  NE1= 2
Toroidal ESA            AE = 0.0500  WE = 156.87  C1 = 0.0000  C2 = 0.0000
Toroidal ESA exit       RO2= 0.0000  GAP= 0.0038  NE2= 2
Drift Space             DL = 0.0218
Electrostatic Q-lens entrance         QR= 0.0050  NQ1= 2
Electrostatic Q-lens                QKE=-36.1600  QLE=  0.0100
Electrostatic Q-lens exit             QR= 0.0050  NQ2= 2
Drift Space             DL = 0.0461
  A-MATRIX
        X         A         C         D          XX         XA         XC         XD         AA         AC
X     0.99997  -0.00003   0.00000   0.00002    0.38379   41.32706   0.00000   -0.00425    0.00143   0.00000
A     0.00230   0.99996   0.00000   0.00005   -0.15294   -0.67270   0.00000 -138.66237  -20.65630   0.00000
T     0.00010   0.00000   0.64177   0.00000 -118.47670    0.02916   0.00005    4.91923   -0.03545   0.00000
        AD         CC         CD         DD         YY         YB         BB
X     0.15697   0.00000   0.00000  -0.00001    0.00001   -0.00001    0.00000
A     0.01475   0.00000   0.00000   1.38775   -0.00021    0.00000   -0.00003
T    -0.00070  -0.16044   0.00000   0.33455   60.12567   -0.00001    0.20528
        Y         B
Y    -0.99998   0.00000
B     0.00052  -0.99998
```

Table 3-8 Physical parameters and overall transfer matrices of ‘MULTUM’ geometry.

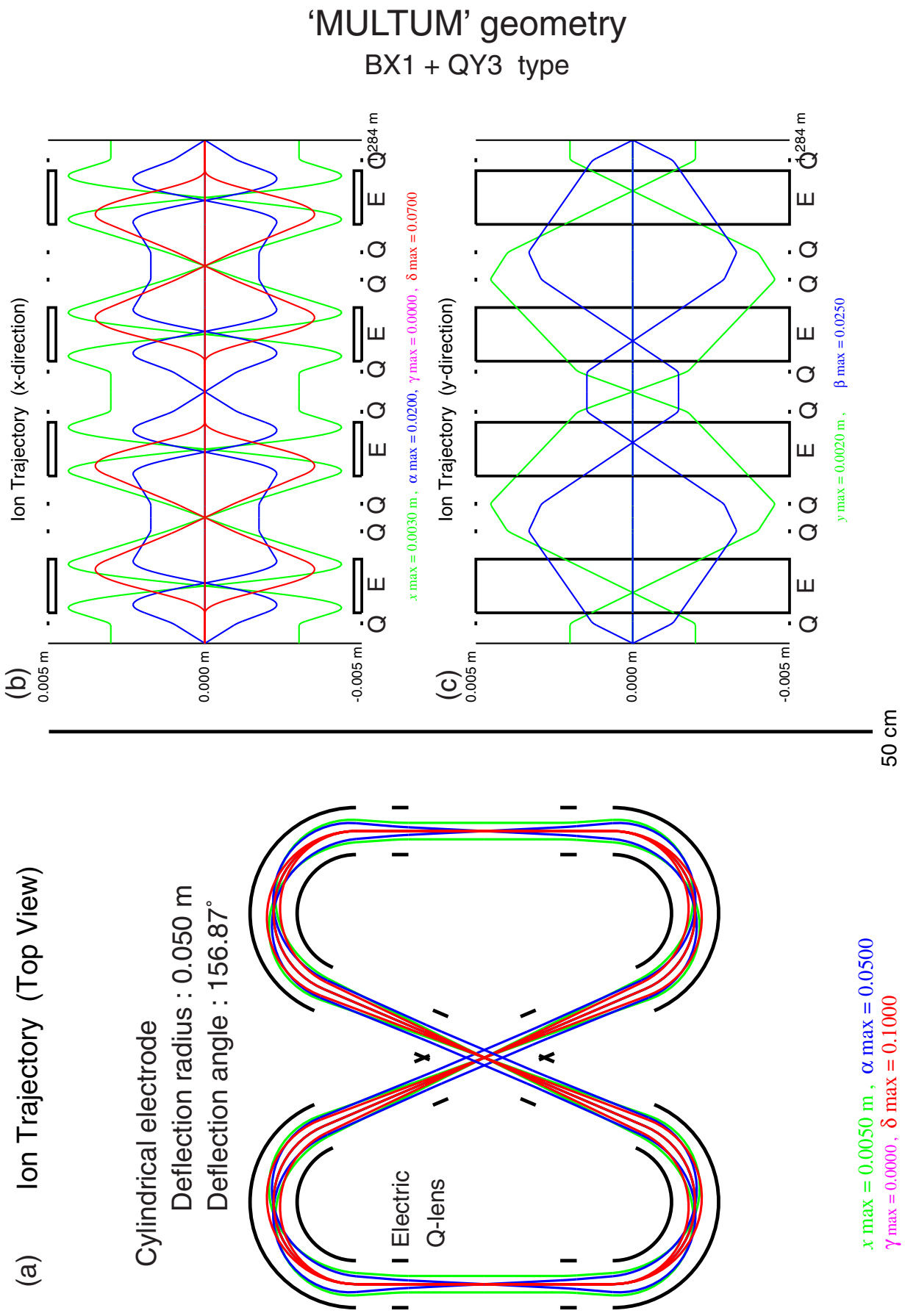

Fig. 3-2 Ion trajectories of the individual beam mode for 'MULTUM' geometry multi-turn TOF mass spectrometer. (a)top view, (b)x-direction, (c)y-direction.

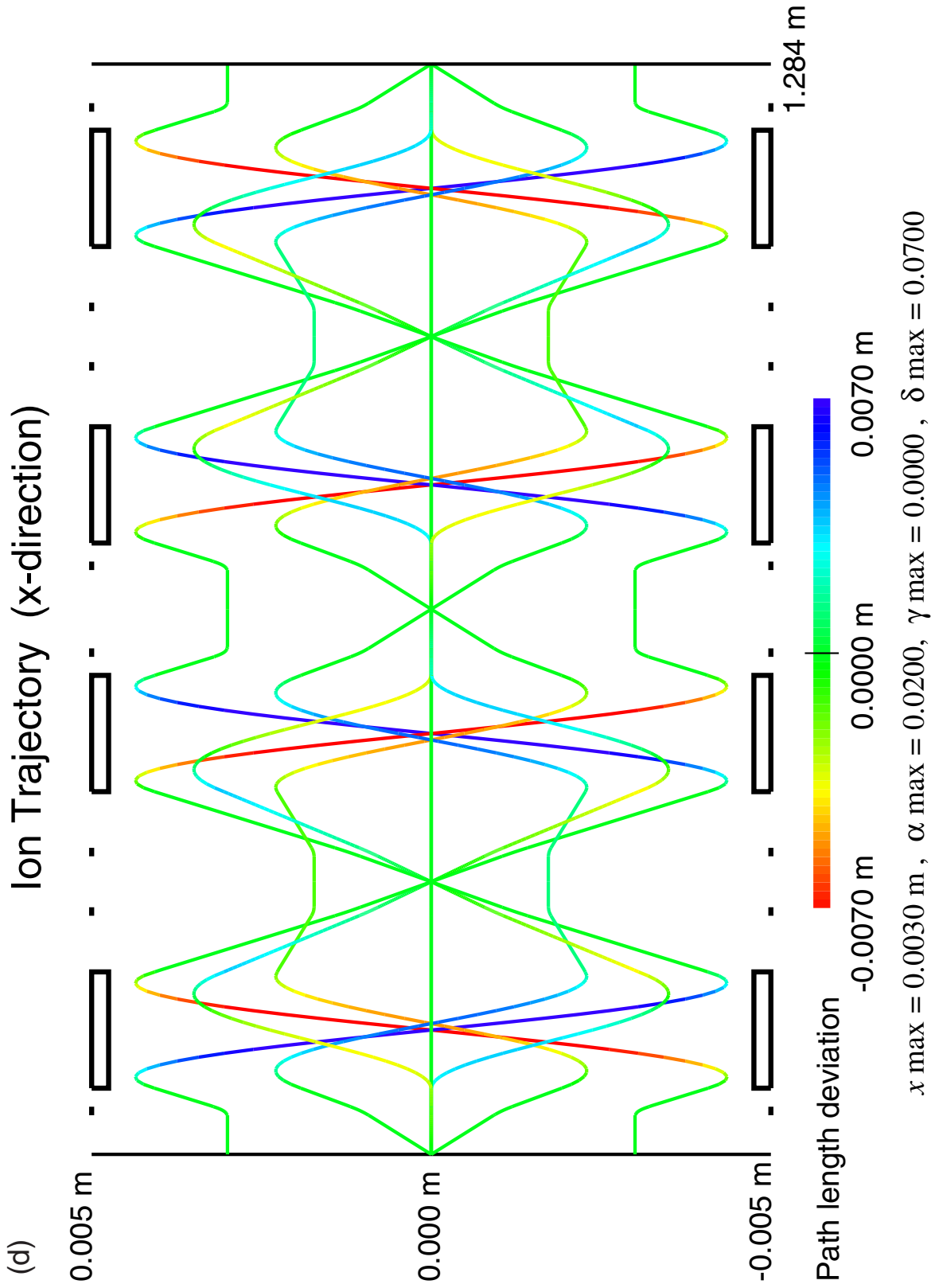

Fig. 3-2(d)Ion trajectories of the path length deviation mode for 'MULTUM' geometry multi-turn TOF mass spectrometer.

```
Drift Space             DL = 0.0724
Electrostatic Q-lens entrance         QR= 0.0050  NQ1= 2
Electrostatic Q-lens                 QKE= 54.2980  QLE=  0.0100
Electrostatic Q-lens exit             QR= 0.0050  NQ2= 2
Drift Space             DL = 0.0100
Electrostatic Q-lens entrance         QR= 0.0050  NQ1= 2
Electrostatic Q-lens                 QKE=-57.0580  QLE=  0.0100
Electrostatic Q-lens exit             QR= 0.0050  NQ2= 2
Drift Space             DL = 0.0100
Toroidal ESA entrance   RO1= 1.0000  GAP= 0.0004  NE1= 2
Toroidal ESA            AE = 0.0500  WE = 227.95  C1 = 0.0000  C2 = 0.0000
Toroidal ESA exit       RO2= 1.0000  GAP= 0.0004  NE2= 2
Drift Space             DL = 0.0100
Electrostatic Q-lens entrance         QR= 0.0050  NQ1= 2
Electrostatic Q-lens                 QKE=-57.0580  QLE=  0.0100
Electrostatic Q-lens exit             QR= 0.0050  NQ2= 2
Drift Space             DL = 0.0100
Electrostatic Q-lens entrance         QR= 0.0050  NQ1= 2
Electrostatic Q-lens                 QKE= 54.2980  QLE=  0.0100
Electrostatic Q-lens exit             QR= 0.0050  NQ2= 2
Drift Space             DL = 0.0724
Deflection Is In Reverse Sense
  A-MATRIX
```

	X	A	C	D	XX	XA	XC	XD	AA	AC
X	0.00016	-0.13779	0.00000	0.02434	-2.78514	-0.85051	0.00000	-2.16933	-0.05861	0.00000
A	7.25553	0.00016	0.00000	0.17662	-22.38365	-6.17036	0.00000	-11.26428	-0.38386	0.00000
T	-0.35325	-0.04869	0.21191	0.00860	16.45989	2.25226	-0.17662	-0.36479	0.31060	-0.02434

	AD	CC	CD	DD	YY	YB	BB
X	-0.21408	0.00000	0.00000	-0.00113	-91.06010	-7.99276	-0.22139
A	-2.18396	0.00000	0.00000	0.10198	-509.28745	-57.98248	-2.08321
T	-0.07517	-0.05298	0.00430	0.11186	104.33482	8.51299	0.35222

	Y	B
Y	0.00039	-0.05613
B	17.81189	0.00039

```
Drift Space             DL = 0.0724
Electrostatic Q-lens entrance         QR= 0.0050  NQ1= 2
Electrostatic Q-lens                 QKE= 54.2980  QLE=  0.0100
Electrostatic Q-lens exit             QR= 0.0050  NQ2= 2
Drift Space             DL = 0.0100
Electrostatic Q-lens entrance         QR= 0.0050  NQ1= 2
Electrostatic Q-lens                 QKE=-57.0580  QLE=  0.0100
Electrostatic Q-lens exit             QR= 0.0050  NQ2= 2
Drift Space             DL = 0.0100
Toroidal ESA entrance   RO1= 1.0000  GAP= 0.0004  NE1= 2
Toroidal ESA            AE = 0.0500  WE = 227.95  C1 = 0.0000  C2 = 0.0000
Toroidal ESA exit       RO2= 1.0000  GAP= 0.0004  NE2= 2
Drift Space             DL = 0.0100
Electrostatic Q-lens entrance         QR= 0.0050  NQ1= 2
Electrostatic Q-lens                 QKE=-57.0580  QLE=  0.0100
Electrostatic Q-lens exit             QR= 0.0050  NQ2= 2
Drift Space             DL = 0.0100
Electrostatic Q-lens entrance         QR= 0.0050  NQ1= 2
Electrostatic Q-lens                 QKE= 54.2980  QLE=  0.0100
Electrostatic Q-lens exit             QR= 0.0050  NQ2= 2
Drift Space             DL = 0.0724
Deflection Is In Reverse Sense
  A-MATRIX
```

	X	A	C	D	XX	XA	XC	XD	AA	AC
X	-0.99977	-0.00004	0.00000	0.00001	-0.00269	1.70040	0.00000	-0.30232	0.00002	0.00000
A	0.00227	-0.99976	0.00000	0.35328	-40.42571	-0.00282	0.00000	-33.66291	-0.85020	0.00000
T	-0.70657	-0.00002	0.42381	0.00001	34.88668	0.60139	-0.35328	1.59857	0.66247	-0.00001

	AD	CC	CD	DD	YY	YB	BB
X	0.63917	0.00000	0.00000	-0.11294	-0.13100	15.98015	0.00031
A	0.29847	0.00000	0.00000	-0.61792	-1322.09680	-0.03858	-3.20982
T	-0.00817	-0.10595	0.00000	0.22613	273.10297	5.64887	0.86037

	Y	B
Y	-0.99976	-0.00004
B	0.01389	-0.99976

continue on the next page

```
Drift Space             DL = 0.0724
Electrostatic Q-lens entrance         QR= 0.0050  NQ1= 2
Electrostatic Q-lens                QKE= 54.2980  QLE=  0.0100
Electrostatic Q-lens exit             QR= 0.0050  NQ2= 2
Drift Space             DL = 0.0100
Electrostatic Q-lens entrance         QR= 0.0050  NQ1= 2
Electrostatic Q-lens                QKE=-57.0580  QLE=  0.0100
Electrostatic Q-lens exit             QR= 0.0050  NQ2= 2
Drift Space             DL = 0.0100
Toroidal ESA entrance   RO1= 1.0000  GAP= 0.0004  NE1= 2
Toroidal ESA            AE = 0.0500  WE = 227.95  C1 = 0.0000  C2 = 0.0000
Toroidal ESA exit       RO2= 1.0000  GAP= 0.0004  NE2= 2
Drift Space             DL = 0.0100
Electrostatic Q-lens entrance         QR= 0.0050  NQ1= 2
Electrostatic Q-lens                QKE=-57.0580  QLE=  0.0100
Electrostatic Q-lens exit             QR= 0.0050  NQ2= 2
Drift Space             DL = 0.0100
Electrostatic Q-lens entrance         QR= 0.0050  NQ1= 2
Electrostatic Q-lens                QKE= 54.2980  QLE=  0.0100
Electrostatic Q-lens exit             QR= 0.0050  NQ2= 2
Drift Space             DL = 0.0724
Deflection Is In Reverse Sense
  A-MATRIX
```

	X	A	C	D	XX	XA	XC	XD	AA	AC
X	-0.00047	0.13776	0.00000	-0.02434	2.78849	-0.84942	0.00000	7.10717	0.05853	0.00000
A	-7.25382	-0.00047	0.00000	0.17675	-22.38500	6.16962	0.00000	11.23707	-0.38393	0.00000
T	-0.35351	0.04867	0.63572	-0.00859	53.30296	2.25207	-0.17676	2.91358	1.01440	0.02434

	AD	CC	CD	DD	YY	YB	BB
X	0.21453	0.00000	0.00000	0.00103	91.27031	-7.98298	0.22066
A	7.09276	0.00000	0.00000	-1.53714	-509.39941	58.00256	-2.08301
T	-0.39278	-0.15893	-0.00430	0.42018	441.68781	8.51407	1.36896

	Y	B
Y	-0.00117	0.05612
B	-17.80766	-0.00117

```
Drift Space             DL = 0.0724
Electrostatic Q-lens entrance         QR= 0.0050  NQ1= 2
Electrostatic Q-lens                QKE= 54.2980  QLE=  0.0100
Electrostatic Q-lens exit             QR= 0.0050  NQ2= 2
Drift Space             DL = 0.0100
Electrostatic Q-lens entrance         QR= 0.0050  NQ1= 2
Electrostatic Q-lens                QKE=-57.0580  QLE=  0.0100
Electrostatic Q-lens exit             QR= 0.0050  NQ2= 2
Drift Space             DL = 0.0100
Toroidal ESA entrance   RO1= 1.0000  GAP= 0.0004  NE1= 2
Toroidal ESA            AE = 0.0500  WE = 227.95  C1 = 0.0000  C2 = 0.0000
Toroidal ESA exit       RO2= 1.0000  GAP= 0.0004  NE2= 2
Drift Space             DL = 0.0100
Electrostatic Q-lens entrance         QR= 0.0050  NQ1= 2
Electrostatic Q-lens                QKE=-57.0580  QLE=  0.0100
Electrostatic Q-lens exit             QR= 0.0050  NQ2= 2
Drift Space             DL = 0.0100
Electrostatic Q-lens entrance         QR= 0.0050  NQ1= 2
Electrostatic Q-lens                QKE= 54.2980  QLE=  0.0100
Electrostatic Q-lens exit             QR= 0.0050  NQ2= 2
Drift Space             DL = 0.0724
Deflection Is In Reverse Sense
  A-MATRIX
```

	X	A	C	D	XX	XA	XC	XD	AA	AC
X	0.99953	0.00009	0.00000	-0.00002	-0.00211	-0.00040	0.00000	0.00683	0.00011	0.00000
A	-0.00454	0.99953	0.00000	0.00008	0.00948	0.00423	0.00000	67.31042	0.00020	0.00000
T	-0.00017	0.00003	0.84763	0.00000	69.75835	0.00105	-0.00008	0.00260	1.32465	0.00002

	AD	CC	CD	DD	YY	YB	BB
X	-1.27809	0.00000	0.00000	0.22581	-0.16463	-0.00383	0.00084
A	0.00668	0.00000	0.00000	-0.00142	0.31473	0.00966	0.00076
T	-0.91966	-0.21191	0.00000	0.61188	546.11859	0.00404	1.72042

	Y	B
Y	0.99953	0.00009
B	-0.02775	0.99952

Table 3-9 Physical parameters and overall transfer matrices of ‘Figure-eight type’ geometry.

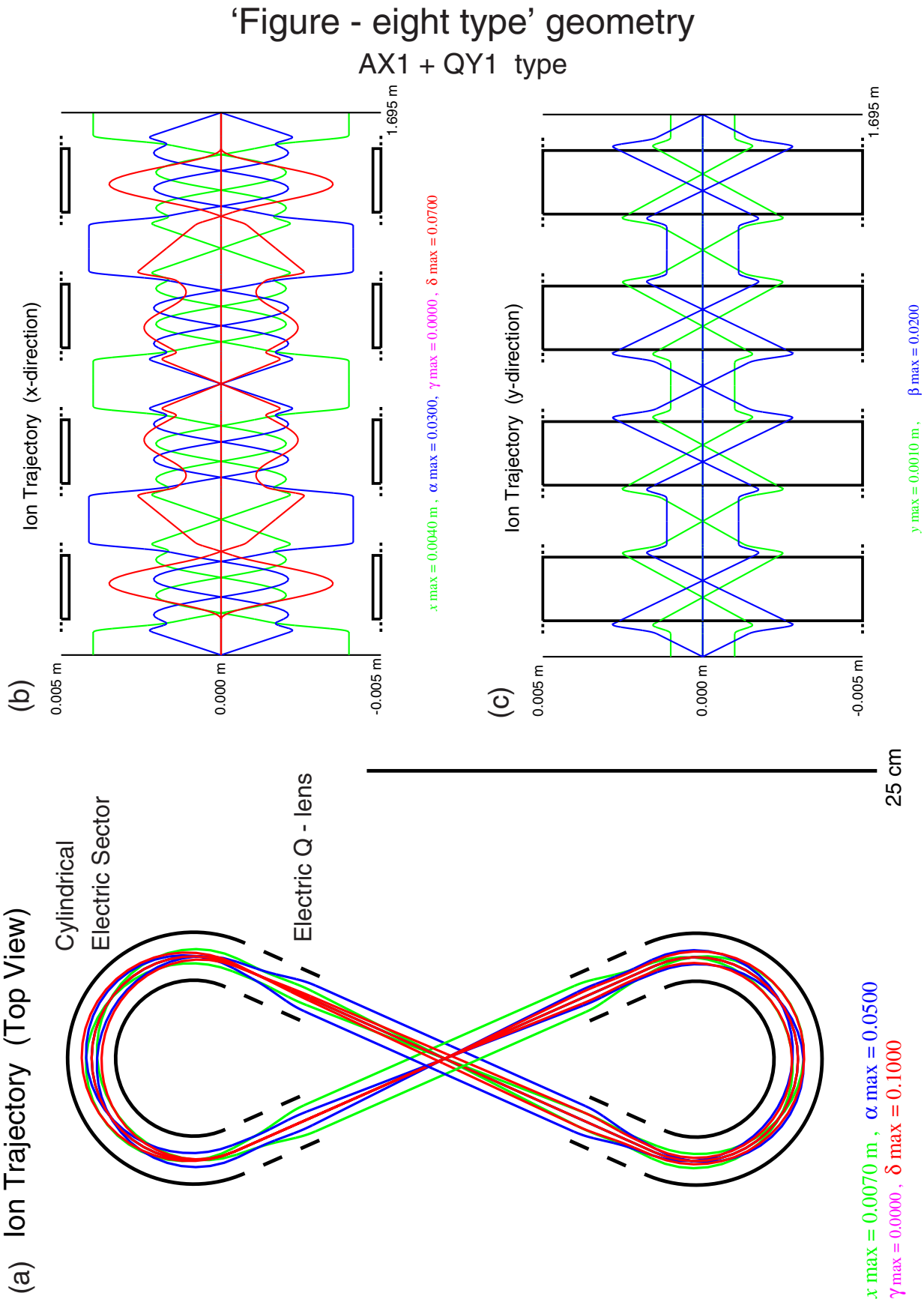

Fig. 3-3 Ion trajectories of the individual beam mode for 'Figure-eight type' geometry multi-turn TOF mass spectrometer. (a)top view, (b)x-direction, (c)y-direction.

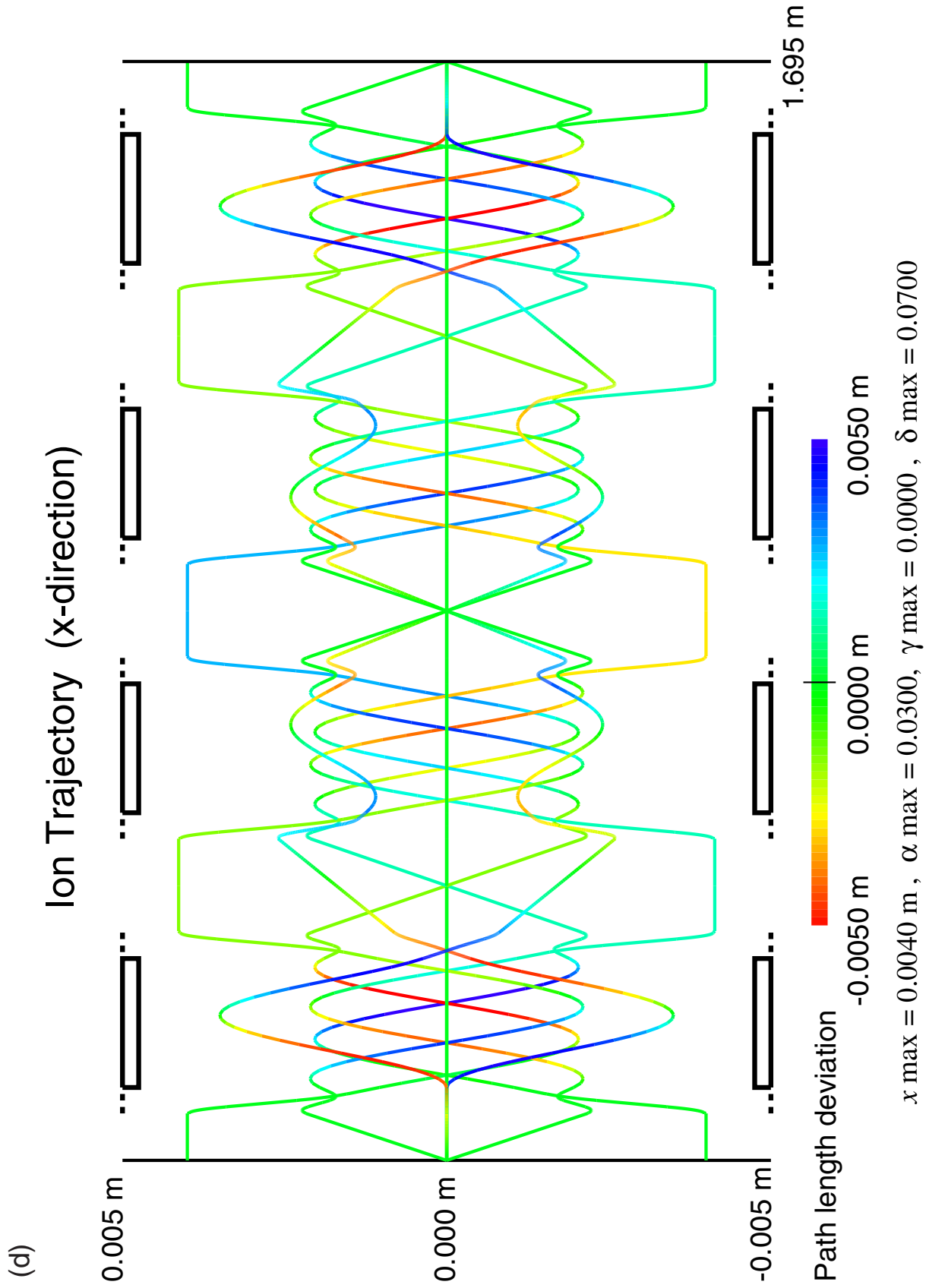

Fig. 3-3(d)Ion trajectories of the path length deviation mode for 'Figure-eight type' geometry multi-turn TOF mass spectrometer.

3.6.3 MULTUM II geometry

'MULTUM II' geometry consists of only four toroidal electrostatic sectors. The image type after one cycle is N-type in the horizontal direction. This optical system has two focusing characteristic according to the starting point. We can classify into the following two case.

3.6.3.1 Start from the point of side

The ion optical parameters and the total transfer matrix elements of 'MULTUM II' starting from the point of side are given in Table 3-10. The ion trajectories simulated by TRIO-DRAW are shown in Fig. 3-4. The basic unit is comprised of two drift spaces and a toroidal electrostatic sector. This system consists of BX3 type in the horizontal direction and QY3 type in the vertical direction. The perfect focusing is satisfied after one cycle (four units) and the image type is the I-type in both the horizontal and the vertical direction.

3.6.3.2 Start from the crossing point

The ion optical parameters and the total transfer matrix elements of 'MULTUM II' starting from the crossing point are given in Table 3-11. The ion trajectories simulated by TRIO-DRAW are shown in Fig. 3-5. In this case, the perfect focusing is satisfied not after one cycle but after two cycles. The basic unit is comprised of two drift spaces and two toroidal electrostatic sectors. This system consists of AX1 type in the horizontal direction and AY1 type in the vertical direction. The perfect focusing is satisfied after two cycles (four units) and the image type is the N-type in both the horizontal and the vertical direction. This system must be operated 2 cycles as a basis.

```
Drift Space              DL = 0.0809
Toroidal ESA entrance    RO1= 0.0000  GAP= 0.0050  NE1= 2
Toroidal ESA             AE = 0.0500  WE = 157.10  C1 = 0.0337  C2 =-0.0023
Toroidal ESA exit        RO2= 0.0000  GAP= 0.0050  NE2= 2
Drift Space              DL = 0.1089
  A-MATRIX
         X         A         C         D         XX         XA         XC         XD         AA         AC
  X    0.96902   -0.03095   0.00000   0.00079  -44.35664   -2.86038   0.00000   2.02607   0.12107   0.00000
  A   16.15310    0.51604   0.00000  -0.40421 -138.61584    8.49187   0.00000   5.11800   2.64651   0.00000
  T   -0.81107    0.02430   0.16347  -0.00064   19.09068   -0.06778  -0.40554  -1.27885  -0.10135   0.01215
         AD         CC         CD         DD         YY         YB         BB
  X    0.05325   0.00000   0.00000  -0.02290  -0.13674   0.10883   0.01871
  A   -0.35358   0.00000   0.00000  -0.04836   1.65087   0.95341   0.53790
  T    0.02120  -0.04087  -0.00032   0.11162   0.10071  -0.04908  -0.01342
         Y         B
  Y    0.68304   0.28207
  B   -1.77099   0.73270
Deflection Is In Reverse Sense
Drift Space              DL = 0.1089
Toroidal ESA entrance    RO1= 0.0000  GAP= 0.0050  NE1= 2
Toroidal ESA             AE = 0.0500  WE = 157.10  C1 = 0.0337  C2 =-0.0023
Toroidal ESA exit        RO2= 0.0000  GAP= 0.0050  NE2= 2
Drift Space              DL = 0.0809
Deflection Is In Reverse Sense
   A-MATRIX
         X         A         C         D         XX         XA         XC         XD         AA         AC
  X    0.00013   -0.03194   0.00000   0.00079  122.17783   -2.96758   0.00000   1.67317  -0.04727   0.00000
  A   31.30524    0.00013   0.00000   0.02522 -1456.11743  -92.56342   0.00000  75.98146   3.92521   0.00000
  T   -0.05025   -0.00160   0.32694  -0.00002  -16.15226   -4.78335  -0.02513   2.42858  -0.02477  -0.00080
         AD         CC         CD         DD         YY         YB         BB
  X    0.07739   0.00000   0.00000  -0.02411   0.03247   0.11214  -0.01038
  A    1.39270   0.00000   0.00000  -0.73259  -1.88894   3.51345   0.17218
  T    0.07591  -0.08173  -0.00001   0.18739   0.00251   0.07833  -0.00041
         Y         B
  Y    0.00092   0.41334
  B   -2.41930   0.00092
Deflection Is In Reverse Sense
Drift Space              DL = 0.0809
Toroidal ESA entrance    RO1= 0.0000  GAP= 0.0050  NE1= 2
Toroidal ESA             AE = 0.0500  WE = 157.10  C1 = 0.0337  C2 =-0.0023
Toroidal ESA exit        RO2= 0.0000  GAP= 0.0050  NE2= 2
Drift Space              DL = 0.1089
Deflection Is In Reverse Sense
   A-MATRIX
         X         A         C         D         XX         XA         XC         XD         AA         AC
  X   -0.96875   -0.03096   0.00000  -0.00080   44.82085   -2.87248   0.00000   0.81714  -0.12204   0.00000
  A   16.15696   -0.51590   0.00000   0.43006 -1371.52808  -87.23325  -0.00001  50.77893   1.40353   0.00000
  T   -0.81086   -0.02752   0.49041  -0.00062   18.99990   -4.87420  -0.40543   1.11416  -0.13901  -0.01376
         AD         CC         CD         DD         YY         YB         BB
  X   -0.03738   0.00000   0.00000   0.02517  -0.01937   0.10894   0.00793
  A    1.80498   0.00000   0.00000  -0.72576  -3.59651   4.57901  -0.36124
  T    0.06307  -0.12260  -0.00031   0.29769  -0.00366   0.13312   0.00418
         Y         B
  Y   -0.68178   0.28259
  B   -1.77425  -0.73135
Drift Space              DL = 0.1089
Toroidal ESA entrance    RO1= 0.0000  GAP= 0.0050  NE1= 2
Toroidal ESA             AE = 0.0500  WE = 157.10  C1 = 0.0337  C2 =-0.0023
Toroidal ESA exit        RO2= 0.0000  GAP= 0.0050  NE2= 2
Drift Space              DL = 0.0809
   A-MATRIX
         X         A         C         D         XX         XA         XC         XD         AA         AC
  X   -0.99996   -0.00001   0.00000  -0.00160   92.86260   -0.00977   0.00000   0.14444  -0.25006   0.00000
  A    0.00805   -0.99996   0.00000  -0.00033  -21.78542 -185.51624  -0.00001  92.10364   0.00610   0.00000
  T    0.00000   -0.00321   0.65388   0.00005  -36.64230   -0.29793   0.00000   0.09965  -0.03730  -0.00160
         AD         CC         CD         DD         YY         YB         BB
  X   -0.09410   0.00000   0.00000   0.05080   0.12135  -0.00015  -0.01109
  A   -0.15257   0.00000   0.00000   0.07349   0.01627   7.02659  -0.00354
  T    0.16428  -0.16347   0.00002   0.36842  -0.00145   0.01128  -0.00019
         Y         B
  Y   -1.00000   0.00076
  B   -0.00445  -1.00000

Total length = 1.307752
```

Table 3-10 Physical parameters and overall transfer matrices of ‘MULTUM II’ geometry starting from the point of side.

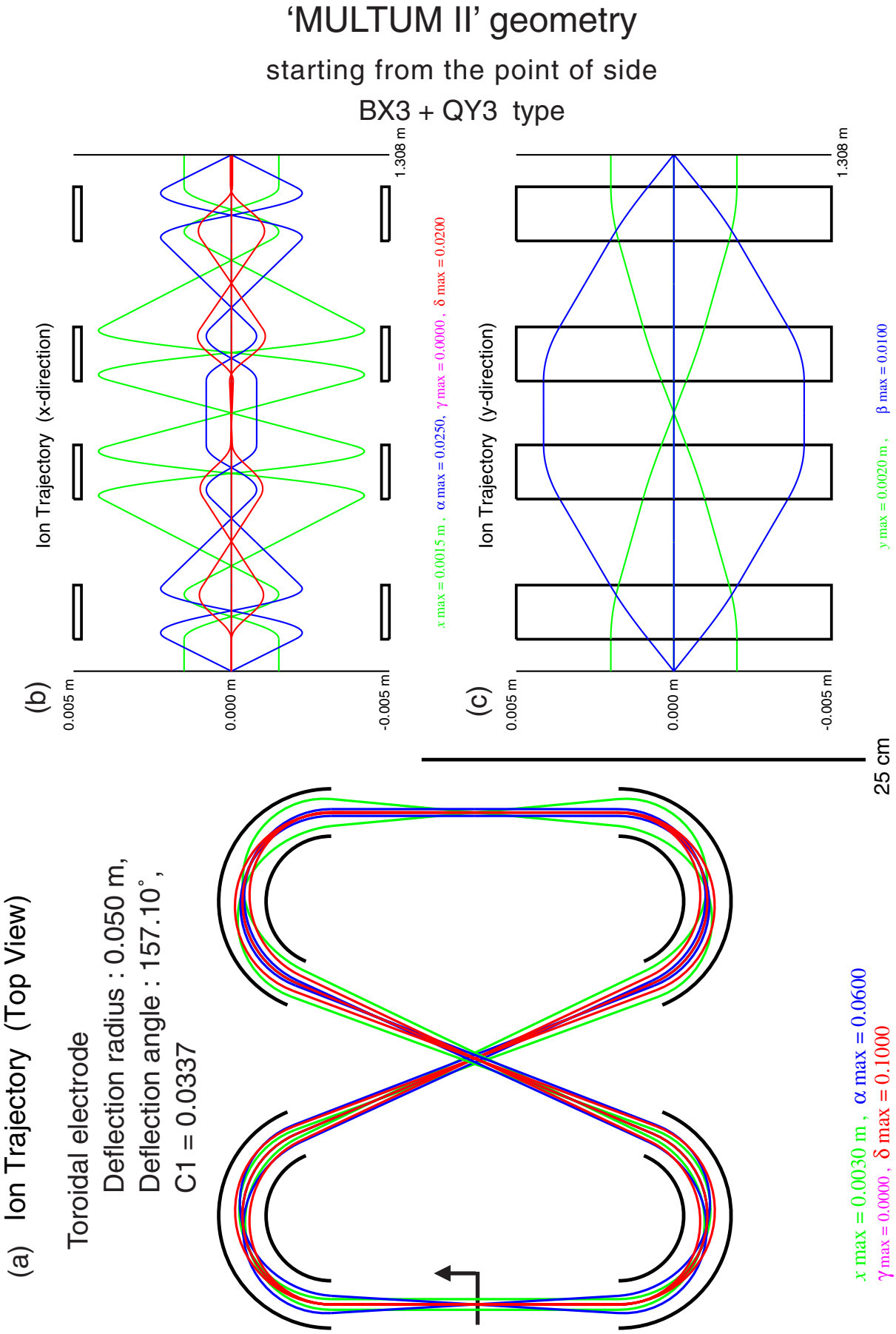

Fig. 3-4 Ion trajectories of the individual beam mode for 'MULTUM II' geometry multi-turn TOF mass spectrometer starting from the point of side. (a)top view, (b)x-direction, (c)y-direction.

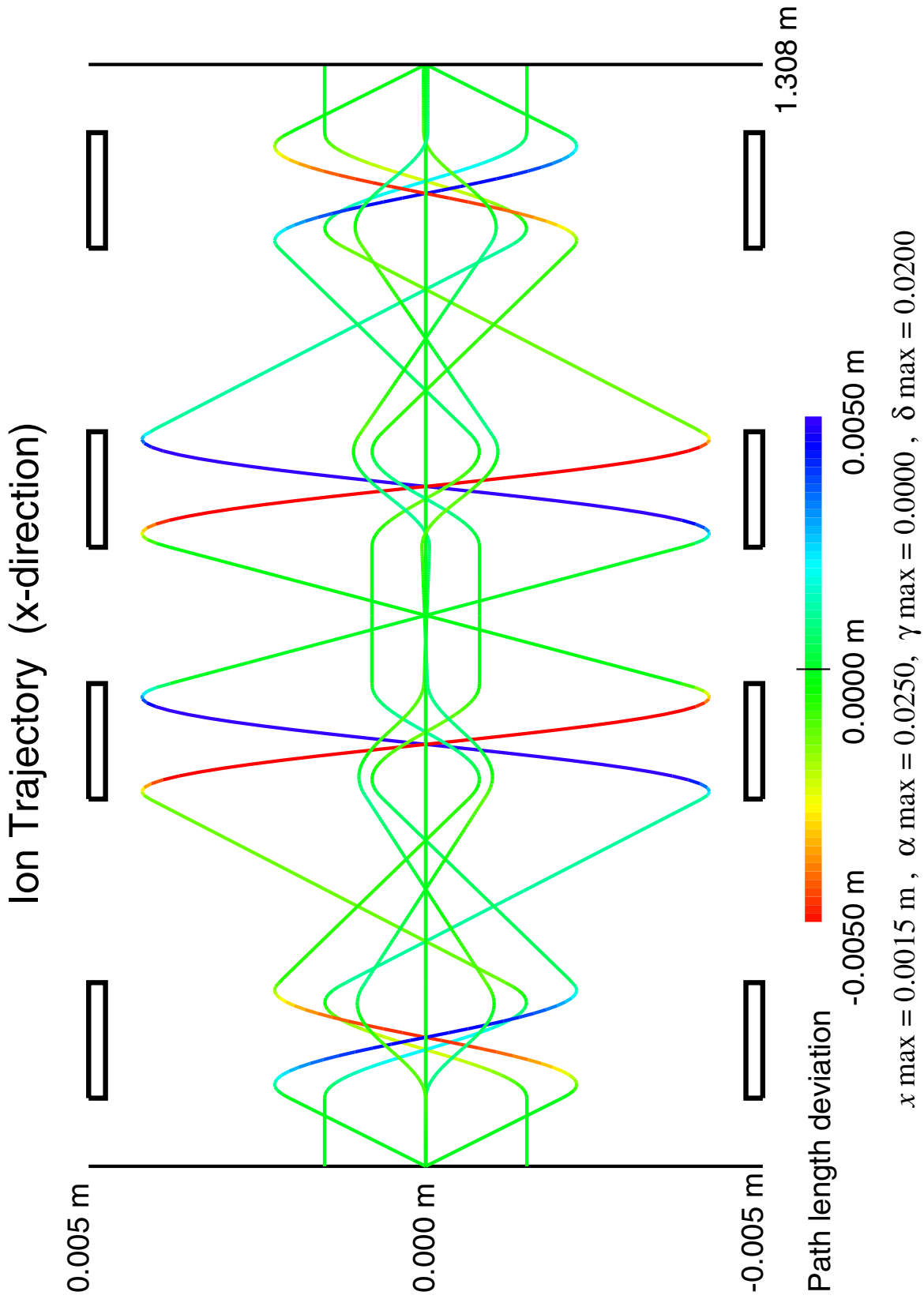

Fig. 3-4(d)Ion trajectories of the path length deviation mode for 'MULTUM II' geometry multi-turn TOF mass spectrometer starting from the point of side.

Deflection Is In Reverse Sense
Drift Space DL = 0.1089
Toroidal ESA entrance RO1= 0.0000 GAP= 0.0050 NE1= 2
Toroidal ESA AE = 0.0500 WE = 157.10 C1 = 0.0337 C2 =-0.0023
Toroidal ESA exit RO2= 0.0000 GAP= 0.0050 NE2= 2
Drift Space DL = 0.0809
Deflection Is In Reverse Sense

A-MATRIX

	X	A	C	D	XX	XA	XC	XD	AA	AC
X	0.51604	-0.03095	0.00000	-0.01212	40.46952	5.36824	0.00000	1.88255	0.07186	0.00000
A	16.15310	0.96902	0.00000	0.40421	138.61584	-0.71762	0.00000	5.11800	-2.77563	0.00000
T	0.81107	-0.00156	0.16347	-0.00064	15.43223	0.56398	0.40554	1.09576	-0.08738	-0.00078

	AD	CC	CD	DD	YY	YB	BB
X	0.11596	0.00000	0.00000	0.02154	0.18303	-0.07183	-0.00579
A	-0.21006	0.00000	0.00000	0.04836	-1.65087	-1.04600	-0.56593
T	0.00368	-0.04087	-0.00032	0.10933	0.05673	-0.00951	-0.00723

	Y	B
Y	0.73270	0.28207
B	-1.77099	0.68304

Deflection Is In Reverse Sense
Drift Space DL = 0.0809
Toroidal ESA entrance RO1= 0.0000 GAP= 0.0050 NE1= 2
Toroidal ESA AE = 0.0500 WE = 157.10 C1 = 0.0337 C2 =-0.0023
Toroidal ESA exit RO2= 0.0000 GAP= 0.0050 NE2= 2
Drift Space DL = 0.1089
Deflection Is In Reverse Sense

A-MATRIX

	X	A	C	D	XX	XA	XC	XD	AA	AC
X	0.00013	-0.05998	0.00000	-0.02504	38.99174	0.01757	0.00000	1.47233	-0.00144	0.00000
A	16.67142	0.00013	0.00000	0.41701	0.83434	-0.93489	0.00000	-6.42220	-2.36918	0.00000
T	0.83711	-0.05020	0.32694	-0.02093	22.96165	1.15282	0.41855	1.25262	-0.03650	-0.02510

	AD	CC	CD	DD	YY	YB	BB
X	-0.02318	0.00000	0.00000	0.01196	0.38439	0.06446	-0.00691
A	-0.49955	0.00000	0.00000	-0.15414	0.76846	-1.08196	-0.95153
T	-0.02071	-0.08173	-0.01047	0.19976	0.32097	0.03169	-0.00588

	Y	B
Y	0.00092	0.38532
B	-2.59521	0.00092

Drift Space DL = 0.1089
Toroidal ESA entrance RO1= 0.0000 GAP= 0.0050 NE1= 2
Toroidal ESA AE = 0.0500 WE = 157.10 C1 = 0.0337 C2 =-0.0023
Toroidal ESA exit RO2= 0.0000 GAP= 0.0050 NE2= 2
Drift Space DL = 0.0809

A-MATRIX

	X	A	C	D	XX	XA	XC	XD	AA	AC
X	-0.51590	-0.03096	0.00000	-0.01371	0.11142	5.40637	0.00000	4.13385	-0.07297	0.00000
A	16.15695	-0.96875	0.00000	-0.40461	1402.09692	-1.32571	-0.00001	52.35277	-2.81774	0.00000
T	0.86293	-0.00156	0.49041	-0.00062	-32.94827	0.57254	0.43147	-1.46355	0.01650	-0.00078

	AD	CC	CD	DD	YY	YB	BB
X	-0.09669	0.00000	0.00000	0.00880	0.21339	-0.00523	-0.00127
A	-1.59949	0.00000	0.00000	0.16799	10.76283	-1.05467	-0.78823
T	0.09527	-0.12260	-0.00031	0.31365	-0.03830	-0.01270	0.00667

	Y	B
Y	-0.73135	0.28259
B	-1.77425	-0.68178

Drift Space DL = 0.0809
Toroidal ESA entrance RO1= 0.0000 GAP= 0.0050 NE1= 2
Toroidal ESA AE = 0.0500 WE = 157.10 C1 = 0.0337 C2 =-0.0023
Toroidal ESA exit RO2= 0.0000 GAP= 0.0050 NE2= 2
Drift Space DL = 0.1089

A-MATRIX

	X	A	C	D	XX	XA	XC	XD	AA	AC
X	-0.99996	-0.00002	0.00000	0.00003	0.35521	0.07426	0.00000	0.02682	0.00182	0.00000
A	0.00428	-0.99996	0.00000	-0.83442	1308.52979	-0.63191	-0.00001	48.76756	-0.02732	0.00000
T	1.67398	0.00001	0.65388	0.00003	-19.77939	-0.06211	0.83699	-0.94600	-0.07164	0.00001

	AD	CC	CD	DD	YY	YB	BB
X	-0.17504	0.00000	0.00000	-0.07326	0.00067	0.12906	-0.00002
A	-0.02694	0.00000	0.00000	0.70773	12.81448	-0.01247	-0.22909
T	0.08888	-0.16347	0.00001	0.41778	-0.00189	-0.10803	-0.00019

	Y	B
Y	-1.00000	0.00071
B	-0.00478	-1.00000

continue on the next page

```
Deflection Is In Reverse Sense
Drift Space              DL = 0.1089
Toroidal ESA entrance    RO1= 0.0000  GAP= 0.0050  NE1= 2
Toroidal ESA             AE = 0.0500  WE = 157.10  C1 = 0.0337  C2 =-0.0023
Toroidal ESA exit        RO2= 0.0000  GAP= 0.0050  NE2= 2
Drift Space              DL = 0.0809
Deflection Is In Reverse Sense
   A-MATRIX
         X         A         C         D         XX        XA        XC        XD        AA        AC
  X   -0.51616   0.03094   0.00000   0.01372   0.12887   5.42636   0.00000   1.09922   0.07373   0.00000
  A  -16.14837  -0.96923   0.00000  -0.40396 1412.33350  -0.10241  -0.00001  41.98512  -2.77245   0.00000
  T    0.86293   0.00156   0.81735   0.00071  -6.09773   0.56426   0.43146  -1.62537  -0.15749   0.00078
         AD        CC        CD        DD        YY        YB        BB
  X   -0.08563   0.00000   0.00000  -0.08496  -0.21356  -0.00515   0.00134
  A   -7.27555   0.00000   0.00000  -2.20640  10.77239   1.02364  -0.78754
  T   -0.20258  -0.20434   0.00035   0.40270   0.03541  -0.01298  -0.00708
         Y         B
  Y   -0.73405  -0.28155
  B    1.76773  -0.68429
Deflection Is In Reverse Sense
Drift Space              DL = 0.0809
Toroidal ESA entrance    RO1= 0.0000  GAP= 0.0050  NE1= 2
Toroidal ESA             AE = 0.0500  WE = 157.10  C1 = 0.0337  C2 =-0.0023
Toroidal ESA exit        RO2= 0.0000  GAP= 0.0050  NE2= 2
Drift Space              DL = 0.1089
Deflection Is In Reverse Sense
   A-MATRIX
         X         A         C         D         XX        XA        XC        XD        AA        AC
  X   -0.00038   0.05998   0.00000   0.02501  -39.49768   0.05670   0.00000  -4.38477   0.00020   0.00000
  A  -16.67082  -0.00038   0.00000   0.41732   6.92793   0.32338   0.00000   6.10996  -2.33861   0.00000
  T    0.83669   0.05020   0.98081   0.02101  -62.22086   1.18553   0.41834  -3.66355  -0.10522   0.02510
         AD        CC        CD        DD        YY        YB        BB
  X    0.02234   0.00000   0.00000  -0.01213  -0.38393   0.06462   0.00678
  A   -6.37223   0.00000   0.00000  -2.60832   0.77609   1.05954  -0.95116
  T   -0.09653  -0.24520   0.01050   0.51256  -0.32355   0.03182   0.00539
         Y         B
  Y   -0.00276  -0.38532
  B    2.59520  -0.00276
Drift Space              DL = 0.1089
Toroidal ESA entrance    RO1= 0.0000  GAP= 0.0050  NE1= 2
Toroidal ESA             AE = 0.0500  WE = 157.10  C1 = 0.0337  C2 =-0.0023
Toroidal ESA exit        RO2= 0.0000  GAP= 0.0050  NE2= 2
Drift Space              DL = 0.0809
   A-MATRIX
         X         A         C         D         XX        XA        XC        XD        AA        AC
  X    0.51575   0.03096   0.00000   0.01211  -40.60268   5.38786   0.00000  -1.14608  -0.07298   0.00000
  A  -16.16051   0.96847   0.00000   0.40415  140.10178   0.55362   0.00001 -100.32430  -2.76161   0.00000
  T    0.81107   0.00155   1.14428   0.00073  -54.45642   0.57429   0.40553   0.94446  -0.05352   0.00078
         AD        CC        CD        DD        YY        YB        BB
  X    0.06591   0.00000   0.00000   0.05455  -0.18367  -0.07175   0.00584
  A   -5.90562   0.00000   0.00000  -2.32722  -1.64546   1.01991  -0.56591
  T   -0.12985  -0.28607   0.00037   0.59905  -0.05959  -0.00921   0.00682
         Y         B
  Y    0.73000  -0.28311
  B    1.77751   0.68052
Drift Space              DL = 0.0809
Toroidal ESA entrance    RO1= 0.0000  GAP= 0.0050  NE1= 2
Toroidal ESA             AE = 0.0500  WE = 157.10  C1 = 0.0337  C2 =-0.0023
Toroidal ESA exit        RO2= 0.0000  GAP= 0.0050  NE2= 2
Drift Space              DL = 0.1089
   A-MATRIX
         X         A         C         D         XX        XA        XC        XD        AA        AC
  X    0.99993   0.00003   0.00000   0.00001  -0.02045   0.00000   0.00000   0.00680   0.00000   0.00000
  A   -0.00855   0.99993   0.00000  -0.00003  -0.04292   0.04089   0.00001 -98.12421   0.00000   0.00000
  T    0.00006  -0.00003   1.30775   0.00009 -38.94629   0.00008   0.00003  -0.00448  -0.14022  -0.00001
         AD        CC        CD        DD        YY        YB        BB
  X    0.35312   0.00000   0.00000   0.14732   0.00042   0.00000  -0.00009
  A    0.00679   0.00000   0.00000   0.00440   0.00035  -0.01982   0.00001
  T   -0.41255  -0.32694   0.00005   0.58888  -0.00301   0.00000  -0.00035
         Y         B
  Y    0.99999  -0.00142
  B    0.00955   0.99999

Total length = 2.615505
```

Table 3-11 Physical parameters and overall transfer matrices of ‘MULTUM II’ geometry starting from the crossing point : 2 cycles.

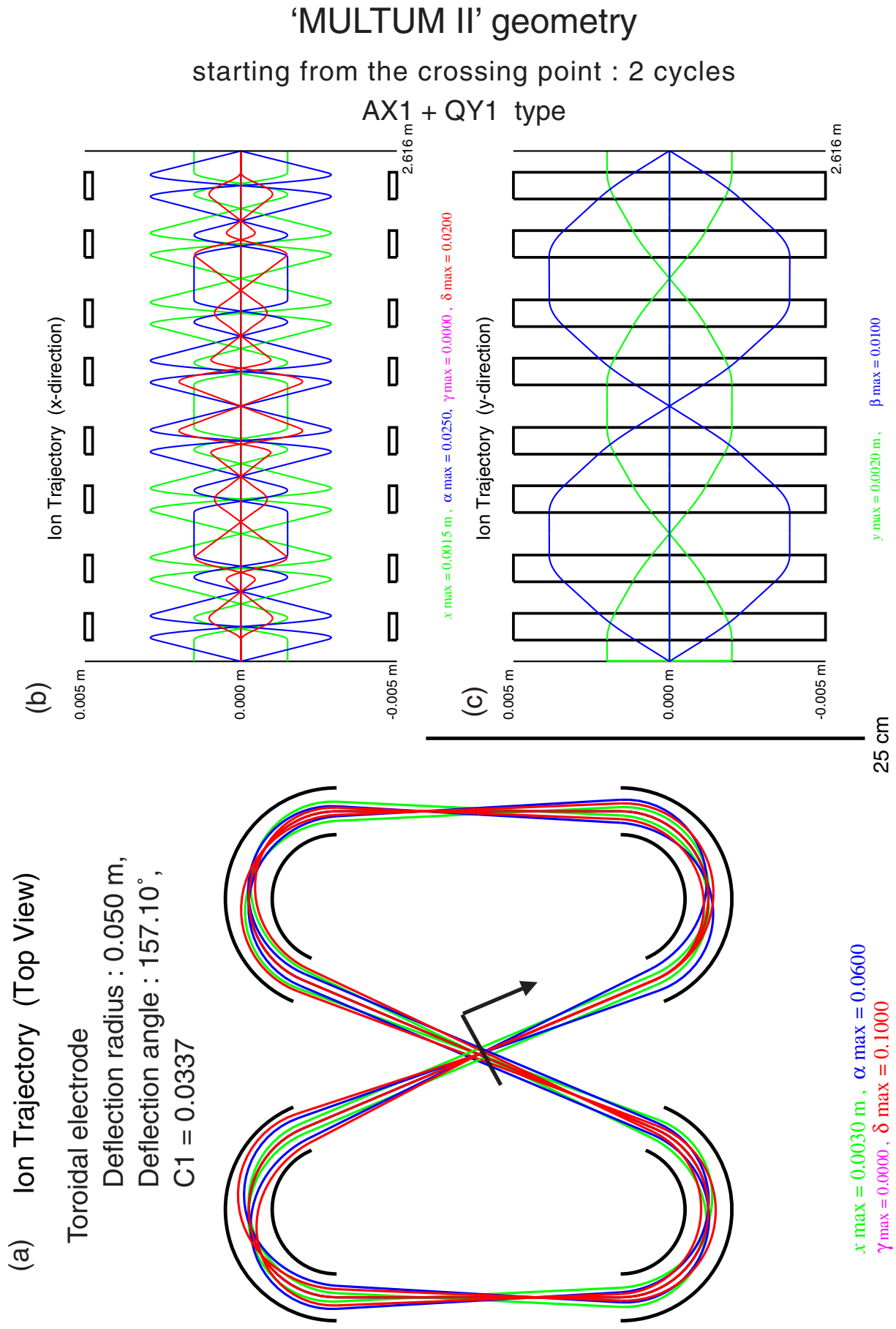

Fig. 3-5 Ion trajectories of the individual beam mode for 'MULTUM II' geometry multi-turn TOF mass spectrometer starting from the crossing point : 2 cycles. (a)top view, (b)x-direction, (c)y-direction.

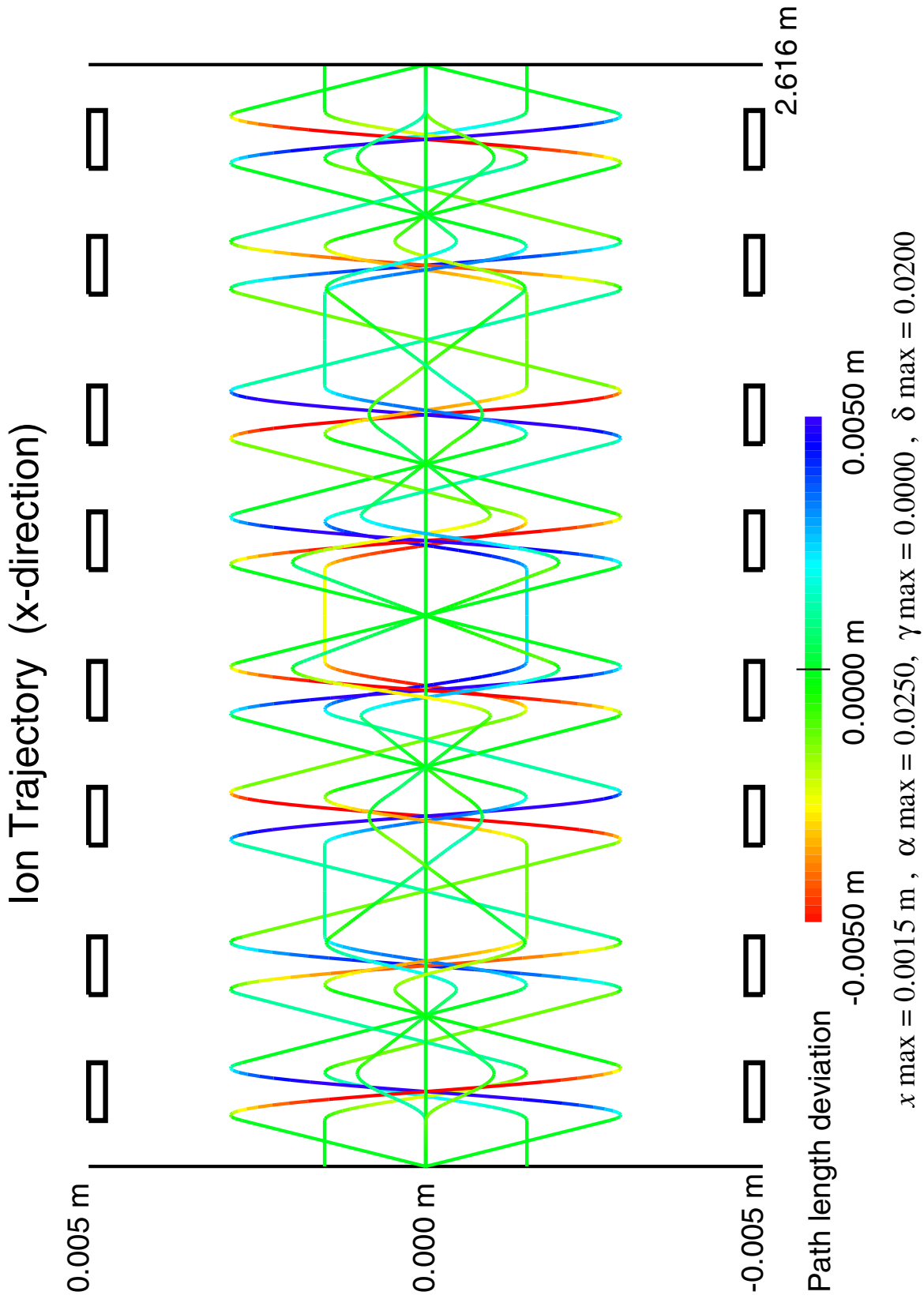

Fig. 3-5(d)Ion trajectories of the path length deviation mode for 'MULTUM II' geometry multi-turn TOF mass spectrometer starting from the crossing point : 2 cycles.

3.7 Conclusion

The required conditions for the perfect space and time focusing for multi-turn TOF mass spectrometers have been investigated. Symmetrical systems consisting of two basic units and four basic units were treated. It was shown that the multiple focusing can be satisfied in few conditions by introducing symmetry in the arrangement. In the case of the system consisting of four basic units, the required conditions can be reduced compared with the case of the system consisting of only two basic units. Some ion optical systems which was satisfied the perfect focusing were also proposed.

References

[3-1] T. Matsuo, M. Toyoda, T. Sakurai and M. Ishihara, *J. Mass Spectrom.*, **32** (1997), 1179-1185.

[3-2] M. Ishihara, M. Toyoda and T. Matsuo, *Int. J. Mass Spectrom. and Ion Proc.*, **197** (2000), 179-189.

[3-3] T. Sakurai, T. Matsuo and H. Matsuda, *Int. J. Mass Spectrom. and Ion Proc.*, **63** (1985), 273-287

[3-4] H. Wollnik and T. Matsuo, *Int. J. Mass Spectrom. and Ion Phys.*, **37** (1981), 209-225.

IV. Construction of The New Multi-turn Time-of-Flight Mass Spectrometer 'MULTUM Linear plus'

4.1 Introduction

In the previous chapter, the ion optics of multi-turn TOF mass spectrometers which satisfy the perfect space and time focusing was studied. By introducing symmetry in the arrangement of sectors, the difficulty of an exhaustive inquiry can be reduced. By using the principle described in Chapter III, the ion optical systems for a multi-turn TOF mass spectrometer have been found. One of these proposed TOF systems has been constructed as a laboratory model of COSAC project of ROSETTA mission. It consists of four cylindrical electrostatic sectors and eight electric quadrupole lenses. In order to inject and eject ions, a linear type TOF mass spectrometer was combined. Four electric quadrupole triplets were used to achieve the perfect space focusing of the linear type TOF mass spectrometer. The flight path length of the multi-turn part is 1.284 m and that of the linear part is 0.429 m. The size of the analyzer and the vacuum chamber is 400 mm × 400 mm × 50 mm and 600 mm × 700 mm × 200 mm, respectively. In this chapter, the technical data of the construction are reported.

4.2 MULTUM Linear plus

A multi-turn TOF mass spectrometer using the 'MULTUM' geometry has been designed and constructed. The system consists of four discrete units, each of which comprises an electric quadrupole lens, a cylindrical electrostatic sector and an electric quadrupole lens. The mean radius of the cylindrical electric sector is 50 mm, the deflection angle is 156.87°, the gap distance between the electrodes is 7.5 mm and the applied voltage is ± 225 V when the accelerating voltage of ions is 1500 V. The drawing of the cylindrical electric sector is shown in Fig. 4-1. The length of the inside electric quadrupole lenses is 10 mm, the radius of the inscribed circle of the

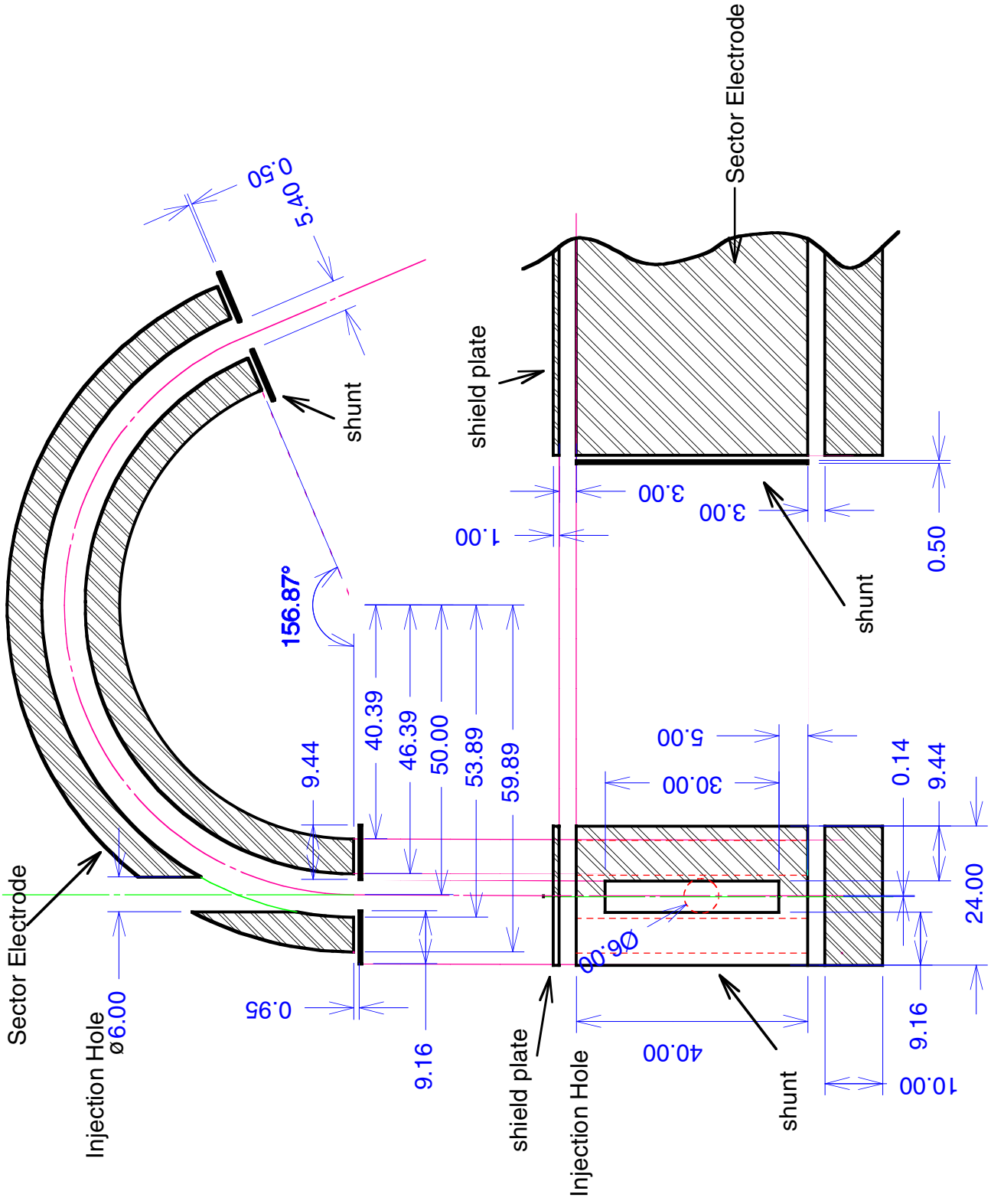

Fig. 4-1 Drawing of the cylindrical electric sector.

electrodes is 10 mm and the applied voltage is ± 16.57 V. The length of the outside electric quadrupole lenses is 10 mm, the radius of inscribed circle is 10 mm and the applied voltage is ± 49.04 V. The drawing of the electric quadrupole lenses is shown in Fig. 4-2. The total path length of one cycle is 1.284 m.

In order to inject and eject ions, the linear type TOF mass spectrometer was combined with 'MULTUM' and the whole system was designated 'MULTUM Linear plus.' The total path length of the linear system is 0.429 m. Four quadrupole triplets were used to achieve the perfect space focusing. A drawing of 'MULTUM Linear plus' is shown in Fig. 4-3. The length of the quadrupole lenses SQ1, SQ3, SQ4, SQ6, CQ1, CQ3, CQ4, CQ6, Q1, Q3, Q6, Q8, Q9, Q11, Q14 and Q16 is 5 mm, the radius of inscribed circle is 10 mm. The drawing of these electric quadrupole lenses is shown in Fig. 4-4. The applied voltage to SQ1, SQ3, SQ4, SQ6, CQ1, CQ3, CQ4 and CQ6 is ± 242.5 V. The applied voltage to Q1, Q3, Q6, Q8, Q9, Q11, Q14 and Q16 is ± 254.9 V when ions are injected and ejected. The dimensions of the quadrupole lenses SQ2, SQ5, CQ2, CQ5, Q2, Q7, Q10 and Q15 are the same as the quadrupole lens using in 'MULTUM.' The applied voltage to SQ2, SQ5, CQ2 and CQ5 is ± 220.9 V. The quadrupole lenses Q2, Q7, Q10 and Q15 share with the quadrupole lenses using in 'MULTUM.' The applied voltage to Q2, Q7, Q10 and Q15 is ± 231.1 V in injection and ejection mode. Ion trajectories of 'MULTUM Linear plus' simulated by TRIO-DRAW are shown in Fig. 4-5. The ion optical parameters and the total transfer matrix elements of 'MULTUM Linear plus' are given in Table 4-1. Twelve ion deflectors are arranged to correct ion trajectory and four ion gates are installed to kick out the undesired ions described later.

Whole system was fixed on the base plate which size is 40 cm × 40 cm. A photograph of the 'MULTUM Linear plus' on the base plate is shown in Fig. 4-6. The base plate was fixed by screws in the vacuum chamber. The size of the vacuum chamber is 60 cm × 70 cm × 20 cm. A photograph of the 'MULTUM Linear plus' in the vacuum chamber and the outside appearance of the vacuum chamber is shown in Fig. 4-7 and Fig. 4-8, respectively. A drawing of the vacuum chamber is shown in Fig. 4-9. The vacuum chamber was evacuated by a turbo molecular pump (Mitsubishi

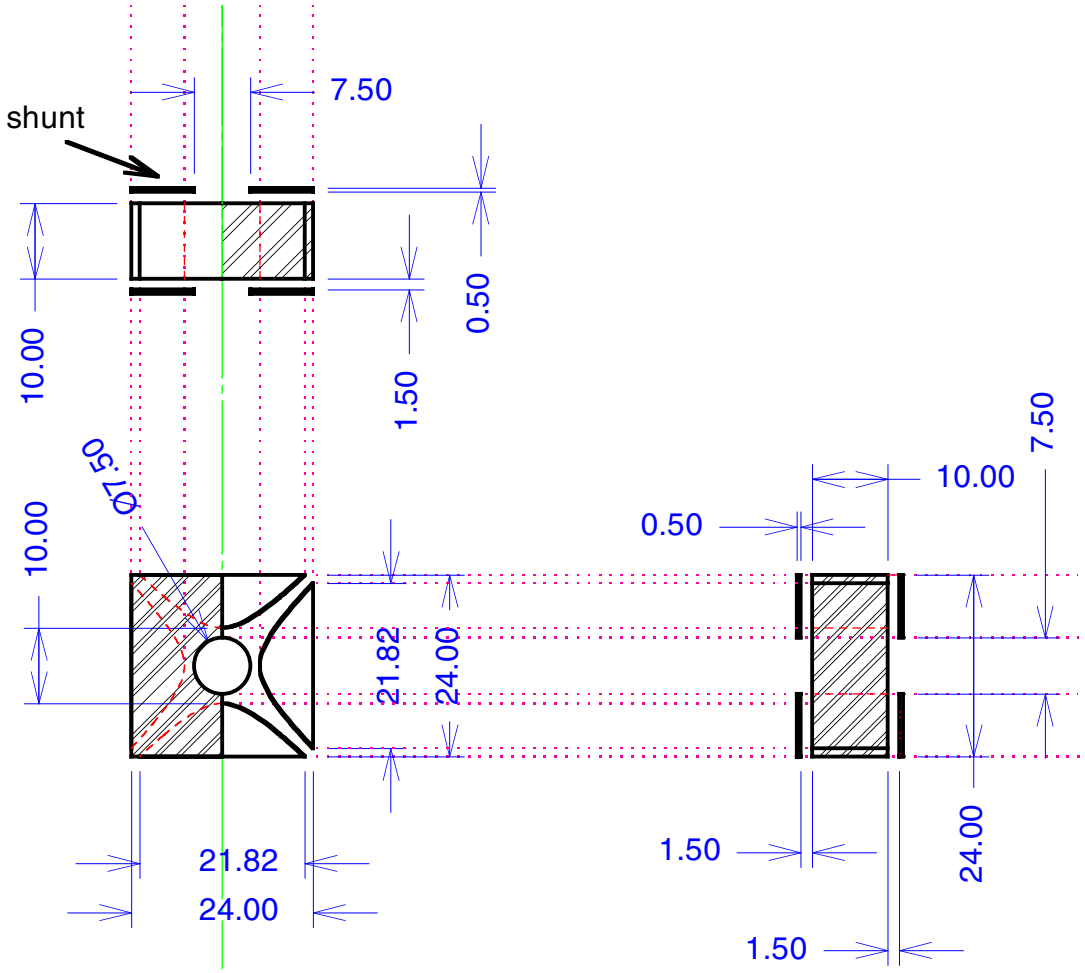

Fig. 4-2 Drawing of the electric quadrupole lenses in 'MULTUM' geometry.

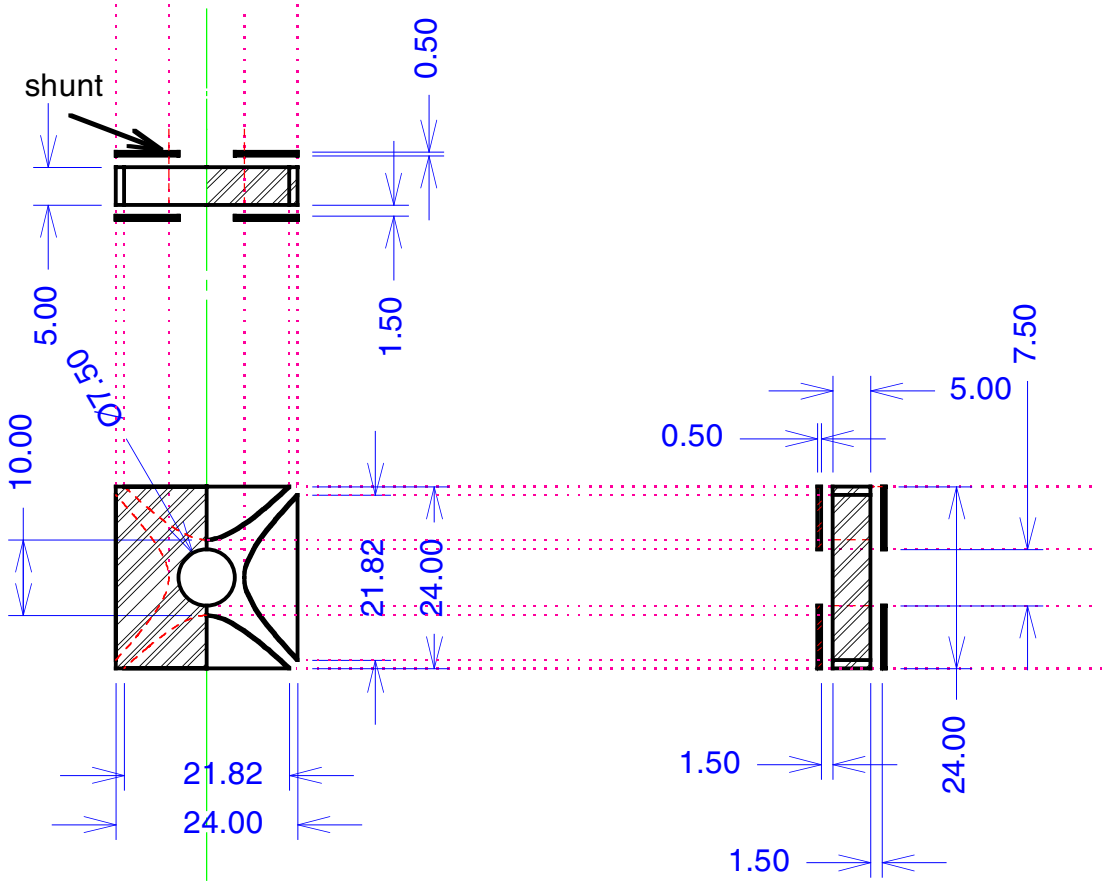

Fig. 4-4 Drawing of the electric quadrupole lenses in the linear-part.

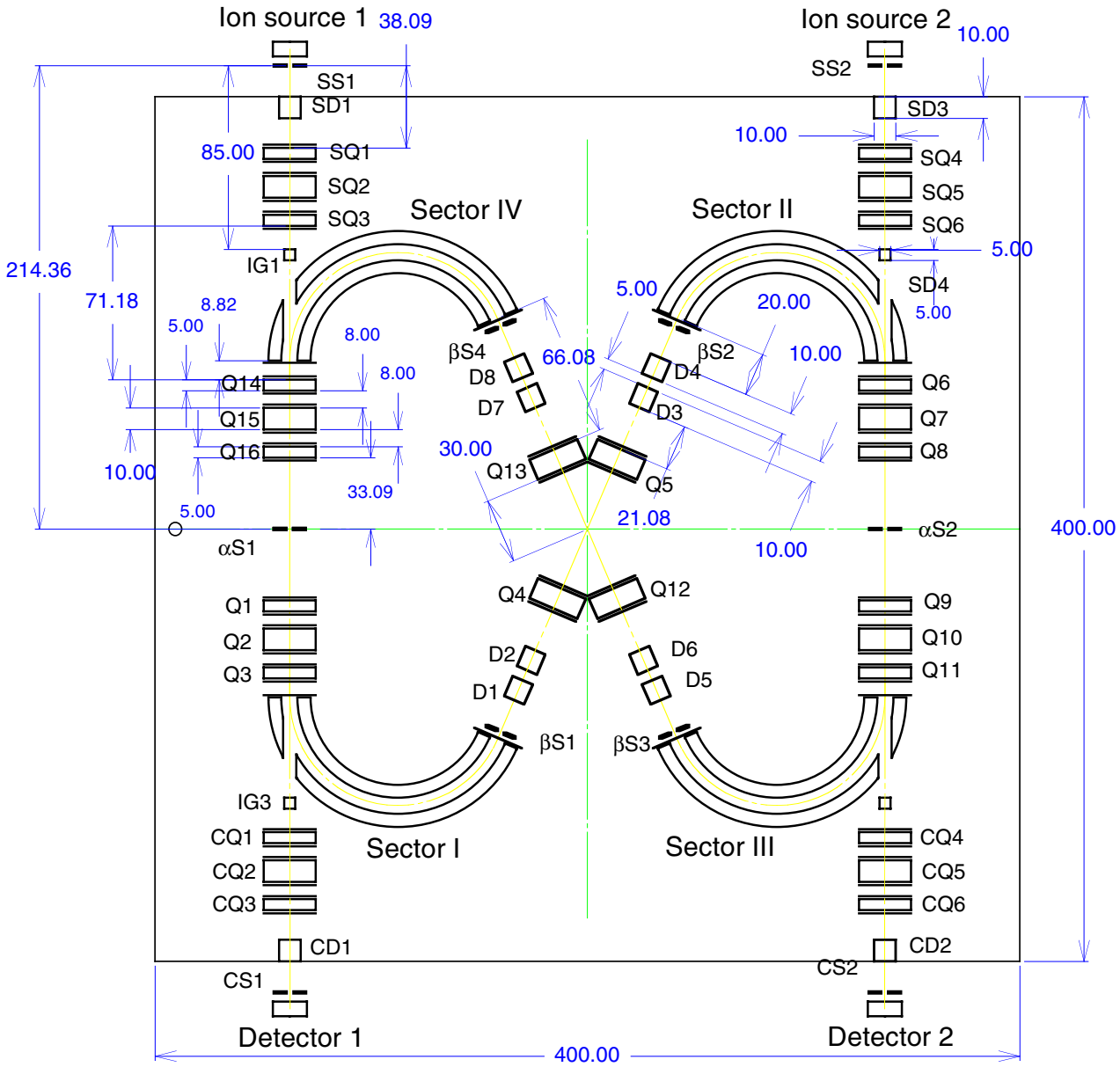

Fig. 4-3 Drawing of 'MULTUM Linear plus.'

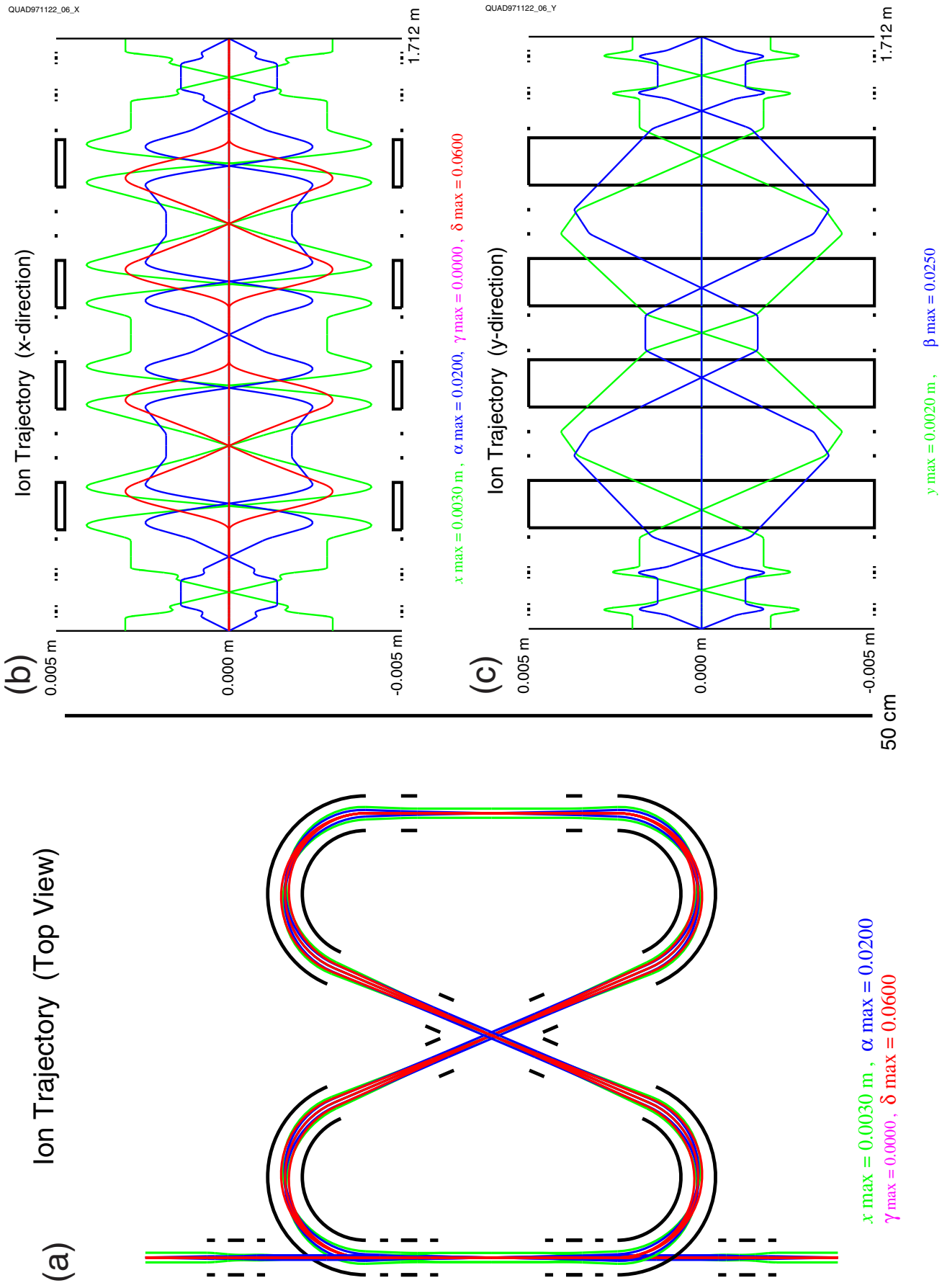

Fig. 4-5 Ion trajectories of 'MULTUM Linear plus' simulated by TRIO-DRAW. (a)Top-view, (b) *x*-direction and (c) *y*-direction in the individual beam mode.

```
Drift Space             DL = 0.0381
 Electrostatic Q-lens entrance         QR= 0.0050  NQ1= 2
 Electrostatic Q-lens                 QKE= 80.4039  QLE=  0.0050
 Electrostatic Q-lens exit             QR= 0.0050  NQ2= 2
 Drift Space             DL = 0.0080
 Electrostatic Q-lens entrance         QR= 0.0050  NQ1= 2
 Electrostatic Q-lens                 QKE=-76.7544  QLE=  0.0100
 Electrostatic Q-lens exit             QR= 0.0050  NQ2= 2
 Drift Space             DL = 0.0080
 Electrostatic Q-lens entrance         QR= 0.0050  NQ1= 2
 Electrostatic Q-lens                 QKE= 80.4039  QLE=  0.0050
 Electrostatic Q-lens exit             QR= 0.0050  NQ2= 2
 Drift Space             DL = 0.0381
 Drift Space             DL = 0.0331
 Electrostatic Q-lens entrance         QR= 0.0050  NQ1= 2
 Electrostatic Q-lens                 QKE= 82.4353  QLE=  0.0050
 Electrostatic Q-lens exit             QR= 0.0050  NQ2= 2
 Drift Space             DL = 0.0080
 Electrostatic Q-lens entrance         QR= 0.0050  NQ1= 2
 Electrostatic Q-lens                 QKE=-78.4961  QLE=  0.0100
 Electrostatic Q-lens exit             QR= 0.0050  NQ2= 2
 Drift Space             DL = 0.0080
 Electrostatic Q-lens entrance         QR= 0.0050  NQ1= 2
 Electrostatic Q-lens                 QKE= 82.4353  QLE=  0.0050
 Electrostatic Q-lens exit             QR= 0.0050  NQ2= 2
 Drift Space             DL = 0.0331
 Drift Space             DL = 0.0461
 Electrostatic Q-lens entrance         QR= 0.0050  NQ1= 2
 Electrostatic Q-lens                 QKE=-36.1600  QLE=  0.0100
 Electrostatic Q-lens exit             QR= 0.0050  NQ2= 2
 Drift Space             DL = 0.0218
 Toroidal ESA entrance   RO1= 0.0000  GAP= 0.0038  NE1= 2
 Toroidal ESA            AE = 0.0500  WE = 156.87  C1 = 0.0000  C2 = 0.0000
 Toroidal ESA exit       RO2= 0.0000  GAP= 0.0038  NE2= 2
 Drift Space             DL = 0.0661
 Electrostatic Q-lens entrance         QR= 0.0050  NQ1= 2
 Electrostatic Q-lens                 QKE=-21.0220  QLE=  0.0100
 Electrostatic Q-lens exit             QR= 0.0050  NQ2= 2
 Drift Space             DL = 0.0300
 Deflection Is In Reverse Sense
 Drift Space             DL = 0.0300
 Electrostatic Q-lens entrance         QR= 0.0050  NQ1= 2
 Electrostatic Q-lens                 QKE=-21.0220  QLE=  0.0100
 Electrostatic Q-lens exit             QR= 0.0050  NQ2= 2
 Drift Space             DL = 0.0661
 Toroidal ESA entrance   RO1= 0.0000  GAP= 0.0038  NE1= 2
 Toroidal ESA            AE = 0.0500  WE = 156.87  C1 = 0.0000  C2 = 0.0000
 Toroidal ESA exit       RO2= 0.0000  GAP= 0.0038  NE2= 2
 Drift Space             DL = 0.0218
 Electrostatic Q-lens entrance         QR= 0.0050  NQ1= 2
 Electrostatic Q-lens                 QKE=-36.1600  QLE=  0.0100
 Electrostatic Q-lens exit             QR= 0.0050  NQ2= 2
 Drift Space             DL = 0.0461
 Drift Space             DL = 0.0461
 Electrostatic Q-lens entrance         QR= 0.0050  NQ1= 2
 Electrostatic Q-lens                 QKE=-36.1600  QLE=  0.0100
 Electrostatic Q-lens exit             QR= 0.0050  NQ2= 2
 Drift Space             DL = 0.0218
 Toroidal ESA entrance   RO1= 0.0000  GAP= 0.0038  NE1= 2
 Toroidal ESA            AE = 0.0500  WE = 156.87  C1 = 0.0000  C2 = 0.0000
 Toroidal ESA exit       RO2= 0.0000  GAP= 0.0038  NE2= 2
 Drift Space             DL = 0.0661
 Electrostatic Q-lens entrance         QR= 0.0050  NQ1= 2
 Electrostatic Q-lens                 QKE=-21.0220  QLE=  0.0100
 Electrostatic Q-lens exit             QR= 0.0050  NQ2= 2
 Drift Space             DL = 0.0300
 Deflection Is In Reverse Sense
```

continue on the next page

```
Drift Space             DL = 0.0300
Electrostatic Q-lens entrance         QR= 0.0050  NQ1= 2
Electrostatic Q-lens                 QKE=-21.0220  QLE=  0.0100
Electrostatic Q-lens exit             QR= 0.0050  NQ2= 2
Drift Space             DL = 0.0661
Toroidal ESA entrance   RO1= 0.0000  GAP= 0.0038  NE1= 2
Toroidal ESA            AE = 0.0500  WE = 156.87  C1 = 0.0000  C2 = 0.0000
Toroidal ESA exit       RO2= 0.0000  GAP= 0.0038  NE2= 2
Drift Space             DL = 0.0218
Electrostatic Q-lens entrance         QR= 0.0050  NQ1= 2
Electrostatic Q-lens                 QKE=-36.1600  QLE=  0.0100
Electrostatic Q-lens exit             QR= 0.0050  NQ2= 2
Drift Space             DL = 0.0461
Drift Space             DL = 0.0331
Electrostatic Q-lens entrance         QR= 0.0050  NQ1= 2
Electrostatic Q-lens                 QKE= 82.4353  QLE=  0.0050
Electrostatic Q-lens exit             QR= 0.0050  NQ2= 2
Drift Space             DL = 0.0080
Electrostatic Q-lens entrance         QR= 0.0050  NQ1= 2
Electrostatic Q-lens                 QKE=-78.4961  QLE=  0.0100
Electrostatic Q-lens exit             QR= 0.0050  NQ2= 2
Drift Space             DL = 0.0080
Electrostatic Q-lens entrance         QR= 0.0050  NQ1= 2
Electrostatic Q-lens                 QKE= 82.4353  QLE=  0.0050
Electrostatic Q-lens exit             QR= 0.0050  NQ2= 2
Drift Space             DL = 0.0331
Drift Space             DL = 0.0381
Electrostatic Q-lens entrance         QR= 0.0050  NQ1= 2
Electrostatic Q-lens                 QKE= 80.4039  QLE=  0.0050
Electrostatic Q-lens exit             QR= 0.0050  NQ2= 2
Drift Space             DL = 0.0080
Electrostatic Q-lens entrance         QR= 0.0050  NQ1= 2
Electrostatic Q-lens                 QKE=-76.7544  QLE=  0.0100
Electrostatic Q-lens exit             QR= 0.0050  NQ2= 2
Drift Space             DL = 0.0080
Electrostatic Q-lens entrance         QR= 0.0050  NQ1= 2
Electrostatic Q-lens                 QKE= 80.4039  QLE=  0.0050
Electrostatic Q-lens exit             QR= 0.0050  NQ2= 2
Drift Space             DL = 0.0381
   A-MATRIX
```

	X	A	C	D	XX	XA	XC	XD	AA	AC
X	0.99844	-0.00004	0.00000	-0.00002	-0.36741	-43.54789	0.00000	-0.00290	-0.00167	0.00000
A	0.00228	0.99844	0.00000	-0.00005	0.12951	0.63596	0.00000	-52.36781	21.76635	0.00000
T	-0.00009	0.00000	0.85613	-0.21436	-28.32825	0.02897	-0.00005	-4.65554	0.35873	0.00000

	AD	CC	CD	DD	YY	YB	BB
X	-0.19279	0.00000	0.00000	0.00002	-0.00001	0.00001	0.00000
A	0.01607	0.00000	0.00000	-1.31361	0.00011	0.00000	0.00004
T	0.00074	-0.21403	-0.10718	0.49532	253.43349	0.00731	0.84392

	Y	B
Y	-0.99846	0.00000
B	0.00044	-0.99846

```
Total length = 1.7122
```

Table 4-1 Ion optical parameters and total transfer matrix elements of ‘MULTUM Linear plus’ for one cycle.

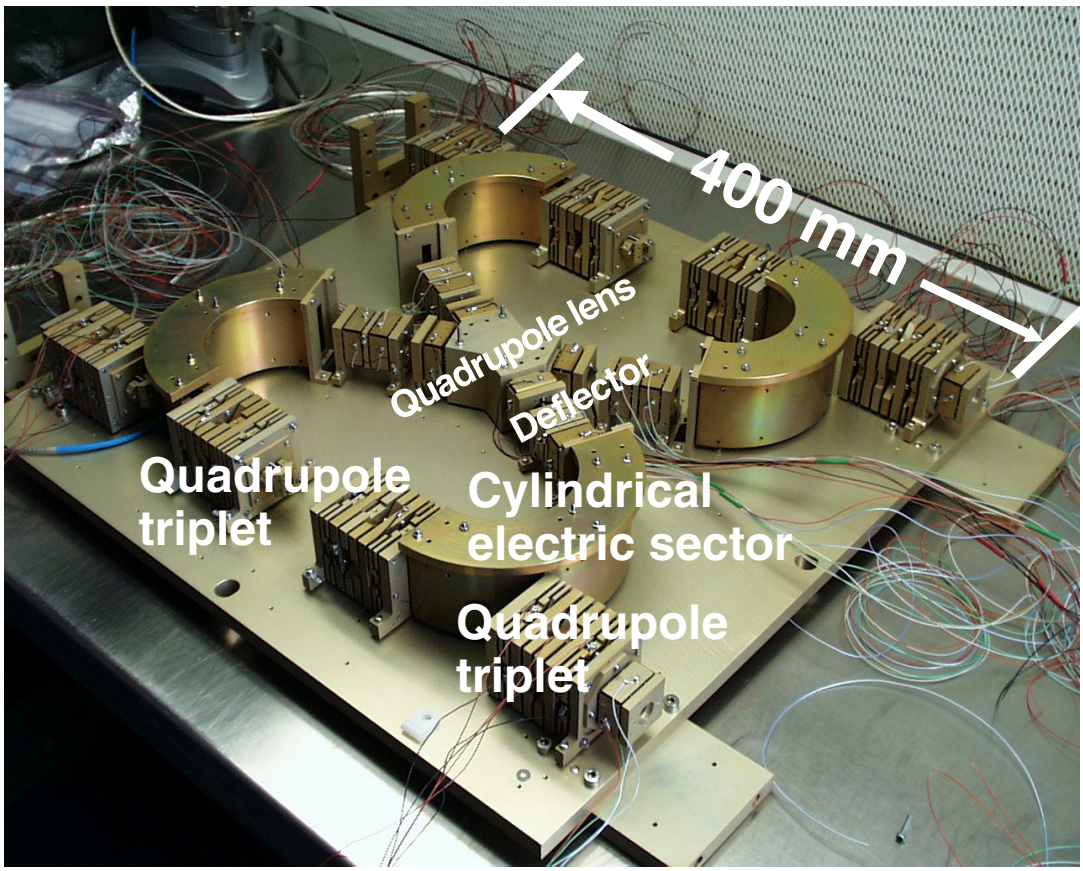

Fig. 4-6 Photograph of the 'MULTUM Linear plus' on the base plate.

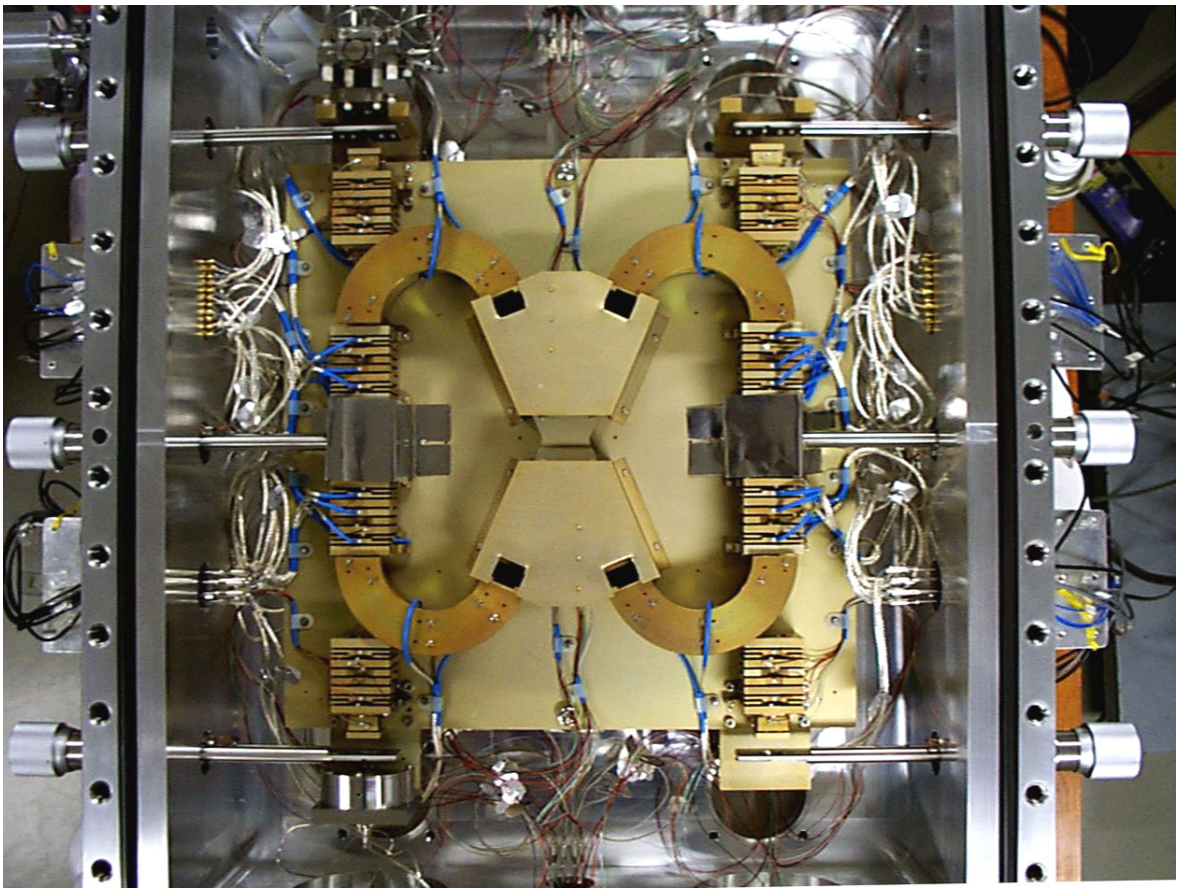

Fig. 4-7 Photograph of the 'MULTUM Linear plus' in the vacuum chamber.

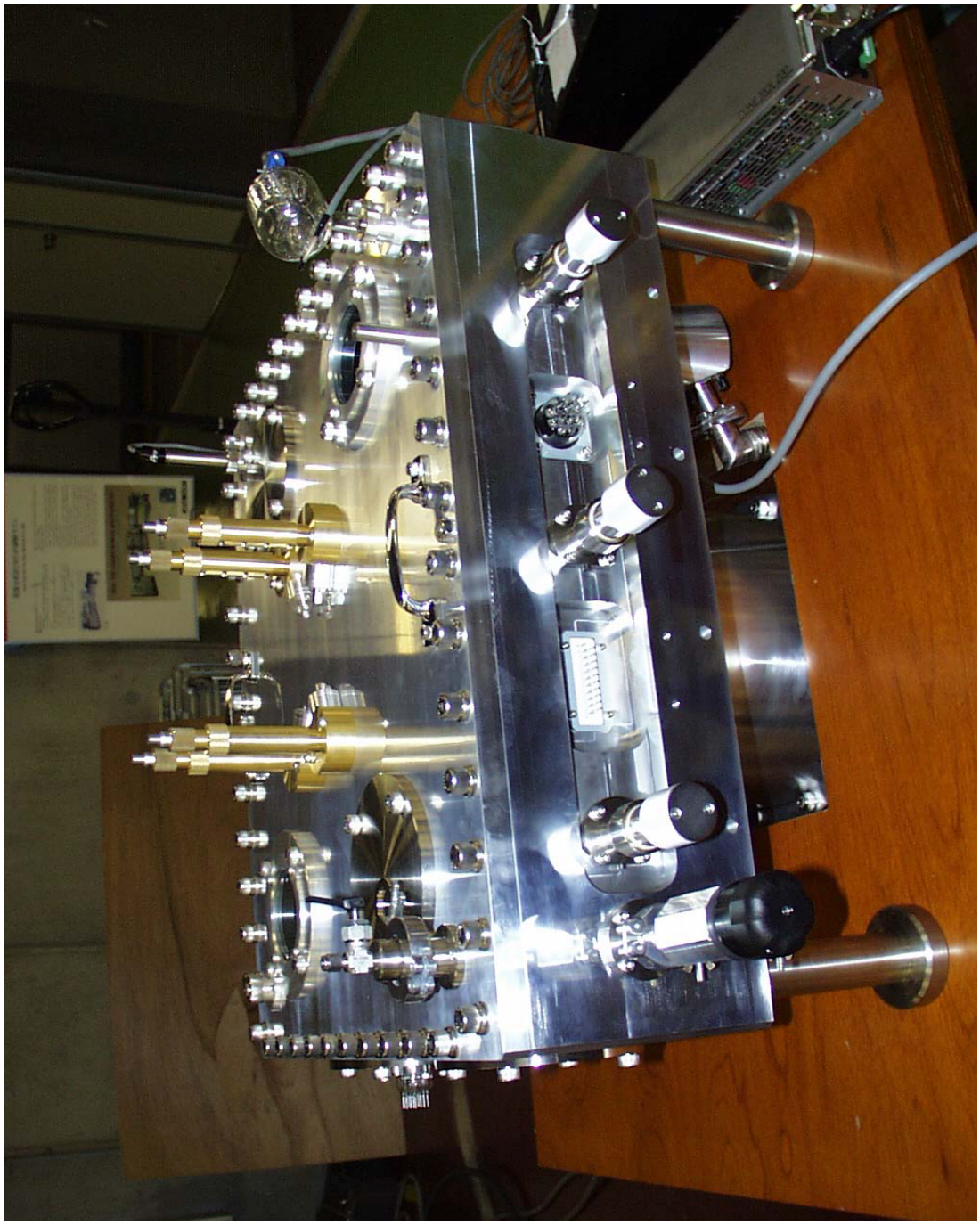

Fig. 4-8 Photograph of the outside appearance of the vacuum chamber.

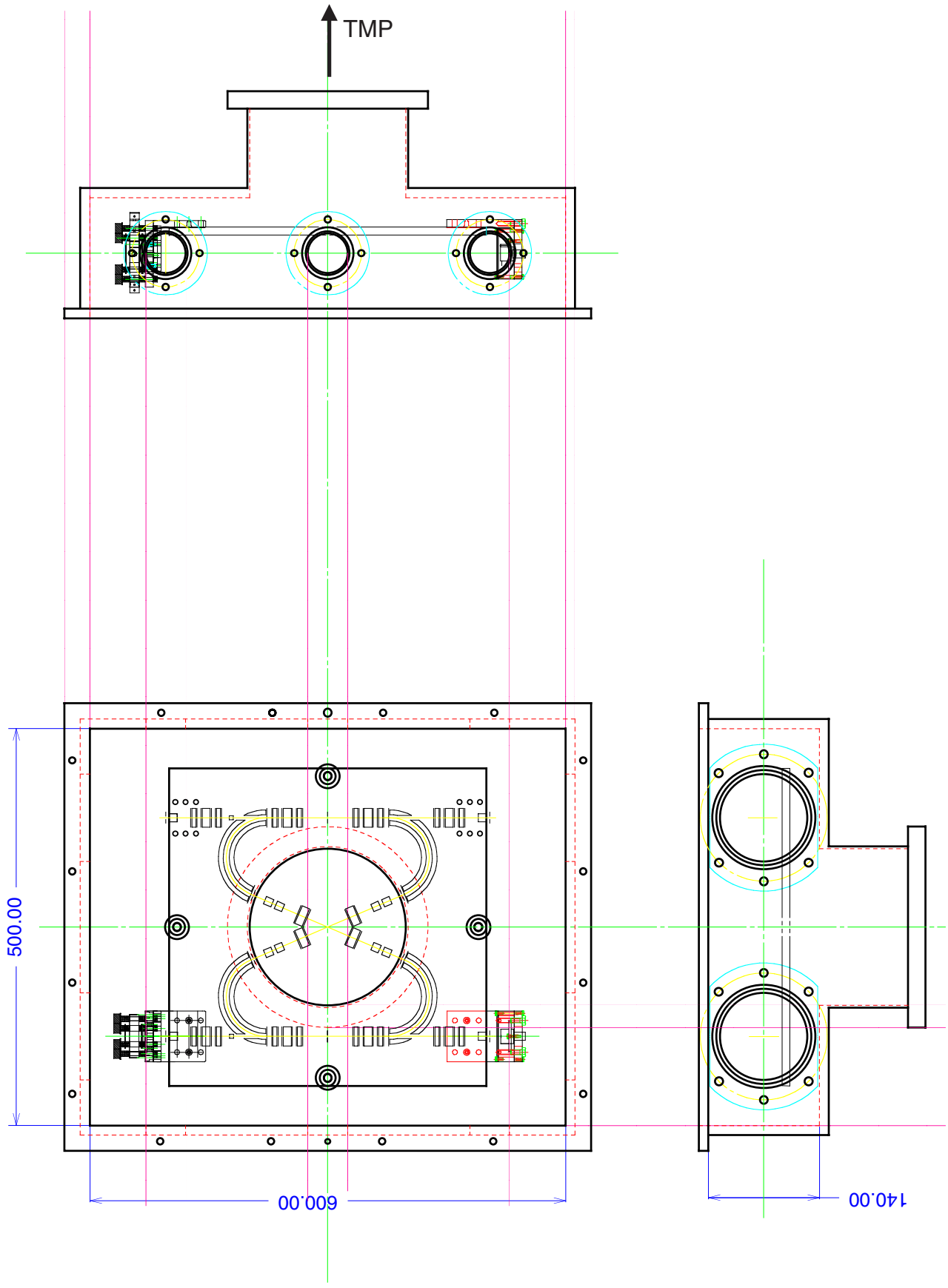

Fig. 4-9 Drawing of the vacuum chamber.

PT1500, Hiroshima, Japan). The vacuum was maintained at 2.5×10^{-7} Torr. Two main slits, two collector slits, two α slits and four β slits are installed.

4.3 Ion source

An electron impact ionization ion source similar to a two-stage acceleration ion source proposed by Wiley and McLaren [4-1] was used. This type of ion source can compensate for the flight time deviation caused by the distribution of the initial position of ions. This focusing is satisfied in the linear part of 'MULTUM Linear plus.' A schematic drawing of a two-stage acceleration ion source is shown in Fig. 4-10. In this ion source, a gaseous sample in the ionization field is ionized by an electron beam. The operating conditions of the electron gun of the ion source were (1) the filament current was about 4.0 A, (2) the electron energy was 160 ~ 200 eV and (3) the transmitted electron current was about 300 μA. The electron gun, the push plate and the center plate were floated at about 1400 V. Ions were bunched by applying pulse voltage of 180 ~ 220 V to the push plate. Then the total acceleration voltage of ions was 1.5 kV. Two types of ion source were made. The first one was used for the preliminary experiments. This source was large and not well vacuum shielded. A photograph of this ion source is shown in Fig. 4-11. The second one was improved on the size and the vacuum shield. A photograph of this ion source is shown in Fig. 4-12.

4.4 Detector and data acquisition system

Two micro-channel plates of 14.5 mm diameter (F4655-10, Hamamatsu, Shizuoka, Japan) were attached at the positions of Detector 1 and Detector 2 in Fig. 4-3. The output signals were accumulated with a digital oscilloscope (LC564A, LeCroy Japan Corp., Osaka, Japan) .

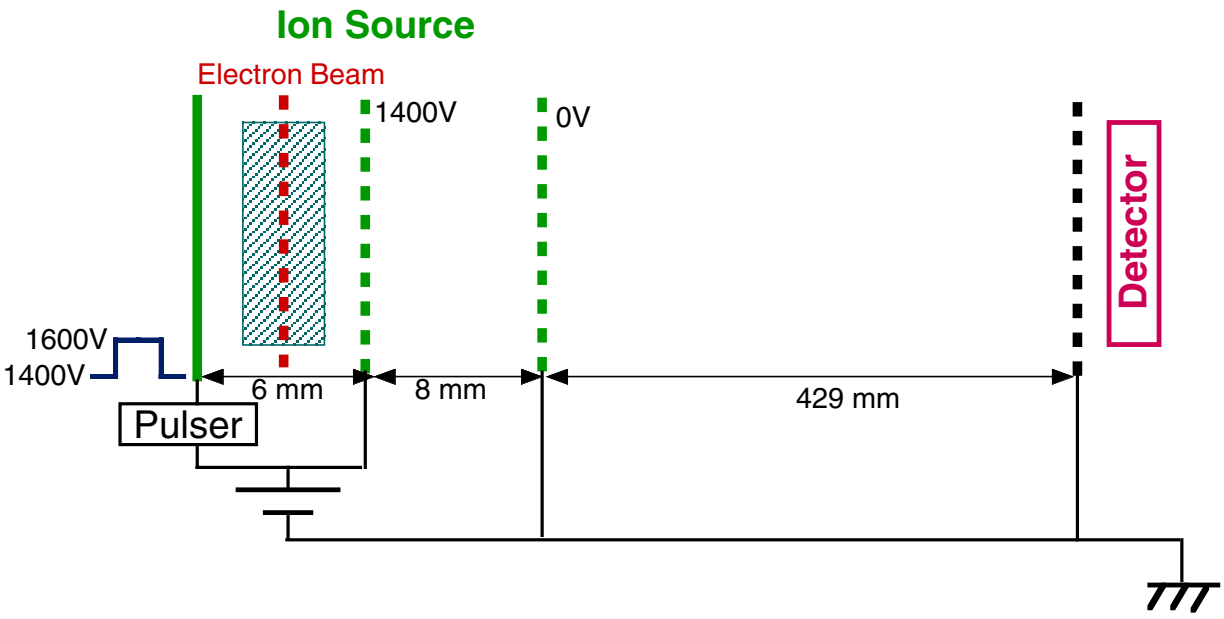

Fig. 4-10 Schematic drawing of a two-stage acceleration ion source.

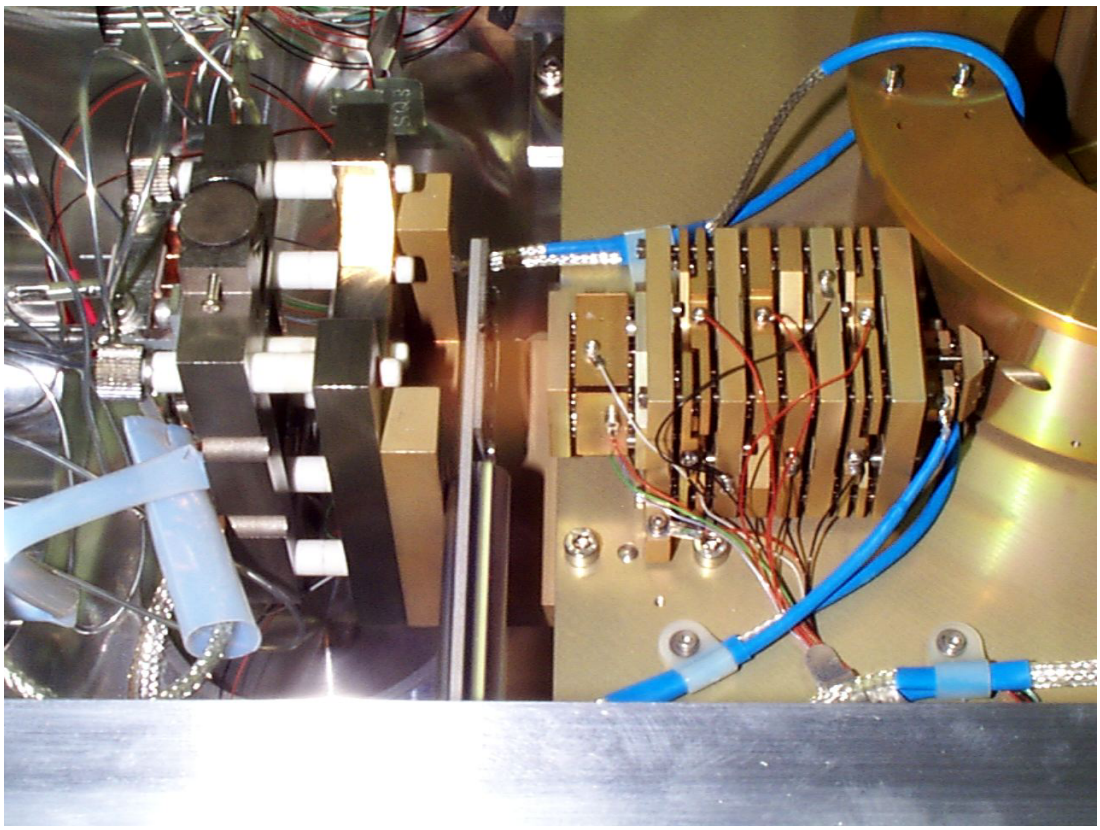

Fig. 4-11 Photograph of the old ion source and the quadrupole triplet.

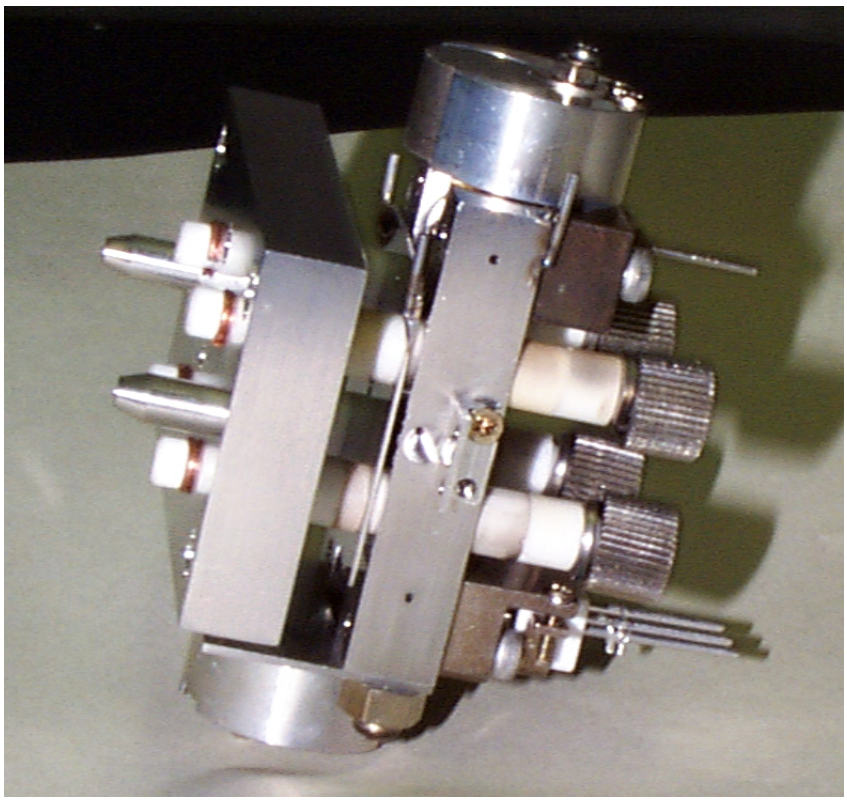

Fig. 4-12 Photograph of the new ion source.

Fig. 4-14 Photograph of the electric circuit unit.

4.5 Operation system

The block diagram of the pulse control circuits is shown in Fig. 4-13. The oscillator provides a trigger pulse for a digital pattern generator (CompuGen T30, Gage Applied Sciences Inc., Montreal, Canada). The digital pattern generator provides the timing signals for the ion source, the ion gate, the sector I or III and IV electrodes, the quadrupole triplets at linear TOF mass spectrometer and the digital oscilloscope. As ions were injected into the multi-turn parts, the voltage of sector IV was off and the voltages of quadrupole lenses Q14, Q15 and Q16 were the voltages for linear TOF mode. Before the ions returned, the voltage of sector IV was turned on, the voltages of quadrupole lenses Q14 and Q16 were turned off and the voltage of quadrupole lens Q15 was switched to the voltage for circulation. After the ions had undergone the desired cycles, the voltage of sector I or III was turned off and the voltages of quadrupole lenses Q1, Q2, Q3 or Q9, Q10, Q11 were switched to the voltages for linear TOF to eject the ions from the multi-turn part. A photograph of the electric circuit unit is shown in Fig. 4-14. This unit consists of electric power supplies and switching electric circuits. The voltage applied to each electrodes can be controlled in discrete by the potentiometers on the front panel of this unit.

Generally, the light ions catch up and pass the heavy ions in a multi-turn part. In order to avoid such complicating phenomena, an ion gate was introduced to eject the undesired ions.

REFERENCES

[4-1] W. C. Wiley and I. H. McLaren, *Rev. Sci. Instrum.*, **26** (1955) 1150 - 1157.

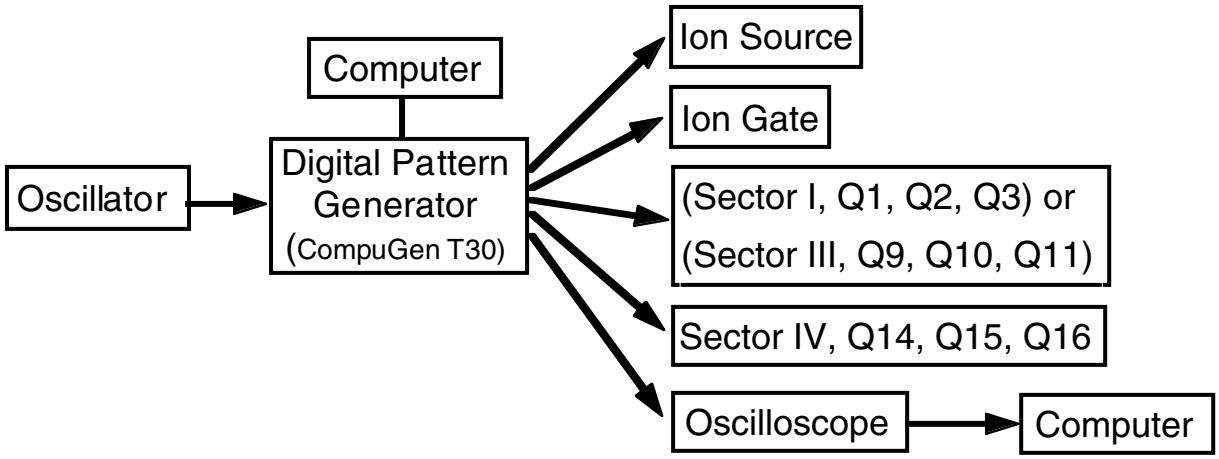

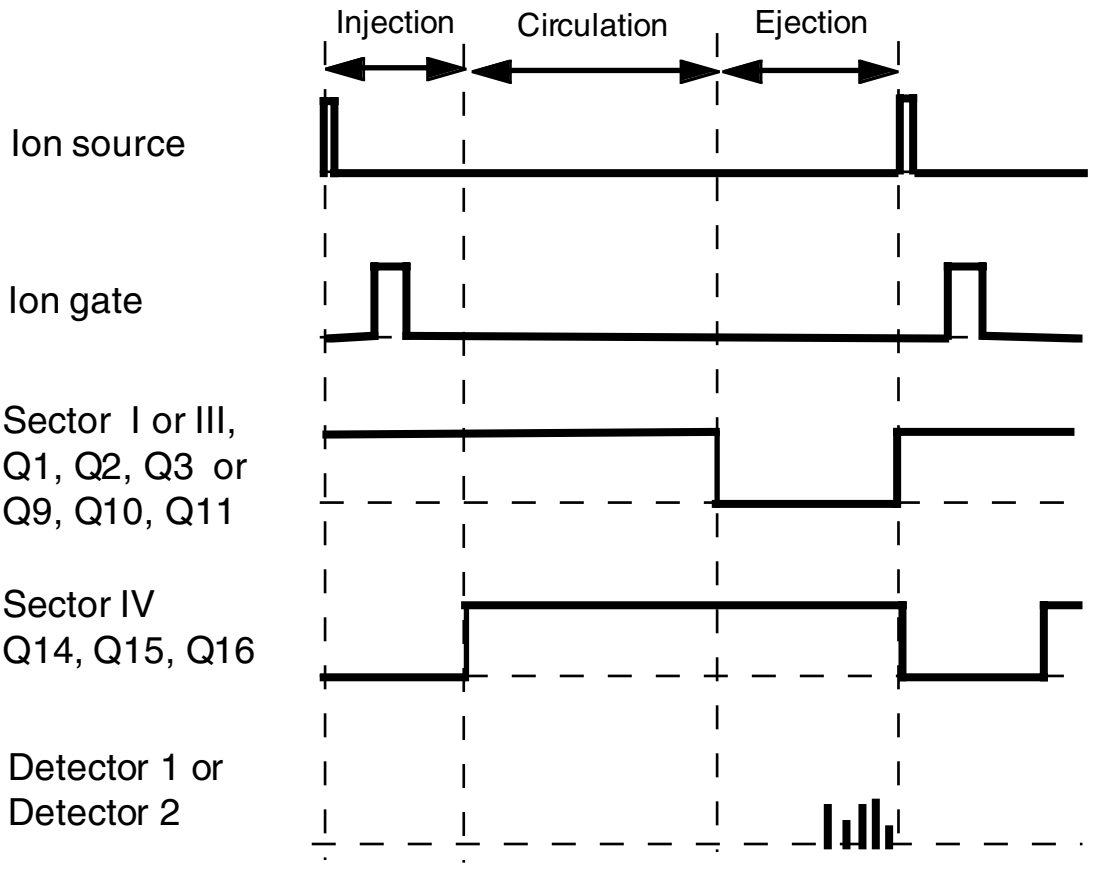

Fig. 4-13 Block diagram of the pulse control circuits.

V. Performance and Results

5.1 Introduction

Generally, the mass resolution of a TOF mass spectrometer is directly proportional to its total flight path length under the assumption of a constant width of ion packet during the flight. However, if the aberrations are too large, mass resolution may decrease after many cycles. Hence, the increase in the mass resolution with the number of cycles should be proved by experiment.

5.2 Measurements of Xe

TOF spectra of Xe^+ were acquired from 0.5 to 13.5 cycles using the micro-channel plate at Detector 2 position. The ion gate was used to inject only Xe^+ ions into the multi-turn part and eject the undesired ions such as multiply charged Xe and ions of residual gases.

The operating conditions of the electron gun of the ion source were (1) the filament current was 3.9 A and (2) the electron energy was 140 eV. Ions were bunched by applying pulse voltage of 180 V to the push plate. The total acceleration voltage of ions was 1.5 kV. The background pressure was 5.5×10^{-7} Torr and the vacuum pressure increased to 1.2×10^{-6} Torr when xenon gas was introduced.

The sampling rate of the digital oscilloscope was 2 GS/s. The following TOF spectra were obtained by summing 5000 spectra on the digital oscilloscope. The oscillator frequency was 100 Hz.

The TOF spectra of Xe^+ acquired using five different flight path lengths (0.5, 3.5, 6.5, 9.5 and 13.5 cycles) are shown in Fig. 5-1. The ordinate is normalized so that the height of the peak of $^{132}Xe^+$ at half cycle is 100. It is clear that the peak width is almost the same in all cases, while the difference in TOF between the peaks of Xe^+ isotopes increases as turning around many times; the mass resolution increases according to the number of cycles. It is clear that the ion transmission through the

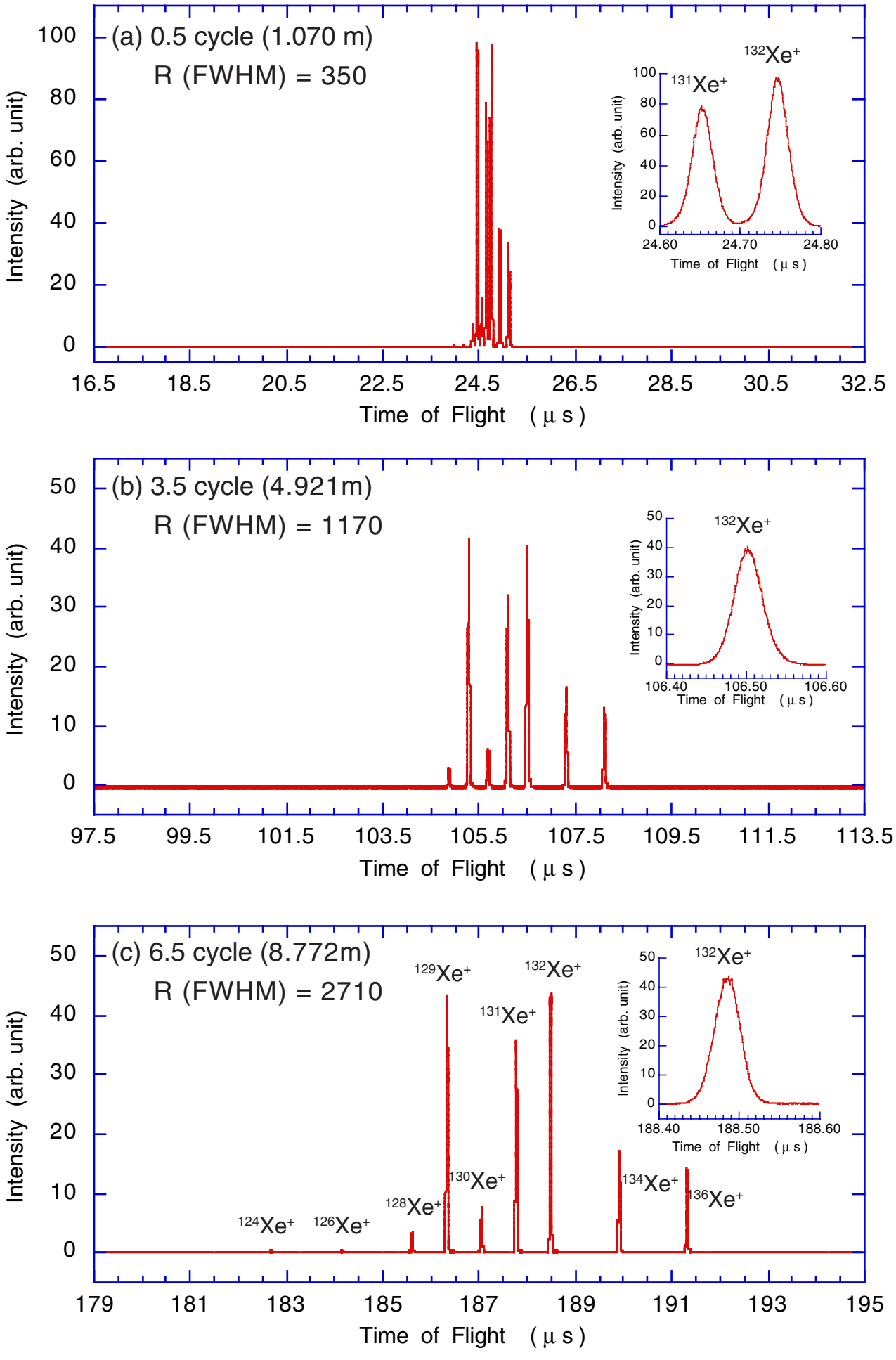
(a) 0.5 cycle (1.070 m)
R (FWHM) = 350
Intensity (arb. unit)
Time of Flight (μs)
131Xe+
132Xe+
(b) 3.5 cycle (4.921m)
R (FWHM) = 1170
Intensity (arb. unit)
Time of Flight (μs)
132Xe+
(c) 6.5 cycle (8.772m)
R (FWHM) = 2710
Intensity (arb. unit)
Time of Flight (μs)
124Xe+
126Xe+
128Xe+
129Xe+
130Xe+
131Xe+
132Xe+
134Xe+
136Xe+

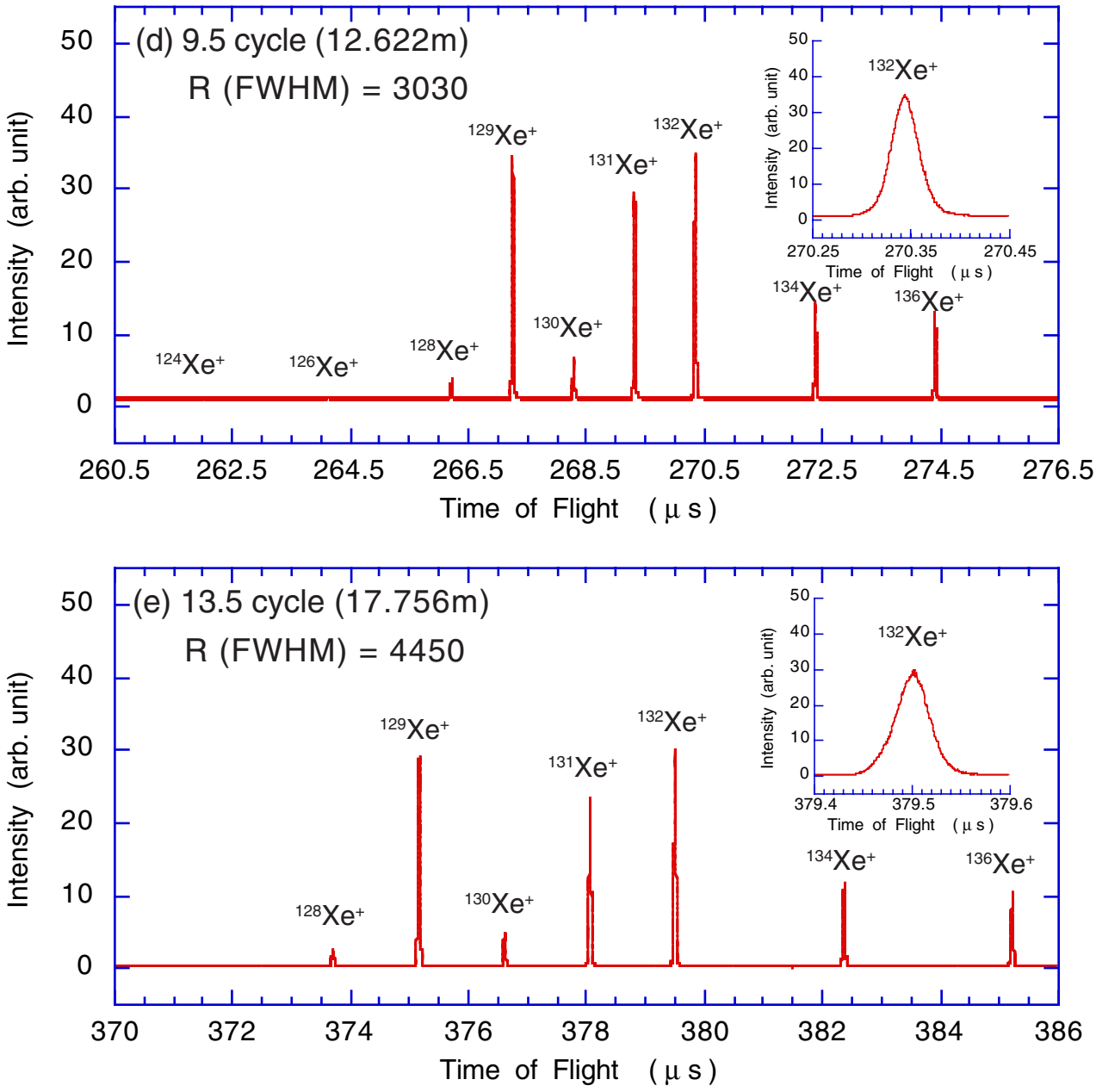

Fig. 5-1 TOF spectra of Xe^+ acquired using five different flight path lengths. (a) Half cycle (the flight path length is correspond to 1.070 m), (b) 3.5 cycles (4.921 m), (c) 6.5 cycles (8.772 m), (d) 9.5 cycles (12.622 m) and (e) 13.5 cycles (17.756 m). The ordinate is normalized so that the height of the peak of $^{132}Xe^+$ at half cycle is 100.

system was more than 90 % after one cycle. The intensity of Xe^+ ions after 10 cycles was still 30% of that after a half cycle. Moreover, from 5.5 to 13.5 cycles no significant decrease of the ion intensity was observed. The detail discussions about the mass resolution and the ion transmission are described in the later section in this chapter.

5.3 Measurements of CO & N_2

TOF spectra of CO^+ and N_2^+ were acquired from 0.5 to 100.5 cycles using CO_2 gas as a sample. The ion gate was used to inject only ions which has m/z = 20 ~ 35 into the multi-turn part.

The operating conditions of the electron gun of the ion source were (1) the filament current was 4.0~4.2 A, (2) the electron energy was 140 eV. Ions were bunched by applying pulse voltage of 185 V to the push plate. The total acceleration voltage of ions was 1.5kV. The background pressure was 2.5×10^{-7} Torr and the vacuum pressure increased to 2.5×10^{-6} Torr when CO_2 gas was introduced.

The sampling rate of the digital oscilloscope was 2 GS/s. The following TOF spectra were obtained by summing 20000 spectra on the digital oscilloscope. The oscillator frequency was 100 Hz.

The TOF spectra of CO^+ and N_2^+ acquired using five different flight path lengths (0.5, 25.5, 50.5, 75.5 and 100.5 cycles) are shown in Fig. 5-2. The mass resolution achieved about 18000 after 100.5 cycles. However, it is seem that the mass resolution was not proportional to the flight path length. The detail discussions about the mass resolution are described in the next section.

5.4 Mass resolution

In a TOF mass spectrometer using only electric sectors and electric quadruple lenses, the path length deviation l_f at a detector is given in the second order approximation as :

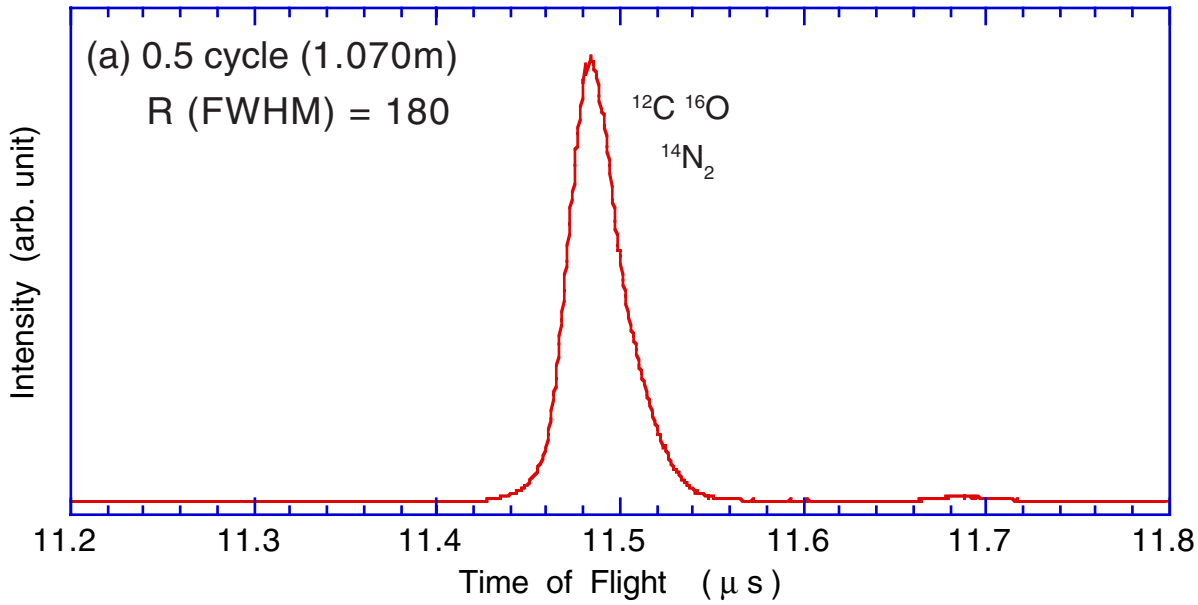
(a) 0.5 cycle (1.070m)
R (FWHM) = 180
$^{12}C\ ^{16}O$
$^{14}N_2$
Intensity (arb. unit)
11.2
11.3
11.4
11.5
11.6
11.7
11.8
Time of Flight (μs)

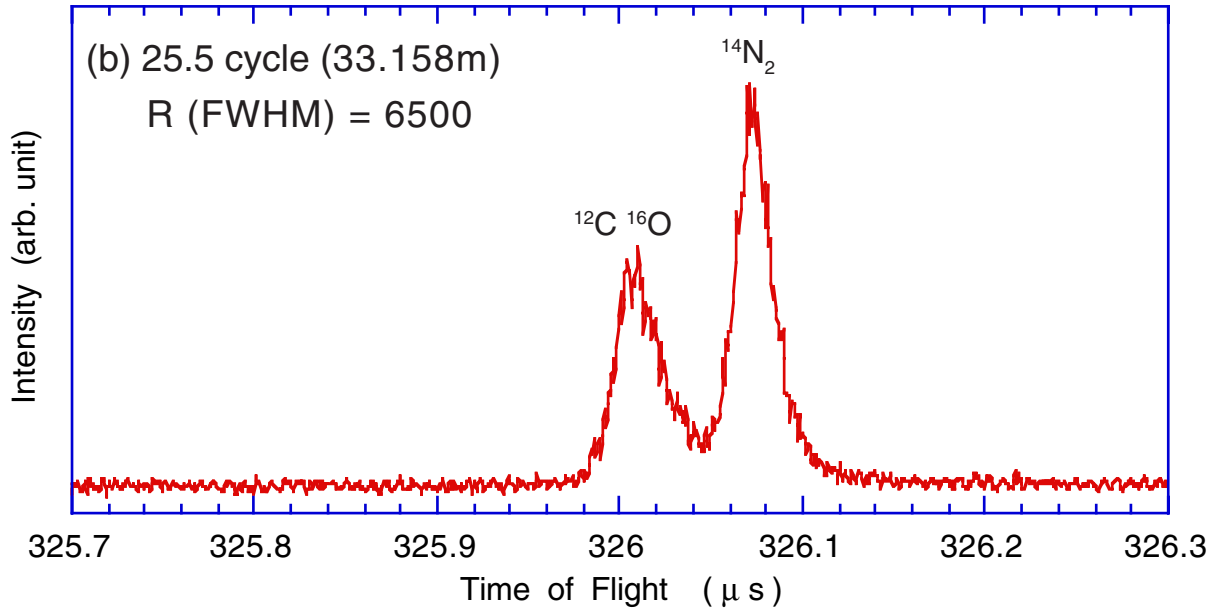
(b) 25.5 cycle (33.158m)
R (FWHM) = 6500
$^{14}N_2$
$^{12}C\ ^{16}O$
Intensity (arb. unit)
325.7
325.8
325.9
326
326.1
326.2
326.3
Time of Flight (μs)

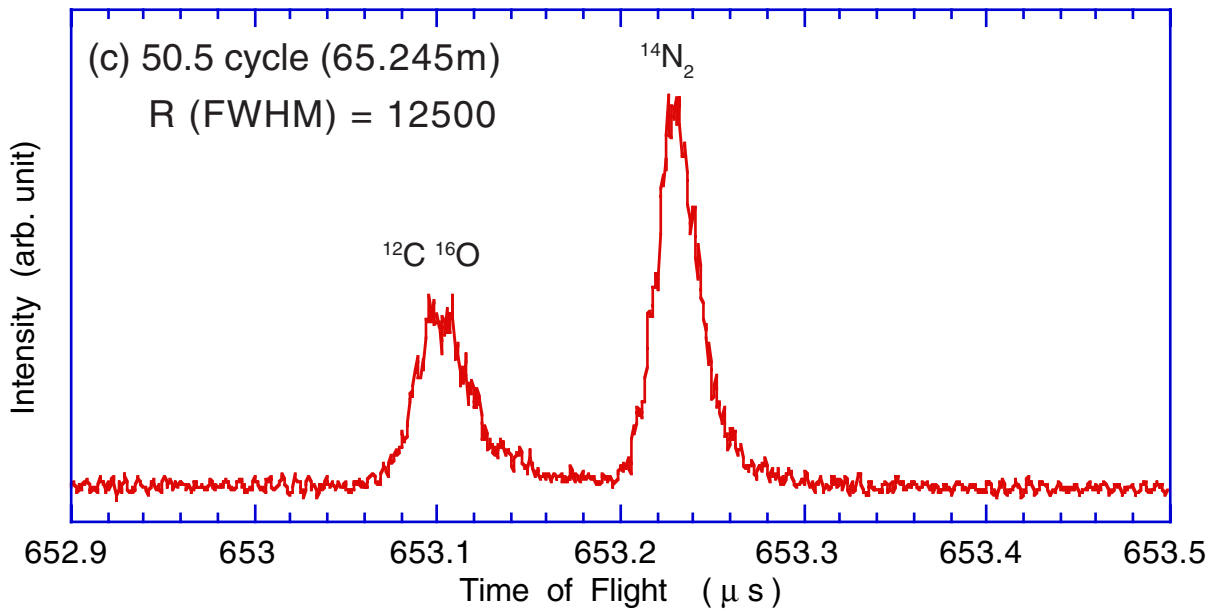
(c) 50.5 cycle (65.245m)
R (FWHM) = 12500
$^{14}N_2$
$^{12}C\ ^{16}O$
Intensity (arb. unit)
652.9
653
653.1
653.2
653.3
653.4
653.5
Time of Flight (μs)

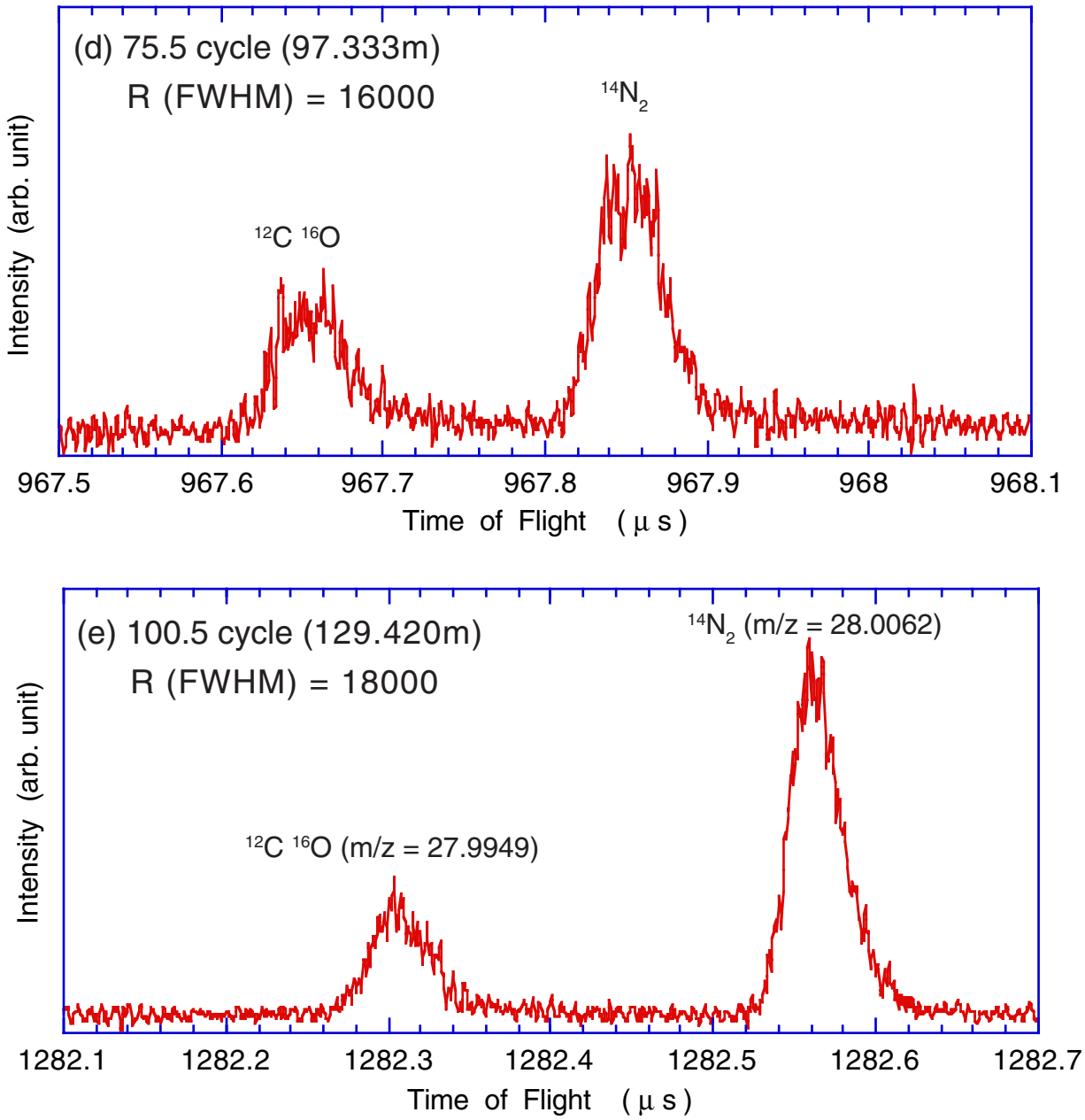

Fig. 5-2 TOF spectra of N_2^+ and CO^+ acquired using five different flight path lengths. (a) Half cycle (the flight path length is correspond to 1.070 m), (b) 25.5 cycles (33.158 m), (c) 50.5 cycles (65.245 m), (d) 75.5 cycles (97.333 m) and (e) 100.5 cycles (129.420 m). The ion source conditions were not identical in these five spectra.

$$l_f = A\,(l \mid x)\,x_0 + A\,(l \mid \alpha)\,\alpha_0 + A\,(l \mid \delta)\,\delta + A\,(l \mid x\,x)\,x_0^2 + A\,(l \mid x\,\alpha)\,x_0\,\alpha_0 + A\,(l \mid x\,\delta)\,x_0\,\delta + A\,(l \mid \alpha\,\alpha)\,\alpha_0^2 + A\,(l \mid \alpha\,\delta)\,\alpha_0\,\delta + A\,(l \mid \delta\,\delta)\,\delta^2 + A\,(l \mid y\,y)\,y_0^2 + A\,(l \mid y\,\beta)\,y_0\,\beta_0 + A\,(l \mid \beta\,\beta)\,\beta_0^2 \quad (5\text{-}1)$$

where x_0 and y_0 are the half width and height of a source slit, respectively, α_0 and β_0 are the horizontal and vertical inclination angles at the source slit, respectively, and δ is the relative energy deviation.

Because the flight time of an ion is proportional to the square root of its mass, the mass resolution, $m / \Delta m$, of a TOF mass spectrometer is given by the half of the time resolution.

$$\frac{m}{\Delta m} = \frac{T_f}{2\,\Delta t} \quad (5\text{-}2)$$

where T_f is the flight time of the ion, and Δt expresses the resolvable time width which is given by $l_f / v_0 + t_0 + t_d$. Here, v_0 is the velocity of a reference ion, t_0 is the initial packet width at the source slit and t_d is the time resolution of the detection system. In these experiments, t_d was almost negligible compared with other elements. Thus, the time resolution of the detection system t_d can be neglected. The flight time T_f is given by L_f / v_0, where L_f is the total flight length. Therefore, the mass resolution of a TOF mass spectrometer can be expressed as :

$$\frac{m}{\Delta m} = \frac{L_f}{2\left(l_f + v_0\,t_0\right)} = \frac{A\,(l \mid \gamma)}{l_f + v_0\,t_0} \quad (5\text{-}3)$$

where $A(l \mid \gamma) = L_f / 2$ at the definition.

It is seemed from Fig. 5-1 and Fig 5-2 that the mass resolution increased according to the number of cycles. Here, detailed experiments using N_2 were done to argue about the relation between the flight path length (the number of cycles) and the mass resolution.

The relation between the number of cycles and the peak width (full width at half maximum, FWHM) of $^{14}N_2^+$ is shown in Fig. 5-3. The relation between the number of cycles and the mass resolution is shown in Fig. 5-4. The mass resolution is defined as the peak width (FWHM) of $^{14}N_2^+$. The operating conditions of the electron gun of the ion source were (1) the filament current was 4.0 A, (2) the electron energy was

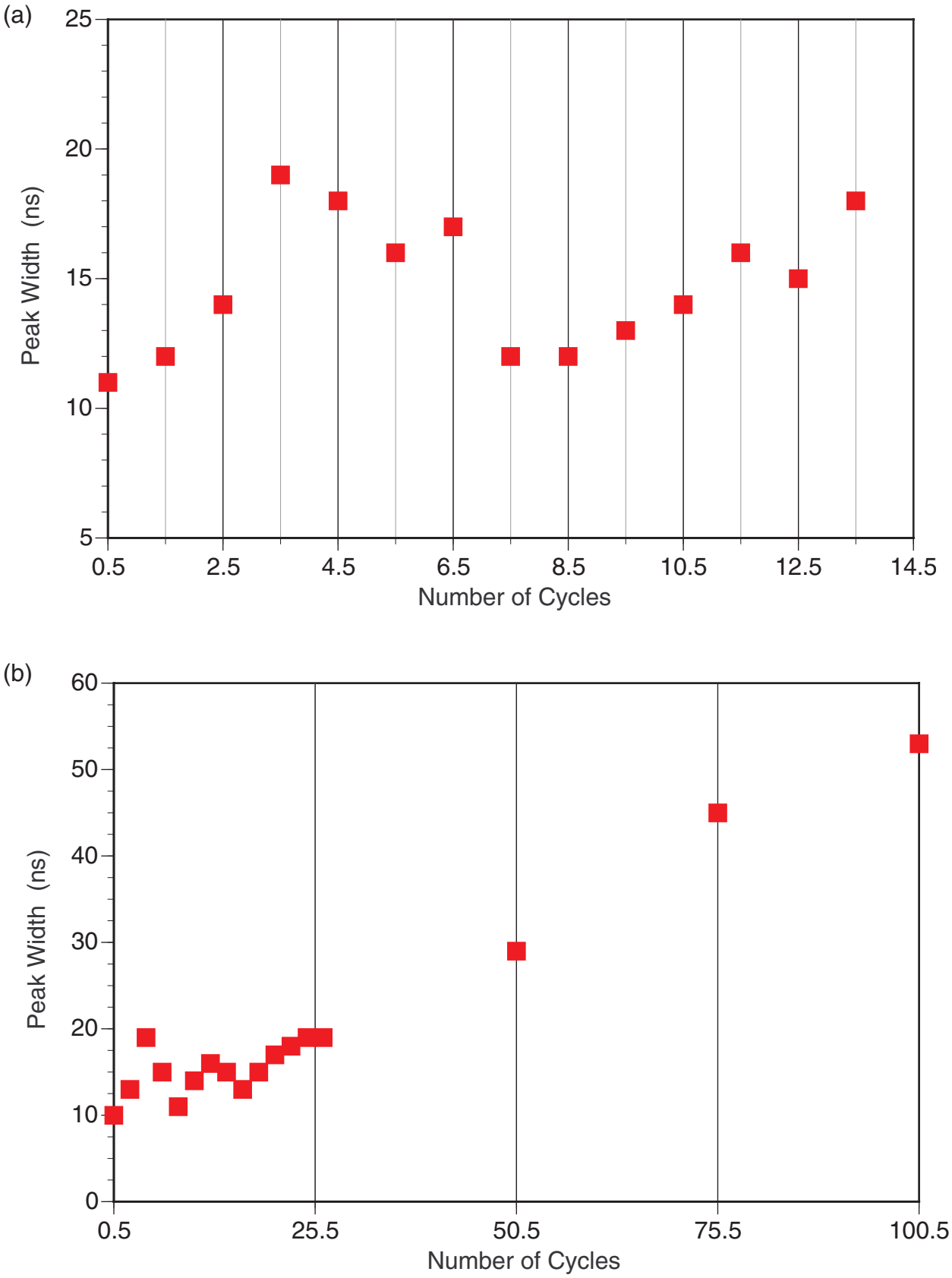

Fig. 5-3 The relation between the number of cycles and the peak width (full width at half maximum, FWHM) of $^{14}N_2^+$ (a) 0.5 ~ 13.5 cycles and (b) 0.5 ~ 100.5 cycles.

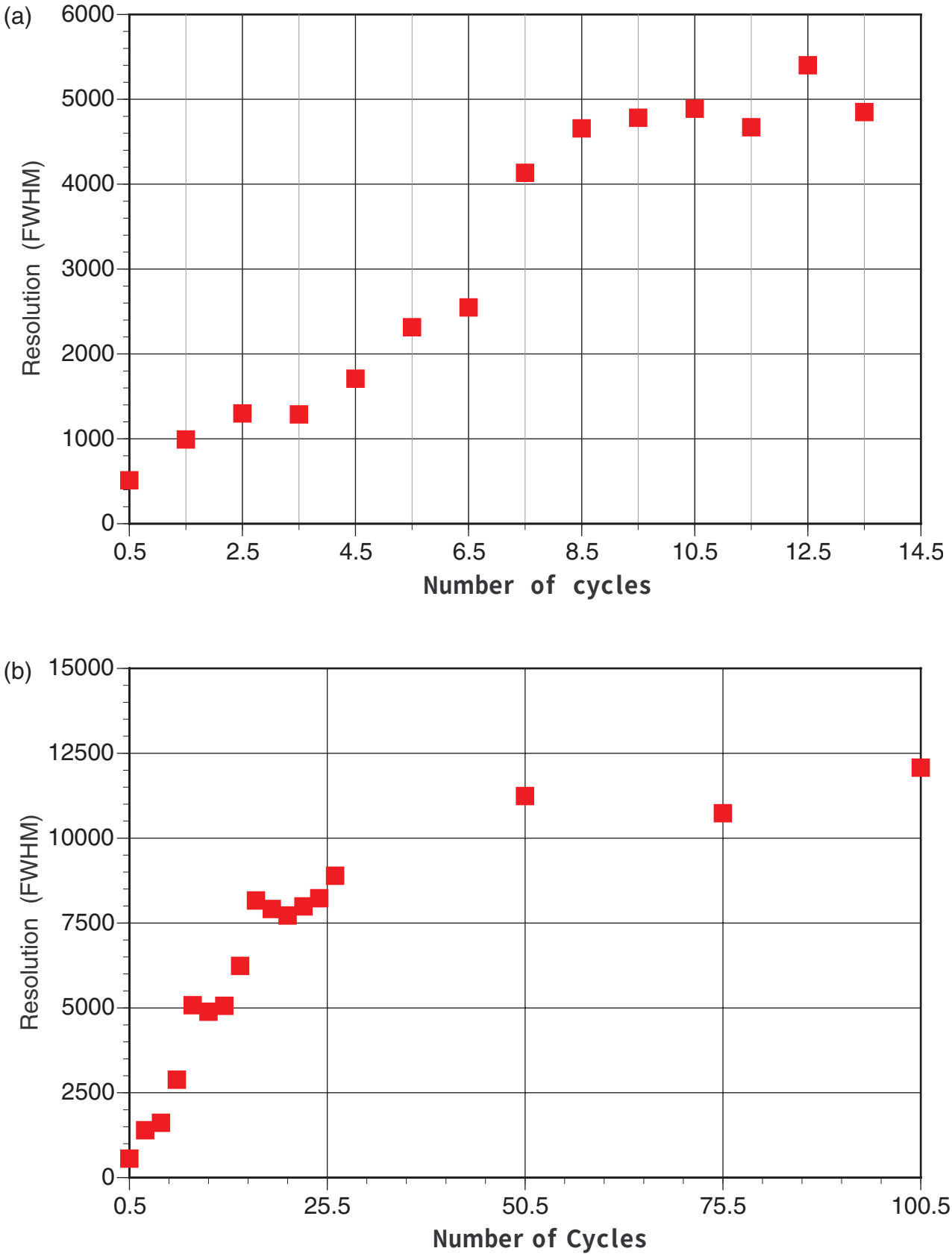

Fig. 5-4 The relation between the number of cycles and the mass resolution (a) 0.5 ~ 13.5 cycles and (b) 0.5 ~ 100.5 cycles. The mass resolution is defined as the peak width (FWHM) of $^{14}N_2^+$.

150 eV and (3) the peak electron current was 300 μA. Ions were bunched by applying pulse voltage of 220 V to the push plate. The total acceleration voltage of ions was 1.5kV. The background pressure was 2.5×10^{-7} Torr, and the vacuum pressure increased to 1.0×10^{-6} Torr when air was introduced. The full width of a source slit was 1 mm in the both horizontal and vertical direction.

If we consider only the path length deviation in the first order approximation, the path length deviation $l_f \sim 0$ in this system. Therefore, the mass resolution is proportional to the flight path length from Eqn. (5-3). It is obvious from Fig. 5-4 that the mass resolution was proportional to the length of flight path from 0.5 ~ 25.5 cycles. However, the mass resolution was gradually approaching the fixed value when the flight path length was more than 25.5 cycles. Two reasons why the mass resolution does not increase proportionally can be considered; (1) the path length deviation l_f is increased by the collisions with neutral particles and (2) the path length deviation l_f is increased because of the influence of higher order terms.

If there is the influence of the collisions with neutral particles, a rate of increase of the peak width is depend on the vacuum pressure in the chamber. The pressure dependence of the peak width is shown in Fig. 5-5. No significant difference in the peak width was found due to the difference of the vacuum pressure. Therefore, it can be concluded that collisions with neutral particles have little effect on the peak width.

Next, we have to consider the influence of the higher order terms. Here, only the multi-turn part is taken into consideration because the linear part can be neglected according to the increase of the number of cycles. It is most likely that the second order term $R(l \mid \delta\delta)$ gives most significant influence. The flight time image shapes were simulated by TRIO-DRAW changing the initial condition of the relative energy deviation δ. The results of the simulation are shown in Fig. 5-6. It is easily found that the experimental results agree approximately with the simulation results whose condition is $\delta\max = 0.01$. Furthermore, more detailed argument about this problem is done. Since the perfect focus is satisfied in the first order approximation, the mass resolution in the MULTUM geometry is expressed from Eqn. (5-3) as :

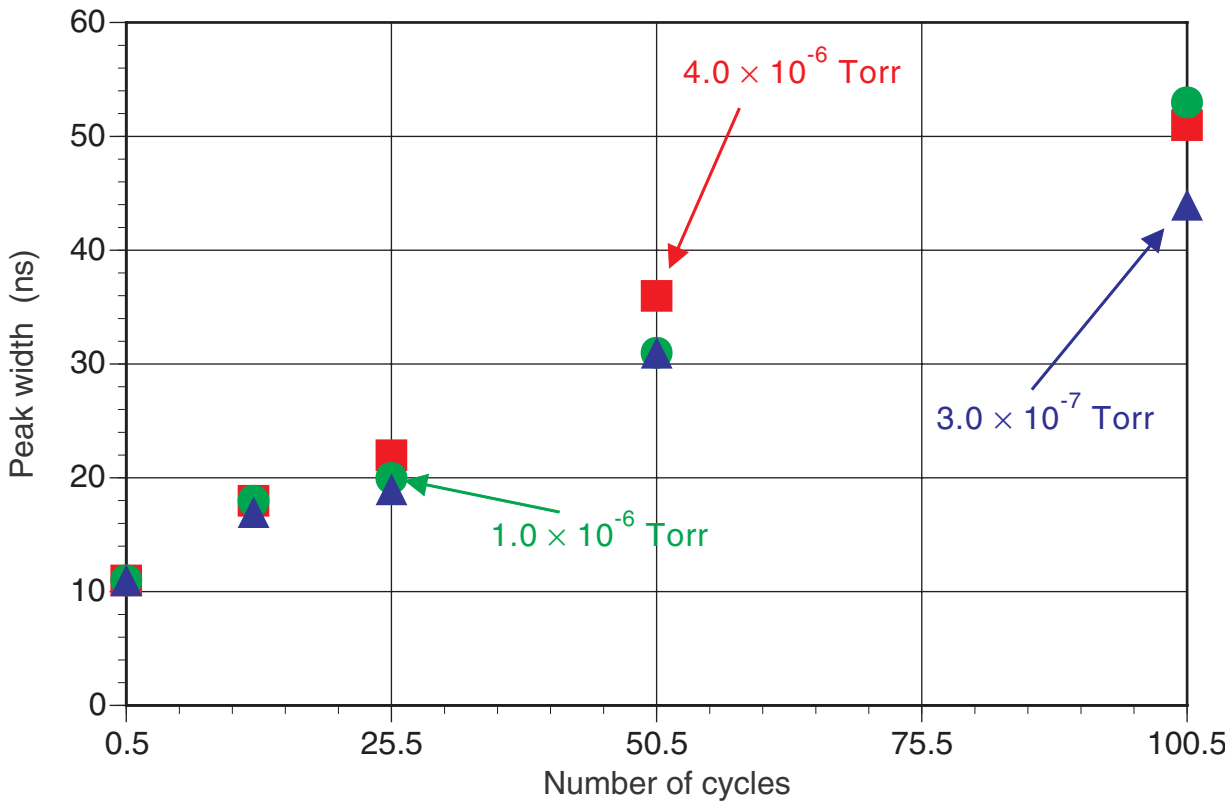

Fig. 5-5 The relation between the number of cycles and the peak width (FWHM) of $^{14}N_2^+$ when the pressure in the vacuum chamber is changed. The ion source conditions were the same as the case of Fig. 5-3.

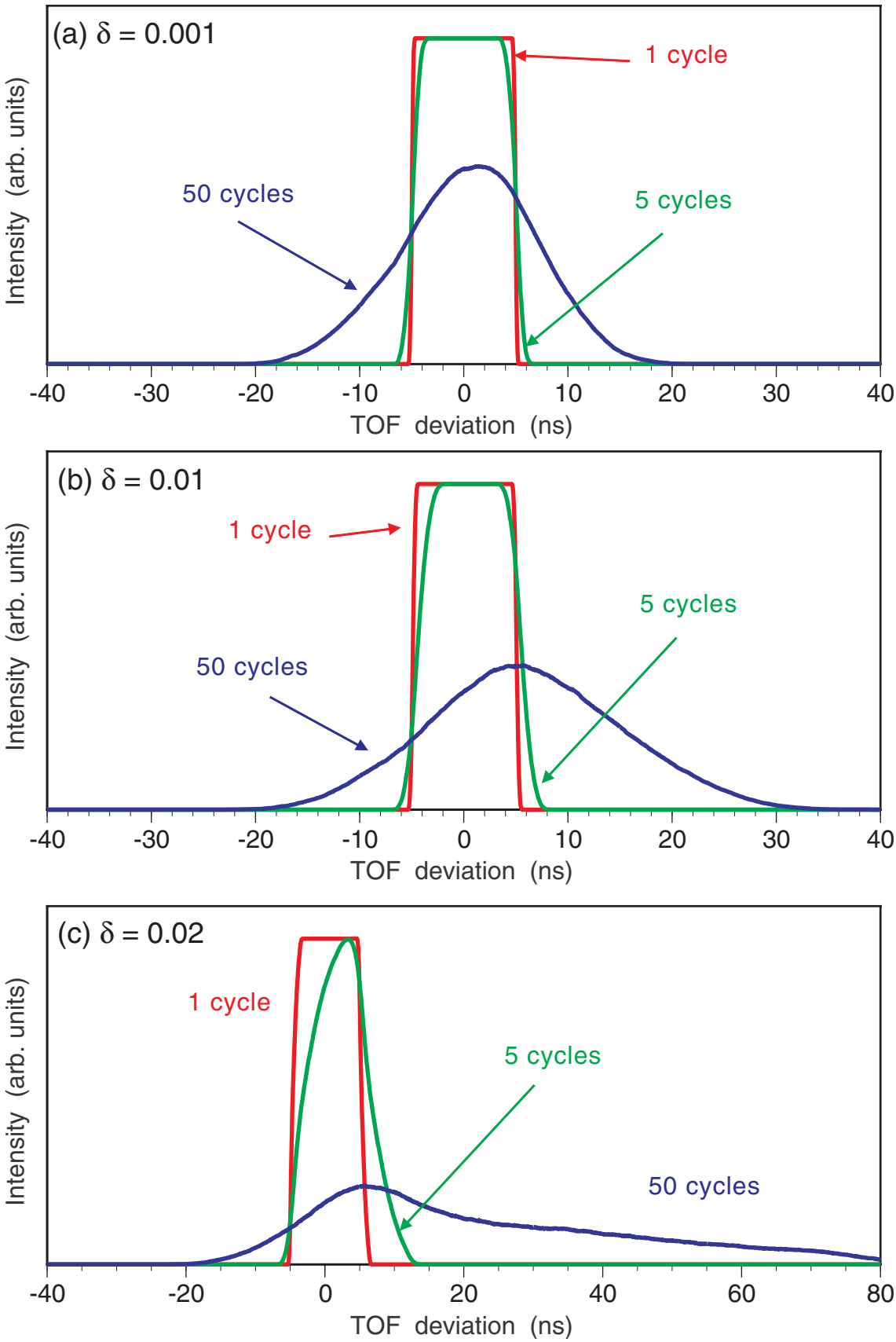

Fig. 5-6 The flight time image shapes simulated by TRIO-DRAW changing the initial condition of the relative energy deviation δ. Pulse width = 20 ns, $x$max = 0.0005 m, αmax = 0.01 rad, $y$max = 0.0005 m, βmax = 0.01 rad, m/z = 28, accelerating voltage = 1500 V. (a) δmax = 0.001, (b) δmax = 0.01 and (c)δmax = 0.02.

$$\frac{m}{\Delta m} = \frac{R(l \mid \gamma) \times n}{l_{2nd} \times n + t_0 \, v_0} \tag{5-4}$$

where n is the number of cycles and l_{2nd} is the second order aberration of one cycle expressed as followings using the major second order coefficients.

$$l_{2nd} = R(l \mid x\,x)\, x_0^2 + R(l \mid x\,\delta)\, x_0\, \delta + R(l \mid \delta\,\delta)\, \delta^2 + R(l \mid y\,y)\, y_0^2 + \cdots \tag{5-5}$$

From Table 3-8, the major second order coefficients are

$$\begin{aligned} &R(l \mid x\,x) = -118.4\,, \;\; R(l \mid x\,\delta) = 4.919 \\ &R(l \mid \delta\,\delta) = 0.3346\,, \;\; R(l \mid y\,y) = 60.13 \end{aligned} \tag{5-6}$$

Substituting the source slit conditions

$$x_0 = 0.0005 \text{ m},\;\; \alpha_0 = 0.01 \text{ rad},\;\; \delta = 0.01,\;\; y_0 = 0.0005 \text{ m},\;\; \beta_0 = 0.01 \text{ rad},\;\; t_0 = 10 \text{ ns} \tag{5-7}$$

for Eqn. (5-4), the limit mass resolution

$$\left(\frac{m}{\Delta m}\right)_{limit} \sim 15000 \tag{5-8}$$

can be estimated. Here, the initial packet width at source slit t_0 = 10 ns was estimated from the experiment result and the relative energy deviation δ = 0.01 was estimated above. This result was in agreement with the observed results.

5.5 Ion transmission

In this multi-turn TOF mass spectrometer, the perfect space focus is satisfied. Therefore, ions should not diverge with an increasing number of cycles around the system. It is clear from Fig. 5-1 that the ion signal intensity after 10 cycles was still 20 ~ 30% of that after a half cycle. Moreover, from 6.5 to 13.5 cycles no significant decrease of the ion intensity was observed. Here, detailed experiments using N_2 were done to argue about the relation between the flight path length (the number of cycles) and the ion signal intensity.

The variation of the relative ion transmission with the numbers of cycles is shown in Fig. 5-7. The ordinate is the area of $^{14}N_2^+$ peaks and is normalized so that the value at half cycle is 1. The experimental conditions were the same as section 5.4.

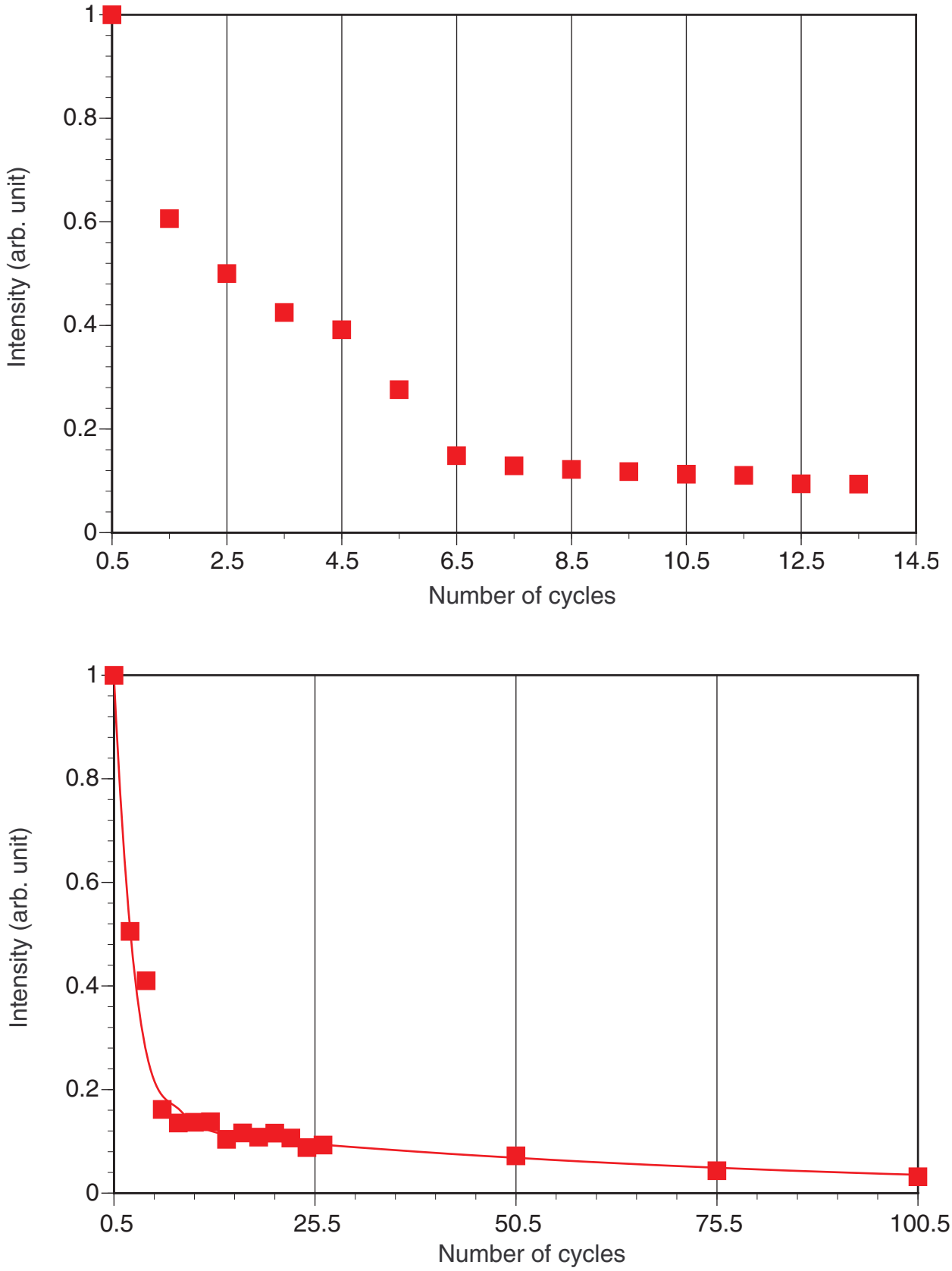

Fig. 5-7 The variation of relative ion transmission with the numbers of cycles. (a) 0.5 ~ 13.5 cycles and (b) 0.5 ~ 100.5 cycles. The ordinate is the area of $^{14}N_2^+$ peaks and is normalized so that the intensity at half cycle is 1.

It is clear from the figure that the transmittance from 0.5 ~ 6.5 cycles was different from the transmittance after 6.5 cycles. The decrease ratio of ion transmittance of the first 6.5 cycles was high and after 6.5 cycles it became low. In the case of the first 6.5 cycles, ions having large initial deviations were lost by hitting against the electrodes. The pressure dependence of the ion transmittance is shown in Fig. 5-8. It is clear that the decrease ratio depended on the pressure after 6.5 cycles. Therefore, the collision with neutral particles became the major reason after 6.5 cycles. To substantiate the above remarks, a collision cross section has been estimated by measuring the vacuum pressure dependence on the signal intensity.

The variation of the relative ion transmission with the vacuum pressure is shown in Fig. 5-9. If the ions were lost by the collision with neutral molecules, the variation of the intensity of ions ΔN are expressed as

$$\frac{\Delta N}{\Delta l} = -\sigma n N \tag{5-9}$$

where l [m], σ [m^2], n [m^{-3}] and N are the flight path length, the cross section, the density of neutral particle and the number of ions, respectively. Then the relation of the number of ions is derived as

$$N = N_0 \exp\left(-\sigma n l\right) \tag{5-10}$$

From the Boyle - Charles' law, Eqn. (5-10) is written as

$$N = N_0 \exp\left(-\frac{133.3 \times 6.022 \times 10^{23}}{R T} \sigma p l\right) \tag{5-11}$$

where p [Torr], R = 8.317 [$J \cdot mol^{-1} \cdot K^{-1}$] and T [K] are the pressure in the chamber, the gas constant and the temperature, respectively. From the result of parameter fitting, the cross section σ is derived. For example, the cross section σ for 100.5 cycles is

$$\sigma = 3.1 \times 10^{-19}\ [m^2] \tag{5-12}$$

The relation between the cross section and the number of cycles is shown in Fig. 5-10. A cross section should not originally depend on the number of cycles, but the experimental result shows that the cross section became large and it was gradually approaching the fixed value as the flight path length grows longer. Even if ions were scattered with small angle, they were lost as flight path length grows longer. Therefore

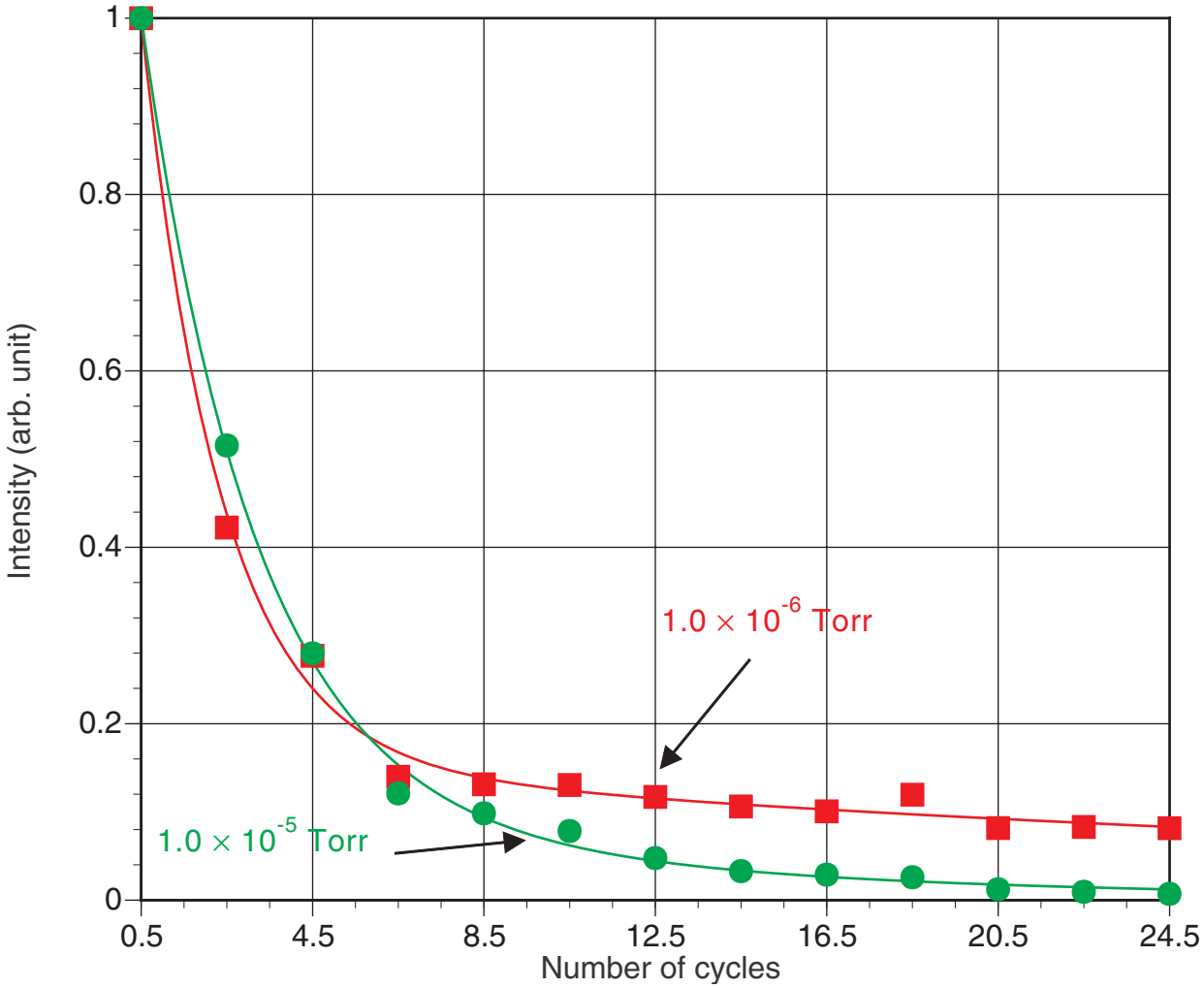

Fig. 5-8 The variation of the relative ion transmission with the numbers of cycles when the pressure in the vacuum chamber was changed. The ordinate is the area of $^{14}N_2^+$ peaks and is normalized so that the intensity at half cycle is 1. The ion source conditions were the same as the case of Fig. 5-7.

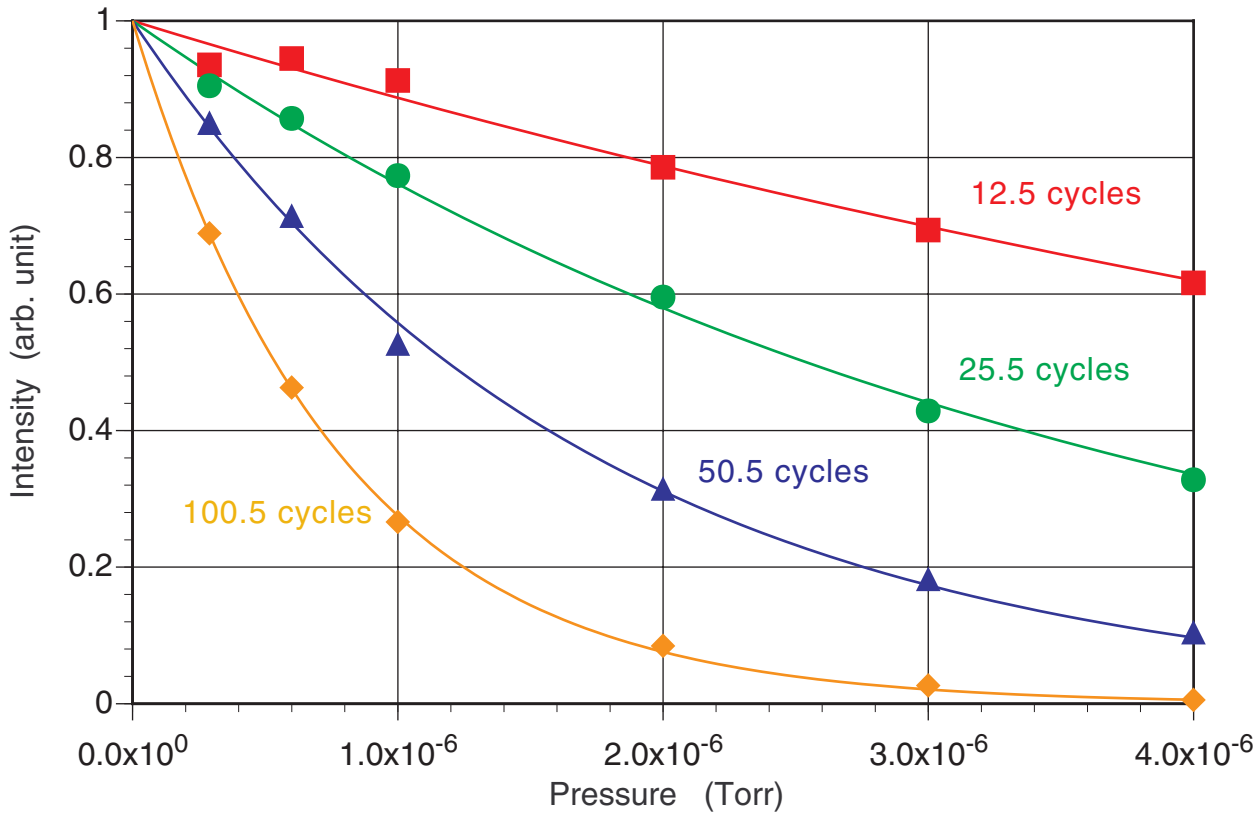

Fig. 5-9 The variation of the relative ion transmission efficiency with the vacuum pressure. The ordinate is the area of $^{14}N_2^+$ peaks divided by the value at half cycle. The ion source conditions were the same as the case of Fig. 5-7.

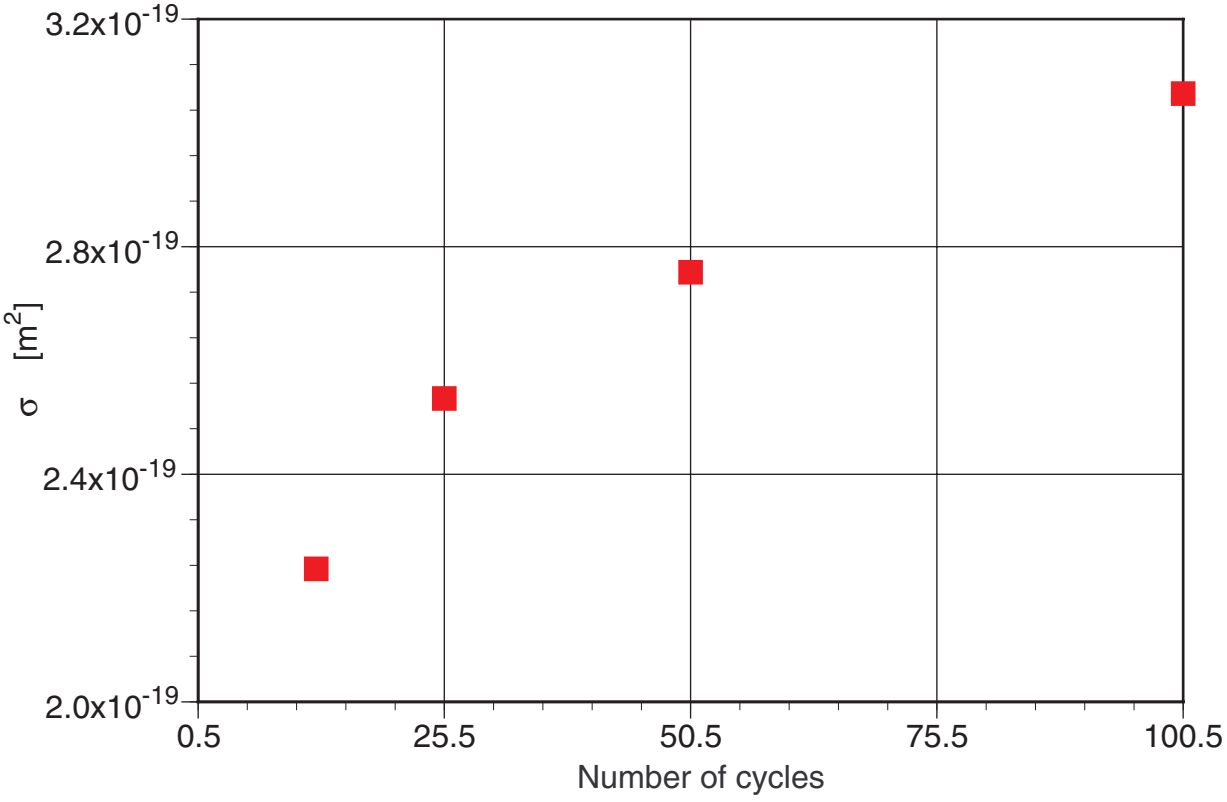

Fig. 5-10 The relation between the cross section and the number of cycles.

the cross section became large. Consequently, it can be concluded that the cross section is $\sigma \sim 3.2 \times 10^{-19}$ [m^2], and this value is proper as a collision cross section between N_2^+ and N_2.

5.6 Tolerance of the voltage applied to the sector and the quadrupole lenses

To estimate the range of energy of ions which can transmit, the ion signal intensity were measured for three different flight path lengths (1.5, 3.5 and 5.5 cycles) while changing the voltage applied to sector II. The operating conditions of the electron gun of the ion source were (1) the filament current was 4.0 A, (2) the electron energy was 100 eV and (3) the peak electron current was 300 μA. Ions were bunched by applying pulse voltage of 220 V to the push plate. The total acceleration voltage of ions was 1.5kV. The background pressure was 2.5×10^{-7} Torr and the vacuum pressure increased to 1.0×10^{-6} Torr when air was introduced. The full width of the source slit was 1 mm in the both horizontal and vertical direction. The intensity is the area of $^{14}N_2^+$ peaks. The variation of ion signal intensity with the voltage applied to sector II is shown in Fig. 5-11. It is clear from the figure that the ion transmission efficiency was maximum around 228 V, while the design value is 225 V. It may be the reason that the acceleration voltage at the ion source was a little high. It is also shown from Fig. 5-11 that the tolerance of energy became narrow as the number of cycles increases and the tolerance of energy was about ±1 % in the case of 6.5 cycles. These results were in agreement with the results which were estimated in section 5.4.

To estimate the effect of the quadrupole lenses, the ion signal intensity for three different flight path lengths (1.5, 3.5 5.5 cycles) were also measured while changing the voltage applied to Q4, Q5, Q12 and Q13. The experimental conditions were the same as the case of the sector. The variation of ion signal intensity with the voltage applied to the quadrupole lenses is shown in Fig. 5-12. It is clear from the figure that the ion transmission efficiency was maximum around 17.5 V, while the design value

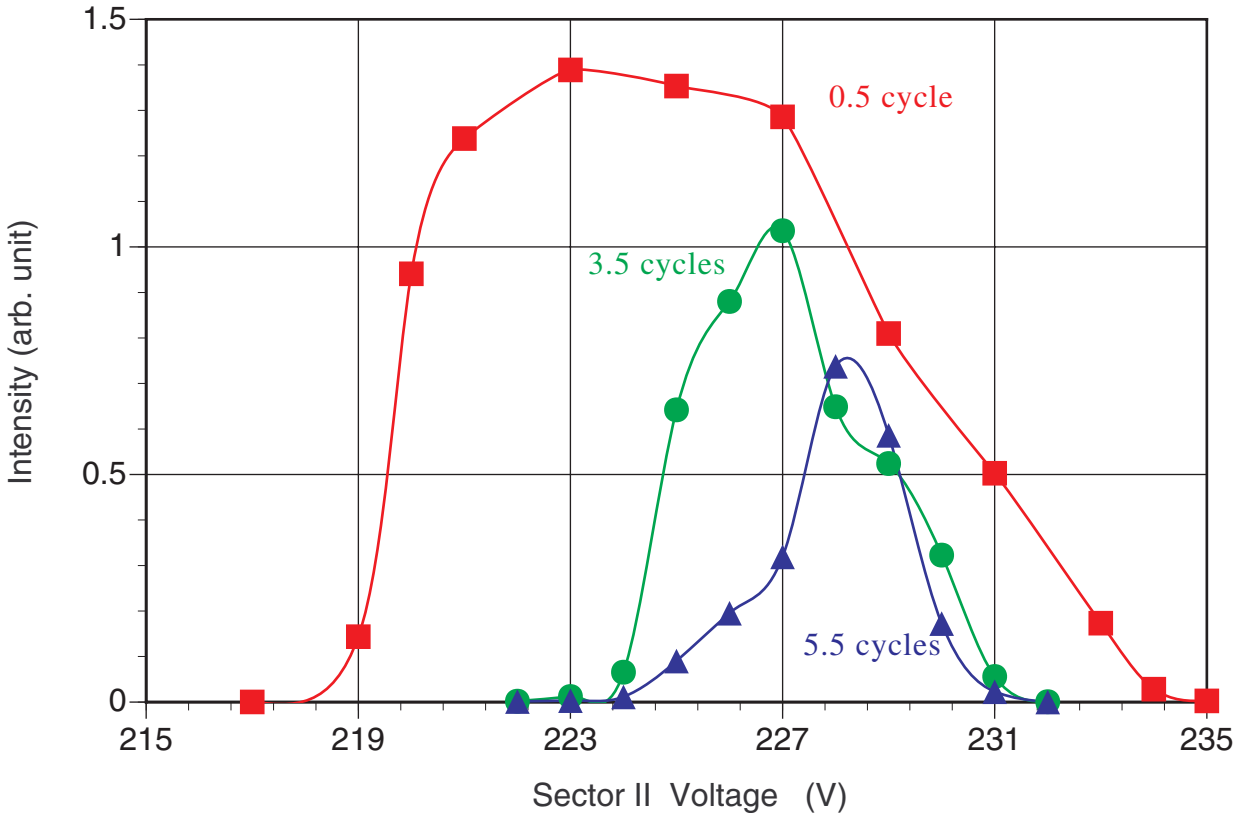

Fig. 5-11 The variation of ion signal intensity with the voltage applied to sector II.

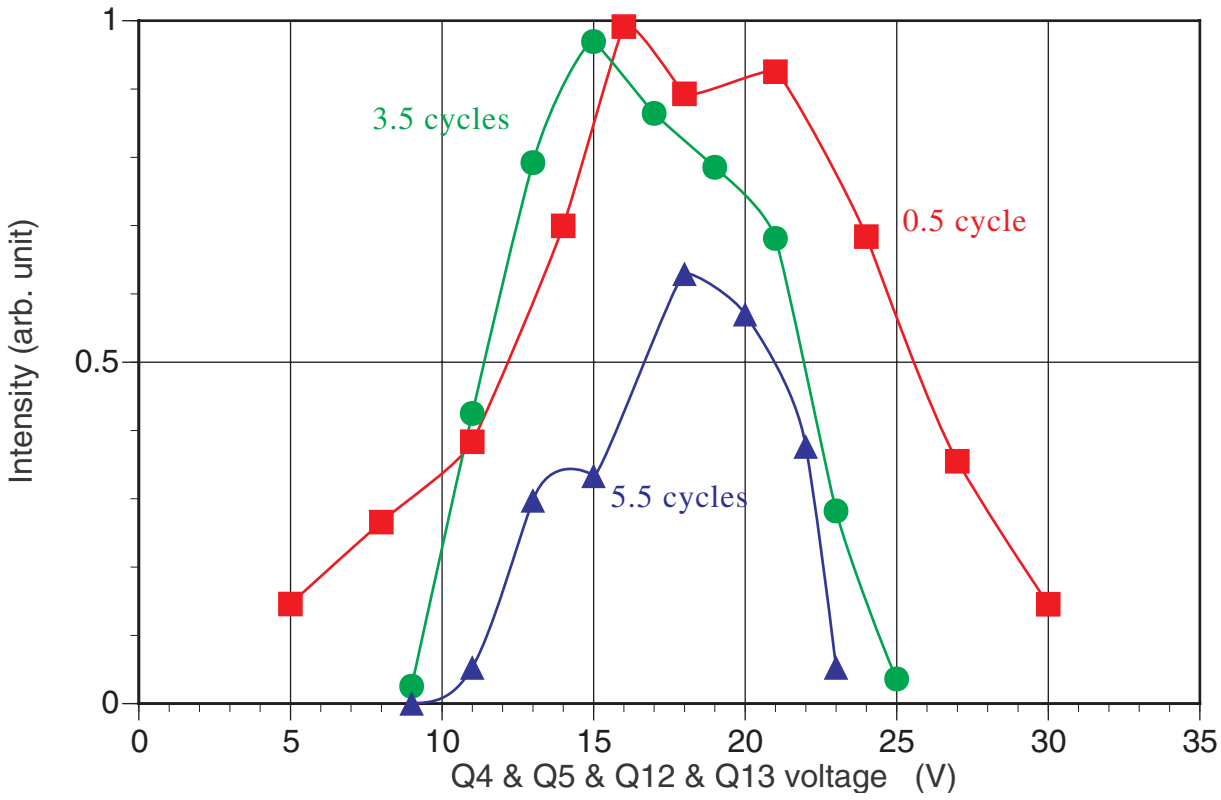

Fig. 5-12 The variation of ion signal intensity with the voltage applied to the quadrupole lenses.

is 16.57 V. The results show that the tolerance became narrow as the number of cycles increases.

5.7 Beam profile at the collector slit

To estimate the space focusing state, the image shapes at the collector slit were measured for four different flight path lengths (0.5, 1.5 3.5 and 6.5 cycles). The experimental conditions were the same as the case of section 5.6. The image shapes were measured by moving the position of the narrow collector slit. The source slit was fixed both the width (1 mm × 1 mm) and position (center). The width of the collector slit were 0.2 mm and it was moved in 0.2 mm step. The relation between the position of the collector slit and the ion signal intensity is shown in Fig. 5-13. It is clear that the image width became wider according the number of cycles.

In the first order approximation, the perfect space focusing should be satisfied. Therefore the width of the image shape should not depend on the number of cycles and should be constant. Here, we consider the higher order influence. The space deviation x_f at the detector slit is given in the second order approximation :

$$\begin{aligned} x_f = {} & A\,(x \mid x)\, x_0 + A\,(x \mid \alpha)\, \alpha_0 + A\,(x \mid \delta)\, \delta + A\,(x \mid x\,x)\, x_0^{\,2} \\ & + A\,(x \mid x\,\alpha)\, x_0\, \alpha_0 + A\,(x \mid x\,\delta)\, x_0\, \delta + A\,(x \mid \alpha\,\alpha)\, \alpha_0^{\,2} + A\,(x \mid \alpha\,\delta)\, \alpha_0\, \delta \\ & + A\,(x \mid \delta\,\delta)\, \delta^2 + A\,(x \mid y\,y)\, y_0^{\,2} + A\,(x \mid y\,\beta)\, y_0\, \beta_0 + A\,(x \mid \beta\,\beta)\, \beta_0^{\,2} \end{aligned} \qquad (5\text{-}13)$$

where x_0 and y_0 are the half width and height of a source slit, α_0 and β_0 are the horizontal and vertical inclination angles at the source slit, respectively, and δ is the relative energy deviation. The image shapes at the collector slit were simulated by TRIO-DRAW for four different number of cycles. The initial conditions used in this simulation were as follows.

$$x_0 = 0.0005 \text{ m},\ \alpha_0 = 0.01 \text{ rad},\ \delta = 0.01,\ y_0 = 0.0005 \text{ m},\ \beta_0 = 0.01 \text{ rad} \qquad (5\text{-}14)$$

The results of the simulation are shown in Fig. 5-14 (a). It is found that the experimental results agree approximately with the simulation results. For comparison, the results of the case of α_0 = 0.001 are shown in Fig. 5-14 (b). In conclusion, the perfect space focusing in the first order approximation was satisfied and the second

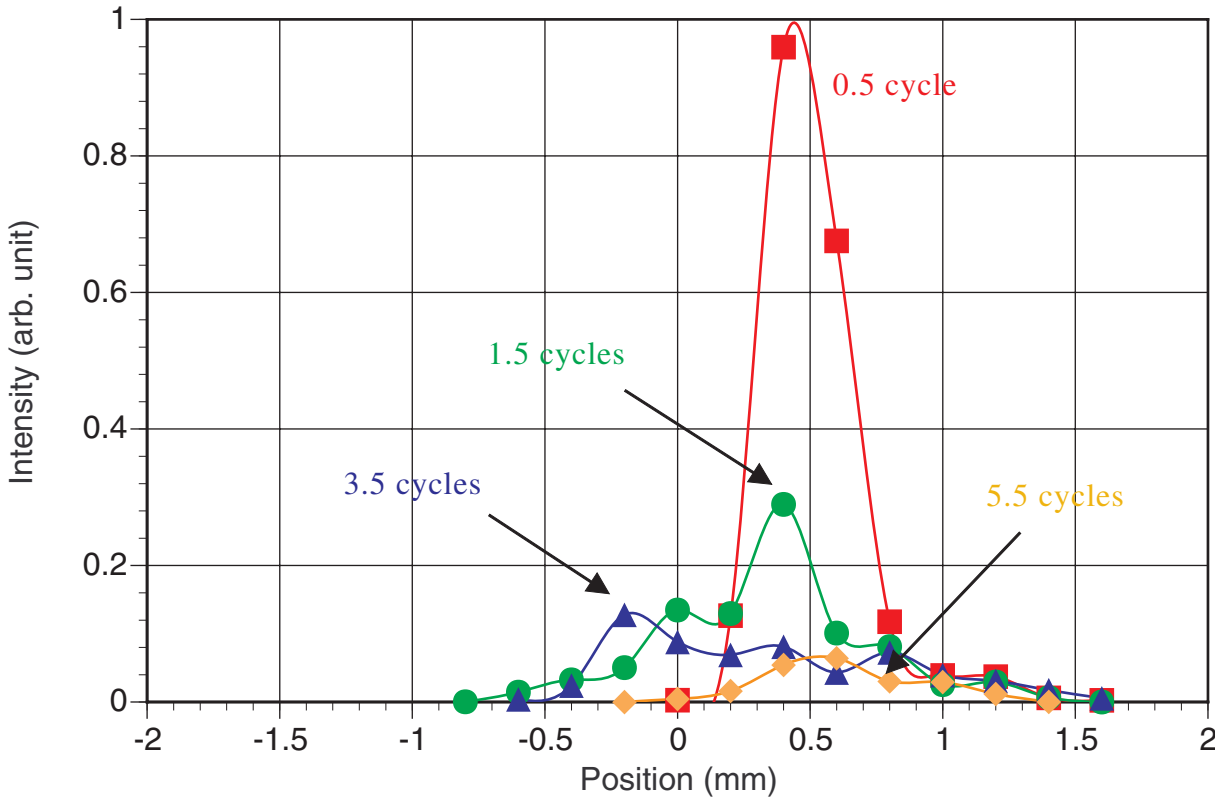

Fig. 5-13 The relation between the position of the collector slit and the ion signal intensity.

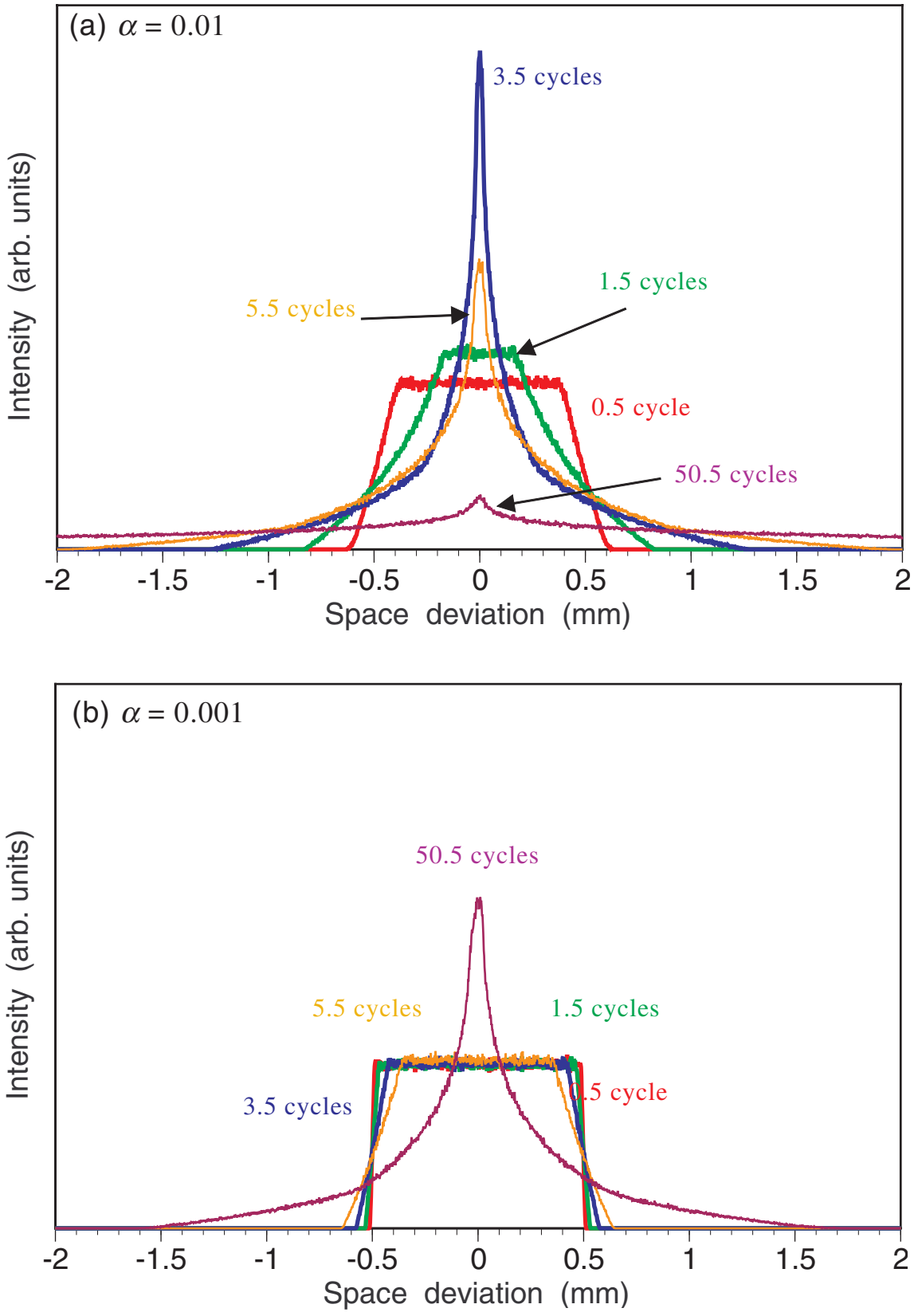

Fig. 5-14 The image shape simulated by TRIO-DRAW changing the initial condition of the relative angle deviation α. $x$max = 0.0005 m, $y$max = 0.0005 m, βmax = 0.01 rad. (a) αmax = 0.01 and (b) αmax = 0.001.

order term $R(x \mid x\alpha)$ (= 21.77 at 0.5 cycle, 65.32012 at 1.5 cycles) gave most significant influence on the beam profile. In order to neglect the influence of higher order term, initial inclination angle should be small.

5.8 Conclusion

The performance of the multi-turn TOF mass spectrometer 'MULTUM Linear plus' was evaluated. It was demonstrated that the mass resolution can increase according to the number of cycles. The mass resolution achieved about 18000 at m / z = 28 after 100.5 cycles. However, it was gradually approaching the saturated value. This phenomenon was explained by the influence of the second order term $R(l \mid \delta\delta)$.

It was also demonstrated that the ion signal intensity after 10 cycles was still 20 ~ 30% of that after a half cycle. Ion intensity of the first 6.5 cycles decreased rapidly and then gradually. The major reason of the ion intensity decrease in the first 6.5 cycles was the escape of ions having large initial deviations by hitting against the electrodes. After 6.5 cycles, small angle scattering with neutral particles became the major reason. The cross section between N_2^+ and N_2 was also estimated.

VI. Discussion

6.1 Performance comparison of 'MULTUM Linear plus' with other multi-turn or multiply-reflected TOF mass spectrometers

Several TOF mass spectrometers which adopt multi-turn or multi-passage ion optical geometries to achieve a long flight path have been proposed and constructed. The specifications of typical such systems are listed in Table 6-1.

The multi-passage TOF mass spectrometer 'OVAL' has been proposed and constructed by Sakurai et al. [6-1]. This spectrometer consists of six electrostatic sectors and the shape of the ion orbit resembles a racetrack oval. This instrument is very large. The size is 2.5 m × 3.5 m and the total flight pass length of 1 turn is 7.4 m. It is estimated theoretically that the high mass resolution (> 30000) can be derived after 1 cycle.

A electrostatic multi-pass mirror systems 'Multi-TOF-MS' has been proposed and constructed by Casares et al. [6-2]. This TOF analyzer consists of two pulsed and one static grid-free ion reflectors. The mass resolution $m / \Delta m$ > 50,000 has been achieved after 31 reflections. This instrument has been also constructed for a laboratory model of 'COSAC' project. However, the instrument is too large to carry on the space craft.

It was proved experimentally that the new TOF mass spectrometer 'MULTUM Linear plus' realized the perfect space and time focusing in the first order approximation. The mass resolution $m / \Delta m$ > 10,000 has been achieved after 50 cycles at m/z = 28. This multi-turn TOF mass spectrometer satisfied the mass resolution and the size that is required in the COSAC project of ROSETTA mission. However, in order to carry on the spacecraft, the number of parts and the weight should be reduced. We are developing a new multi-turn TOF mass spectrometer 'MULTUM II' which improves these problems. The design concepts of 'MULTUM II' are described in the next section.

	MULTUM	MULTUM2	OVAL	Multi-TOF-MS
Type	Multi-turn four cylindrical electric sectors + 28 Q-lenses	Multi-turn four toroidal electric sectors	Multi-turn six toroidal electric sectors	Multiply reflected three ion mirrors
size (1 turn)	60 cm ×70 cm (1.28 m)	45 cm × 50 cm (1.31 m)	250 cm × 350 cm (7.4 m)	? (1.2 m)
Resolution	>10,000 (50 turns) at m/z = 28	Theoritical >10,000 (50 turns)	Theoritical >33,000 (3 turns) at m/z = 2000	>50,000 (31 passages) at m/z = 28
Transmission	10~30% (after 10turns)	?	?	95% for every passage (50%: first passage)
	Osaka Univ. laboratory model for COSAC project	Osaka Univ. modified model of MULTUM now constructing	JAIST	Justus-Liebig Univ. laboratory model for COSAC project

Table 6-1 Specifications of typical multi-turn or multi-passage TOF mass spectrometers.

6.2 The design concepts of 'MULTUM II'

An ion optical system 'MULTUM II' geometry described in Chapter 3.6.3 consisting of only four toroidal electric sectors was found. This system was simple, compact and light, because no quadrupole lens is used. In addition, with employing an orthogonal acceleration ion source to inject ions into the multi-turn ion optical system and employing an ion mirror to eject ions from the system, more high resolution will be achieved. The second order term $R(l \mid \delta\delta)$ may give big influence to the mass resolution in the same as 'MULTUM' geometry. The affect of the term $R(l \mid \delta\delta)$ can be canceled by using an ion mirror. A drawing of the proposed system is shown in Fig. 6-1. A drawing of electric toroidal sector is shown in Fig. 6-2. The miniaturization is possible by putting both an ion source and an ion mirror inside the multi-turn part.

REFERENCES

[6-1] T. Sakurai, H. Nakabishi, T. Hiasa and K. Okanishi, *Nucl. Instrum. Methods A*, **427** (1999), 182-186.

[6-2] A. Casares, A. Kholomeev, N. Nankov, R. Roll, H. Rosenbauer and H. Wollnik, *Proceedings of the 47th ASMS Conference on Mass Spectrometry and Allied Topics*, (1999)

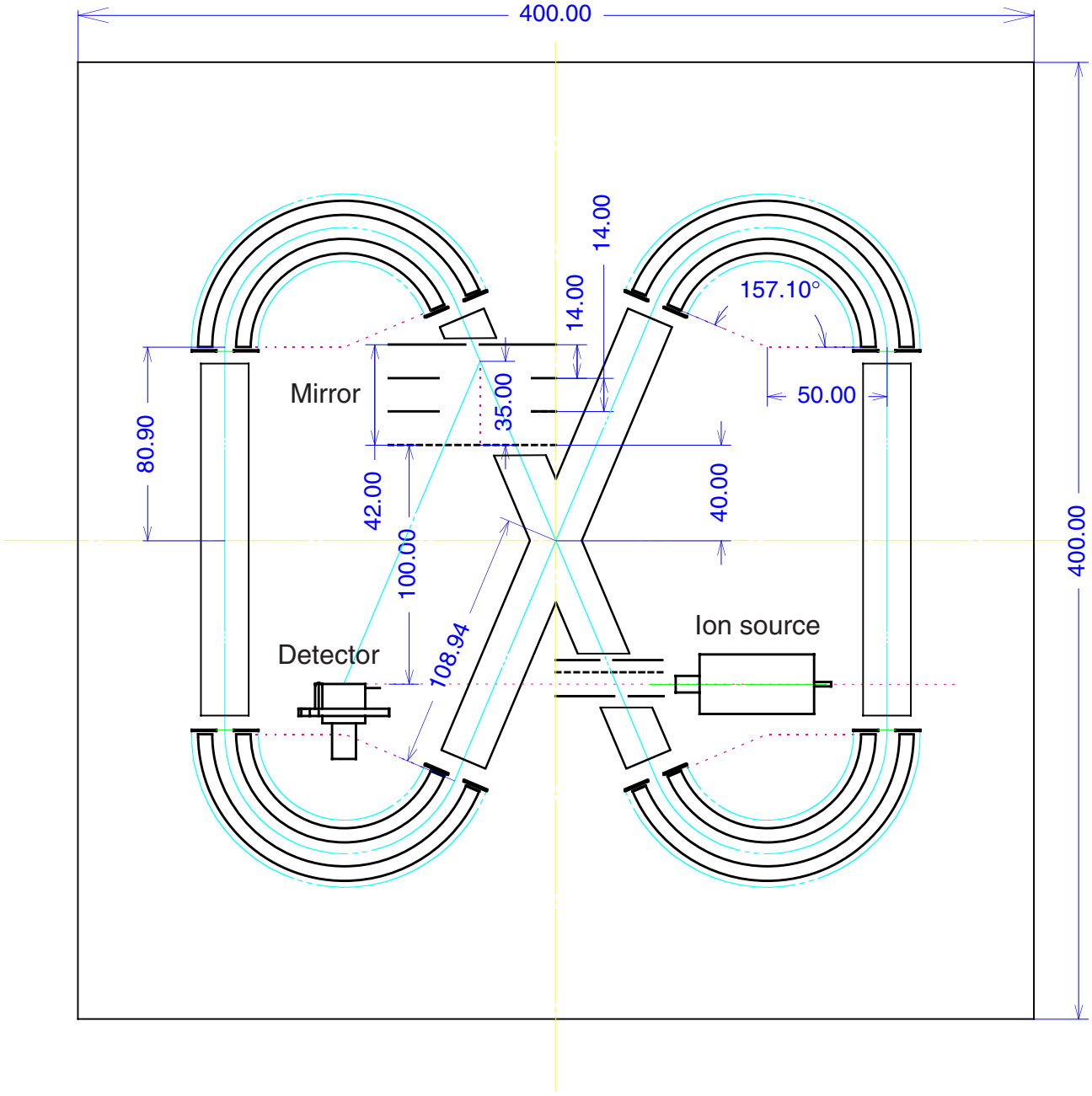

Fig. 6-1 Drawing of the new multi-turn TOF mass spectrometer using 'MULTUM II' geometry.

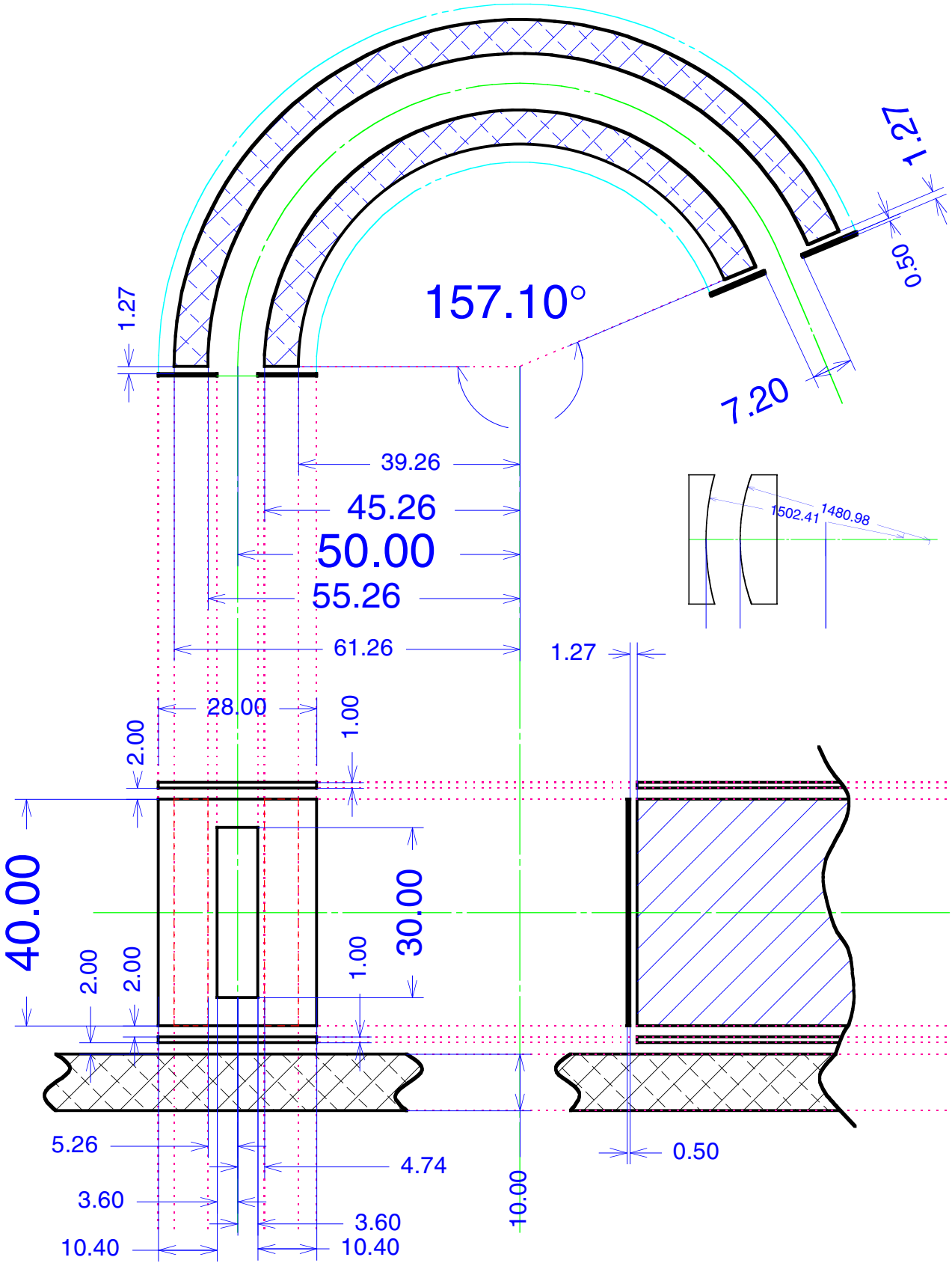

Fig. 6-2 Drawing of electric toroidal sector for the new multi-turn TOF mass spectrometer using 'MULTUM II' geometry.

Acknowledgments

The author would like to express his sincere appreciation and gratitude to Professor Takekiyo Matsuo, under whose guidance the work was conducted and completed. He is also greatly indebted to Dr. Morio Ishihara for encouragement and many useful suggestions and advice. He also thanks to Professor Shuichi Kinoshita for his encouragement and suggestions and to Professor Itsuo Katakuse for enlightening discussions.

He also expresses his thanks to Dr. Helmut Rosenbauer and Dr. Reinhard Roll of Max Planck Institute for Aeronomy for the construction of the new multi-turn time-of-flight mass spectrometer. He wish to express his gratitude to Dr. Arthur Ghielmetti of Lockheed Martin Advanced Research Center for helpful discussions.

He also expresses his thanks to Dr. Toru Sakurai of the Japan Advanced Institute of Science and Technology for using calculation code ‘unify’ and for the helpful discussions on the ion optics. He is also greatly indebted to Mr. Shin-ichi Yamaguchi for the development of the ion sources and for helpful discussions.

He also thanks to Professor Masahiro Kimura of Kochi University of Technology for his encouragement and suggestions. He also would like to acknowledge the contributions of Mr. Hiroyuki Ito for helpful suggestions and observations.

He also expresses his thanks to the staff of MS group of JEOL Ltd. Akishima Tokyo for the construction of the new time-of-flight mass spectrometer and helpful discussions.

He also thanks to Professor Koichiro Tsuruda of The Institute of Space and Astronautical Science for his supports.

This work was supported by JSPS Research Fellowship (2258), a Grant-in-Aid for Scientific Research (B) (No. 09559012, No. 10044085 and No. 11559012) from the Ministry of Education, Science, Sports and Culture. He is also thankful to the Institute of Space and Astronautical Science and the Yamada Science Foundation for financial support.